University of Miskolc

Faculty of Mechanical Engineering and Informatics

Institute of Applied Mechanics

Dávid Gönczi

Thermoelastic Problems of Functionally Graded and Composite Structural Components

PhD dissertation

Scientific Supervisor:
István Ecsedi
Professor Emeritus

István Sályi Doctoral School
Main Topic Group: Fundamental Sciences in Mechanical Engineering
Topic Group: Mechanics of Solid Bodies

Head of Doctoral School:
Miklós Tisza, Doctor of Science, Full Professor

Head of the Main Topic Group:
István Páczelt, Member of the Hungarian Academy of Sciences, Professor Emeritus

Head of the Topic Group:
György Szeidl, Doctor of Sciences, Professor Emeritus

Miskolc-Egyetemváros

2016

Table of Content

Declaration

The author hereby declares that the work in this dissertation contains no material previously published or written by another person and no part of the dissertation has been submitted, either in the same or different form, to this or any other university for a PhD degree. The author confirms that the work presented in this dissertation is his own and the appropriate credit has been given where reference has been made to the work of the others.

Miskolc, June 29, 2016. Dávid Gönczi

Nomenclature

Here the most important notations are gathered, although each notation is described in the text when first used. Due to the large number of constants and notations, a few symbols might appear in a section as for example integration constants.

Latin symbols:

a	inner radius of spheres, curved beams and disks
A	surface
b	outer radius of spheres, curved beams and disks
B_i	body force vector
B_{ij}	dielectric constants (for *e*-form)
C	constant of integration
C_{ijkl}	material stiffness
D, D_i	electrical displacement
e_{ijk}	piezoelectric constants
E	Young modulus, modulus of elasticity
E_i	coordinates of the electrical field, negative of potential gradient
E_{ij}	Almansi strain tensor
f	distributed load at the boundary of the layers
g_{ijk}	piezoelectric constants
G	shear modulus
$h(r)$, h_i	thickness of radially graded disks, thickness of layers
M	general notation for material parameters
$(\dots)^M$	elastic part of (…)
n	number of layers
p	pressure
P_i	material dependent coefficients of temperature
q	heat flow
r	radial coordinate of cylindrical and spherical coordinate systems
r_{mi}	average radius of the *i*-th layer
R_i	radius values of layers and curved bodies
T	temperature difference function, temperature field ($T(\boldsymbol{r})=t_{abs}-t_{ref}$)
t	temperature value
t_{abs}	absolute temperature (in K)
t_{ref}	reference temperature (where the stresses are zero if the body is undeformed)
$(\dots)^T$	thermal part of (…)
u	radial displacement
u_i	coordinates of the displacement vector
U_0	complementary energy per unit volume
V	volume
$V(r)$	stress function

Greek symbols:

α	coefficient of linear thermal expansion
β_{ij}	dielectric constants (for *g*-form)
γ_{ij}	shear strain on the *ij* plane
γ	heat transfer coefficients
δ_{ij}	Kronecker delta
ε_i	normal strain in the direction *i*
ε_{ij}	strain tensor
ϑ	circumferential coordinate of spherical coordinate system
Θ	function of the Kirchoff integral transformation
λ	thermal conductivity
ν	Poisson's ratio
$\tilde{\Pi}_c$	total complementary energy
ρ	density
σ_i	normal stress in the direction *i*
τ_{ij}	shearing stress on the *ij* plane
φ	tangential coordinate of spherical and cylindrical coordinate systems
ω	angular velocity of rotating disks

1. Introduction

As technology progresses at an ever increasing rate, the need for advanced capability materials becomes a priority in the engineering of more complex and higher performance systems. This need can be seen in many fields in which engineers are exploring the applications of these new engineered materials. Pure metals are used rarely in engineering applications because of the demand of conflicting property requirements. In many cases an application may require a material that is hard as well as ductile. To solve this problem, metals are combined with other metals or non-metal components to improve their material properties.

1.1. Composite and functionally graded materials

One method of producing materials with improved properties is to combine them in solid state which is referred to as composite materials [1]. These advanced inhomogeneous materials are made of one or more materials in solid state with distinct mechanical and chemical properties. The composites offer excellent properties which are different from the individual constituent materials and in most cases lighter in weight. The basic types of composite materials are particle-reinforced, fiber-reinforced, laminated or layered structural and filled composites. The utilization of these materials is limited because under extreme working conditions a phenomenon called delamination [2] will occur. This process is especially problematic in high temperature environments when the parent materials have different coefficients of linear thermal expansion.

To solve this problem, researchers in Japan in the mid 1980s created the concept of the functionally graded material during a hypersonic space plane project where the body of the spaceplane is exposed to very high temperature environment with huge temperature gradient. The researchers wanted to create a material by gradually changing the material composition in order to improve both the thermal resistance and the mechanical properties of the structural members of the plane.

Functionally Graded Materials (FGMs) are advanced material in which the composition and structure gradually change resulting in a corresponding change in the properties of the material. In functionally graded materials the sharp interfaces between the constituent materials are eliminated [3]. It replaces this sharp interface, which is where failure can be initiated, with a gradient interface which produces smooth transition from one material to the next [4, 5]. This solution lessens the stress concentrations which become troublesome in a laminated composite material. At high temperature, the smooth transition of material properties provides thermal protection, great mechanical behaviour and structural integrity without introducing a single point for failure within the structure. In recent years this concept has become more popular in Europe.

From the point of view of material processing methods, the functionally graded structural components can be divided into two groups, thin and bulk functionally graded materials. Thin functionally graded materials or surface coatings can be produced for example by vapour deposition, plasma spraying or self-propagating high-temperature synthesis [1]. These methods are energy intensive and produce poisonous gases as their byproducts. All the above mentioned processes cannot be used to produce bulk functionally graded materials because they are generally slow and energy intensive, therefore they are uneconomical.

Bulk functionally graded materials are produced using powder metallurgy technique, centrifugal casting method, solid freeform technology [6], etc. Powder metallurgy technique is used to produce functionally graded material through weighing and mixing of powders according to the predesigned spatial distribution as dictated by the functional requirement, stacking and

ramming of the premixed-powders, and finally sintering. Despite the excellent characteristics of powdered metallurgy, there exist some limitations, for example certain shapes and features cannot be produced. The centrifugal method is utilized to create continuous structures, where the force of gravity is used through the spinning of the mould, which contains molten metal matrix and ceramic powder, to form bulk functionally graded materials. One of the main problems of the centrifugal method is the limit to which type of gradient can be produced, because the gradient is formed through natural processes with two main components, which are the centrifugal force and the density difference. To solve these problems, researchers are using an advanced manufacturing method known as solid freeform (SFF) method. This is an additive manufacturing process that offers lots of advantages that include: higher speed of production, less energy consumption, maximum material utilization, ability to produce complex shapes and design freedom as parts are produced directly from CAD data [7]. SFF involves five basic steps, which are the generation of CAD data from softwares like AutoCAD, Solid Edge, etc., conversion of the CAD data to Standard Triangulation Language (STL) file, the slicing of the STL into two- dimensional cross section profiles, building of the component layer by layer, and lastly removal and finishing. To produce bulk functionally graded components the laser based SFF methods are utilized generally, such as 3D printing, laser cladding based method, selective laser sintering and selective laser melting. A big disadvantage of the solid freeform method is the poor surface quality, therefore a second finishing operation is necessary.

The fabrication processes are constantly improving, the cost of powders and the overall process expense are decreasing, therefore the application of functionally graded materials are expanding. These advanced materials are utilized in high efficiency engine components, light weight structures for aircraft and space industry, implants, cutting inserts, tools, numerous military applications, etc.

1.2. Preliminaries

The dissertation deals with the steady-state thermoelastic problems of simple structural components, such as disks, spheres and beams, which are subjected to thermal and mechanical loadings. These components are made from inhomogeneous materials, especially functionally graded materials and laminated composites.

A lot of books and papers deal with the thermoelastic problems of homogeneous, isotropic materials. In the past few years many researchers dealt with the mechanics of structures made from inhomogeneous materials, in recent years the concept and the mechanics of functionally graded materials have become more popular in Europe.

Lots of works deal with the mechanics of functionally graded materials from various aspects. One of the main fields of the mechanical analysis for FGMs is finite element modelling for these materials, another areas are the stress, stability, dynamic analysis and fracture mechanics mostly for FGM beams, plates and shells [8, 9]. There are several textbooks dealing with the analytical, semi-analytical and numerical solutions for the thermomechanical problems of hollow spheres, cylinders, beams and disks.

The analytical solution for the stresses and displacements in spheres and cylinders made from functionally graded materials are given by Lutz and Zimmerman [10]. Their paper considered thick radially graded spherical and cylindrical bodies under radial thermal loading, where the composition of the constituent materials was linear.

The work by Tutuncu and Ozturk [11] derived closed-form analytical solutions for the stresses in functionally graded cylindrical and spherical bodies, subjected to internal pressure alone.

Radially varying inhomogeneous material properties are considered with a material stiffness-matrix in which the parameters are obeying a simple power-law, furthermore the stress distributions depends on the inhomogeneity constant. This work presents specific applications to control the stress distribution. The paper of Obata and Noda [12] studied one-dimensional steady-state thermal stress problem for functionally graded hollow circular cylinders and hollow spheres by use of a perturbation approach in order to investigate the effect of the composition on stresses and to design the optimum functionally graded hollow circular cylinder and hollow sphere, under different assumptions of temperature distributions. The unsteady-state thermal stress of graded circular hollow cylinders is based on the multilayered method and Green function were presented by Kim and Noda [13].

Another general analysis of one-dimensional steady-state thermal stress problems in a hollow thick FGM cylinder was obtained by Eslami et al. [14]. This work uses a direct method to solve the heat conduction and Navier equations, the temperature distribution is assumed to be a function of the radial coordinate. In a similar work (2005), Eslami et al. [15] investigated the thermal and mechanical stresses in hollow functionally graded spheres using the same method as in [14].

Liew et al. [16] investigated the thermomechanical behavior of hollow circular cylinders made from functionally graded material. The exact solutions are obtained by a novel limiting process that employs the solutions of homogeneous hollow circular cylinders, with no recourse to the basic theory or the equations of nonhomogeneous thermoelasticity with the results that thermal stresses occur in the FGM cylinder, except in the trivial case of zero temperature and heat resistance may be improved by the proper variation of material composition. The thermal stresses in the FGM cylinder are governed by more factors than in the case of homogeneous materials.

Zamani N. and Rahimi [17] investigated the thermal and mechanical stresses under generalized plane strain and plane stress assumptions, respectively. Concerning the stress analysis of cylindrical and spherical structural elements, Tutuncu and Temel [18] presented a novel approach to stress analysis of pressurized FGM cylinders, disks, and spheres. In this work axisymmetric displacements and stresses in functionally graded hollow cylinders, disks and spheres subjected to constant internal pressure were determined using plane elasticity theory and the method of complementary functions.

The work of Nayak and Mondal [19] presented an analysis of a functionally graded thick cylindrical vessel with radially varying properties in the form of the displacement field, strains and associated stresses for thermal, mechanical and thermomechanical loads. This contains a reducing method for the FGM pressure vessels to thick cylindrical bodies made of isotropic homogeneous materials. The paper of Shao [20] presented the solution of a functionally graded hollow circular cylinder using a multilayered approach and the theory of laminated composites. That case is considered when the layers have finite lenght, the body is subjected to axisymmetric thermal and mechanical loads. Furthermore the material properties are homogeneous in each layer, varying radially between the layers and they are independent of the temperature field. The results are also presented for a mullite-molybdenum functionally graded circular hollow cylinder. The work by Vitucci and Mishuris [21] investigated multilayered cylinders with perfect and imperfect contact between the isotropic homogeneous layers, and the residual stresses in ceramic layers. Arefi [22] applied the general shell deformation theory to functionally graded cylinders shells.

You et al. [23] presented an accurate method to carry out elastic analysis of two kinds of thick spherical pressure vessels subjected to internal pressure. In the first case a spherical body is considered which consists of two homogeneous layers near the inner and outer surfaces of the vessel and one functionally graded layer in the middle. The other investigated case consideres a functionally graded sphere. In this paper the effects of the Young's modulus of the outer and inner layers and geometric size of the middle layer on the displacement field and on the associated

stresses are examined. A method to obtain an almost constant circumferential stress in the spherical vessels made of functionally graded material only is presented.

Ahmet and Tolga [24] dealt with the plane strain analytical solutions for functionally graded elastic and elastic–plastic pressurized tubes using small deformation theory. The modulus of elasticity and the uniaxial yield limit of the material are assumed to vary radially according to parabolic forms. The plastic model is based on Tresca yield criterion, its flow rule and ideally plastic material behaviour. By the suitable selection of the material parameters, the inhomogeneous elastic-plastic solution can be reduced to a homogeneous one. Chen and Lin [25] carried out the elastic analysis for thick cylinders and spherical pressure vessels made of functionally graded materials when the material parameters are varying exponentially along the radial coordinate. This work investigates the stress distribution along the radial direction. Shao and Ma [26] presented thermo-mechanical analysis of functionally graded hollow circular cylinders subjected to mechanical loads and linearly increasing boundary temperature. Thermomechanical properties of functionally graded material are temperature independent and vary continuously in the radial direction of the cylinder. Using the Laplace transformation technique and methods for ordinary differential equation, the solutions for the time-dependent temperature and thermomechanical stresses are calculated, furthermore an example is presented for a molybdenum-mullite graded cylinder in which the material properties vary exponentially along the radial coordinate.

Nayak et al. [27] elaborated an analytical solution to obtain the radial, tangential and effective stresses within thick spherical pressure vessels made of FGMs subjected to axisymmetric mechanical and thermal loadings. The properties of the material for the vessel are assumed to be graded in the radial direction based on a power-law function of the radial coordinate but the Poisson's ratio has constant value. With thermal boundary conditions of the third kind and steady-state unidirectional radial heat conduction, the equilibrium equation reduces to Navier equation. A work by Bayat, Mahdi and Torabi [28] dealt with the previously presented problem too, and investigated the effect of the index parameter of the power-law functions on the stress distribution.

In paper by Pen, X. and Li, X. [29] the thermoelastic problem of isotropic functionally graded disks with arbitrary radial inhomogeneity was considered. The numerical solution of the steady-state thermoelastic problem is reduced to a solution of a Fredholm integral equation. A general analysis of one-dimensional steady-state thermal stresses in thick cylinder made of isotropic radially inhomogeneous elastic materials is presented by Jabbari et. al [30]. An analytical method is used to solve the heat conduction and Navier equations in [30].

Some textbooks such as Timoshenko and Goodier [31], Solecki and Conant [32], Barber [33], Baroumi and Ragab [34], Hetnarski and Eslami [35], Noda et. al [36] give detailed analysis of the thermal stress problem for homogeneous isotropic elastic disk with axisymmetric temperature field. Furthermore these books and papers [31-36] neglect the convective heat transfer on the lower and upper plane surfaces of the disks. Numerous papers, such as [37-41], present thermomechanical problems of functionally graded disks but the material parameters are special functions of the radial coordinate.

Wang et al. [61] studied the dynamic problem of a multilayered piezoelectric spherical body under symmetric loading. The superposition principle is used to divide the problem into quasi-static and dynamic parts. Wang and Xu [42] investigated the effect of material inhomogeneity on the electromechanical behaviors of exponentially graded piezoelectric spheres using the Frobenius series method. The paper by Sburlati and Atashipour [43] investigated the electromechanical problem of piezoelectric spherical bodies with functionally graded coating. The material properties are power-law based functions of the radial coordinate. The work of Ghorbanpour et. al. [44] presents analytical solutions for a few cases of radially graded piezoelectric spheres under axisymmetric mechanical loading.

As for functionally graded beams, paper [45] dealt with the two-dimensional problem of exponentially graded beams under uniaxial tension and bending. The governing equation is derived by means of the Airy stress function method together with the strain compatibility equation. Sankar [46] studied a bending problem of a simply supported FGM beam based on the theories of beams and two-dimensional elasticity. Zhong and Yu [47] obtained the general solution for a cantilever made from functionally graded beam subjected to different kinds of loads. The paper by Ying et al. [48] gave a two-dimensional elasticity solution for functionally graded beams resting on elastic foundations. Wang and Liu [49] analysed a bi-material beam with graded intermediate layer subjected to uniform loading on the upper surface. A paper by Li et al. [50] made a stress analysis of FGM beams using effective principal axes. Papers [62-65] dealt with the problem of bimetallic strips made from two different homogeneous components, although the curved beams were not investigated.

1.3. Objectives

As we have seen in the previous section, analytical solutions were derived only in special cases, for example for power-law based material properties, constant Poisson's ratio, etc. Most of the papers and works neglect the temperature dependency of the material properties. The aim of the dissertation is to deal with the problems of functionally graded simple structural components made from isotropic functionally graded materials and layered -laminated- composites subjected to thermal and mechanical loads. I intend to derive methods for thermoelastic problems of functionally graded materials with properties described by arbitrary spatial and temperature-dependent functions. I will investigate stationary or steady-state thermoelastic problems. The time-independence of the functions involved separates the analysis of the temperature field from that of the elastic field, therefore these problems become uncoupled. As we have seen in Section 1.1 in many cases the functionally graded structural components are built with additive methods layer by layer, therefore we can approximate the problem of functionally graded components with methods of layered components (we will refer to this model as multilayered approach) with finite layer number n. Obviously when $n \to \infty$ we get to the functionally graded materials. In view of this, the objectives of the dissertation are

- ***(a)*** to derive analytical methods to calculate the temperature field, displacements and stress field within layered spherical bodies;
- ***(b)*** to develop fast and accurate numerical methods for determining the temperature-, displacement- and stress field within functionally -radially- graded spherical components, when the material properties are arbitrary functions of the radial coordinate and temperature;
- ***(c)*** investigation of special problems of functionally graded spherical bodies, such as incompressible or piezoelectric, radially polarized materials;
- ***(d)*** to present analytical solutions for functionally graded spheres, then compare the developed one-dimensional numerical and analytical methods to each other and to finite element simulations;
- ***(e)*** to develop analytical solutions for calculating the temperature field, displacements and normal stresses in layered composite disks;
- ***(f)*** derivation of numerical methods for rotating thin functionally graded disks with arbitrary thickness profile when the material properties are arbitrary functions of the radial coordinate and the temperature field, furthermore there are combined thermal and mechanical loads on the cylindrical boundary surfaces;

(g) to determine the thermal stresses and displacements in nonhomogeneous prismatic bars caused by mechanical and thermal loads when the cross section of the bar is an arbitrary bounded plain domain, the material properties and the temperature field do not depend on the axial coordinate;

(h) to deal with the problems of curved layered composite and functionally graded curved beams subjected to special thermal and mechanical loads;

(i) to compare the developed methods to each other, to finite element solutions and to results of the literature.

The text of the dissertation is organized into seven chapters. After the introduction and the overview of the literature, the basic concepts and equations of thermoelasticity are presented in Chapter 2. In Chapters 3 and 4 several methods are derived to deal with the thermoelastic problem of layered composite and functionally graded spherical bodies, objectives *(a)-(d)*. Chapter 3 presents analytical methods for composite and radially graded spheres, while Chapter 4 focuses on numerical methods for functionally graded spherical bodies. Chapter 5 contains a few thermoelastic problems of thin radially graded disks *(e)-(f)*. Objectives *(g)*, *(h)* and *(i)* are presented in Chapter 6. The dissertation closes with a brief summary and the list of the most important theoretical results, i.e., the theses.

2. Basics of thermoelasticity

In this chapter the basic equations are presented for the thermoelastic problems which will be investigated in the next chapters.

2.1. Displacement and strain tensors

Consider an elastic body in its original undeformed configuration described in the coordinate system (g_1, g_2, g_3) fixed to the body [35]. A point P of the body has the coordinates g_i (i = 1, 2, 3) in this system (Fig. 2.1), after the loading, point P is deformed and moved to a new position Q. Along with the body, the original coordinate system is transformed into the deformed configuration (x_1, x_2, x_3). The coordinates of the point Q in the deformed coordinates are x_i, (i= 1, 2, 3). It is assumed that the change and deformation of the body is continuous and the point transformation is one-to-one.

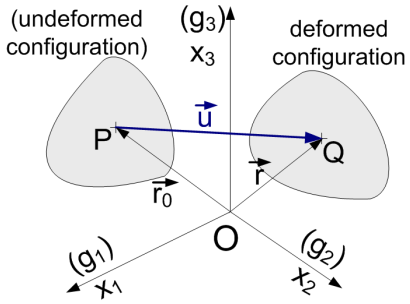

Figure 2.1. The displacement vector.

Let us confine ourselves to the rectangular Cartesian coordinates, and assume that the law of coordinate transformation between the original and the deformed coordinates and its inverse transformation law are known and given as

$$x_i = X_i(g_1, g_2, g_3), \tag{2.1.1}$$

$$g_i = G_i(x_1, x_2, x_3). \tag{2.1.2}$$

From these equations we get

$$\mathrm{d}x_i = \frac{\partial x_i}{\partial g_k}\mathrm{d}g_k, \tag{2.1.3}$$

$$\mathrm{d}g_i = \frac{\partial g_i}{\partial x_k}\mathrm{d}x_k. \tag{2.1.4}$$

The differentials of position vector in the original and deformed configurations are

$$\mathbf{dr_0} = \mathbf{g_i}\mathrm{d}g_i, \tag{2.1.5}$$

$$\mathbf{dr} = \mathbf{a_i}\mathrm{d}x_i, \tag{2.1.6}$$

where $\mathbf{g_i}$ and $\mathbf{a_i}$ are the unit vectors in the original and deformed coordinates, respectively. Here the summation conventions are valid. The differentials of line elements in the original and the deformed coordinates are

$$dS_0^2 = \mathbf{dr_0} \cdot \mathbf{dr_0} = \mathbf{g_i} \cdot \mathbf{g_j} dg_i dg_j = \delta_{ij} dg_i dg_j, \tag{2.1.7}$$

$$dS^2 = \mathbf{dr} \cdot \mathbf{dr} = \mathbf{a_i} \cdot \mathbf{a_j} dx_i dx_j = \delta_{ij} dx_i dx_j. \tag{2.1.8}$$

The substitution of Eqs. (2.1.3), (2.1.4) into Eqs. (2.1.7), (2.1.8) gives

$$dS_0^2 = \delta_{ij} \frac{\partial g_i}{\partial x_k} dx_k \frac{\partial g_j}{\partial x_l} dx_l, \tag{2.1.9}$$

$$dS^2 = \delta_{ij} \frac{\partial x_i}{\partial g_k} dg_k \frac{\partial x_j}{\partial g_l} dg_l. \tag{2.1.10}$$

With the combination of Eqs. (2.1.7)-(2.1.10) we get

$$dS^2 - dS_0^2 = \left(\delta_{kl} - \delta_{ij} \frac{\partial g_i}{\partial x_k} \frac{\partial g_j}{\partial x_l} \right) dx_k dx_l, \tag{2.1.11}$$

$$dS^2 - dS_0^2 = \left(\delta_{ij} \frac{\partial x_i}{\partial g_k} \frac{\partial x_j}{\partial g_l} - \delta_{kl} \right) dg_k dg_l. \tag{2.1.12}$$

Let e_{ij} and E_{ij} denote the Green strain tensor in terms of the strains in the original coordinates and the Almansi strain tensor in terms of the strains in the deformed coordinates, respectively as

$$e_{kl} = \frac{1}{2}\left(\delta_{ij} \frac{\partial x_i}{\partial g_k} \frac{\partial x_j}{\partial g_l} - \delta_{kl} \right), \quad E_{kl} = \frac{1}{2}\left(\delta_{kl} - \delta_{ij} \frac{\partial g_i}{\partial x_k} \frac{\partial g_j}{\partial x_l} \right). \tag{2.1.13}$$

The displacement vector **u** is defined as

$$\mathbf{u} = \mathbf{r} - \mathbf{r_0}, \qquad u_i = x_i - g_i. \tag{2.1.14}$$

The relation for the Almansi strain tensor is

$$E_{ij} = \frac{1}{2}\left(\frac{\partial u_j}{\partial x_i} + \frac{\partial u_i}{\partial x_j} - \frac{\partial u_k}{\partial x_i} \frac{\partial u_k}{\partial x_j} \right). \tag{2.1.15}$$

For the infinitesimal theory of elasticity the displacement gradient $u_{k,i}$ is small, so that the quadratic term in Eqs. (2.1.15) may be neglected and strain tensors e_{ij} and E_{ij} are both reduced to the linear form as

$$\varepsilon_{ij} = E_{ij} + \frac{1}{2}\left(\frac{\partial u_k}{\partial x_i} \frac{\partial u_k}{\partial x_j} \right) = \frac{1}{2}\left(u_{j,i} + u_{i,j} \right). \tag{2.1.16}$$

In terms of the O*xyz* conventional Cartesian coordinate system, the six strain-displacement relations reduce to

$$\begin{gathered} \varepsilon_{11} = \varepsilon_x = \frac{\partial u_x}{\partial x}, \ \varepsilon_{22} = \varepsilon_y = \frac{\partial u_y}{\partial y}, \ \varepsilon_{33} = \varepsilon_z = \frac{\partial u_z}{\partial z}, \\ \varepsilon_{12} = \frac{1}{2}\gamma_{xy} = \frac{1}{2}\left(\frac{\partial u_x}{\partial y} + \frac{\partial u_y}{\partial x} \right), \varepsilon_{23} = \frac{1}{2}\gamma_{yz} = \frac{1}{2}\left(\frac{\partial u_z}{\partial y} + \frac{\partial u_y}{\partial z} \right), \varepsilon_{13} = \frac{1}{2}\gamma_{xz} = \frac{1}{2}\left(\frac{\partial u_x}{\partial z} + \frac{\partial u_z}{\partial x} \right). \end{gathered} \tag{2.1.17}$$

In equations (2.1.17) u_x, u_y and u_z denote the components of the displacement vector in the direction of *x*, *y* and *z*, respectively. Here we note that the strain tensor ε_{ij} is symmetric. In O*rφz* cylindrical coordinate system the strain-displacement relations are

$$\varepsilon_r = \frac{\partial u_r}{\partial r},\ \varepsilon_\varphi = \frac{1}{r}\left(\frac{\partial u_\varphi}{\partial \varphi} + u\right),\ \varepsilon_z = \frac{\partial u_z}{\partial z},$$
$$\gamma_{r\varphi} = \frac{1}{r}\frac{\partial u_r}{\partial \varphi} + \frac{\partial u_\varphi}{\partial r} - \frac{u_\varphi}{r}, \gamma_{\varphi z} = \frac{1}{r}\frac{\partial u_z}{\partial \varphi} + \frac{\partial u_\varphi}{\partial z}, \gamma_{zr} = \frac{\partial u_r}{\partial z} + \frac{\partial u_z}{\partial r}, \tag{2.1.18}$$

where u_r, u_φ and u_z are the components of the displacement vector. In O$r\varphi\vartheta$ spherical coordinate system the strain-displacement relations can be written in the following forms:

$$\varepsilon_r = \frac{\partial u_r}{\partial r},\ \varepsilon_\vartheta = \frac{1}{r}\left(\frac{\partial u_\vartheta}{\partial \vartheta} + u_r\right),\ \varepsilon_\varphi = \frac{1}{r\sin\vartheta}\left(\frac{\partial u_\varphi}{\partial \varphi} + u_r \sin\vartheta + u_\vartheta \cos\vartheta\right),$$
$$\gamma_{r\vartheta} = \frac{1}{r}\frac{\partial u_r}{\partial \vartheta} + \frac{\partial u_\vartheta}{\partial r} - \frac{u_\vartheta}{r}, \gamma_{r\varphi} = \frac{1}{r\sin\vartheta}\frac{\partial u_r}{\partial \varphi} + \frac{\partial u_\varphi}{\partial r} - \frac{u_\varphi}{r}, \tag{2.1.19}$$
$$\gamma_{\varphi\vartheta} = \frac{1}{r}\left[\frac{1}{\sin\vartheta}\frac{\partial u_\vartheta}{\partial \varphi} + \left(\frac{\partial u_\varphi}{\partial \vartheta} - u_\varphi \cos\vartheta\right)\right],$$

where u_r, u_φ and u_ϑ are the components of the displacement vector in the current coordinate system.

2.2. Constitutive law and equilibrium equations

In the classical theory of linear thermoelasticity the components of the strain tensor are linear functions of the components of the stress tensor and the components of the strain tensor due to the mechanical load and temperature change, that is [35]

$$\varepsilon_{ij} = \varepsilon_{ij}^M + \varepsilon_{ij}^T, \tag{2.2.1}$$

where $\varepsilon_{ij}{}^M$ and $\varepsilon_{ij}{}^T$ denote the elastic and thermal strain tensors. The thermal strain due to temperature change is

$$\varepsilon_{ij}^T = \alpha\left(t_{abs} - t_{ref}\right)\delta_{ij}. \tag{2.2.2}$$

Here a cubic element was considered whose temperature is raised from the reference temperature t_{ref} at which strains and thermal stresses are zero, to the absolute temperature value t_{abs}. The sides of the element are free from tractions, α is the coefficient of linear thermal expansion. The relation (2.2.2) represents a property of an isotropic body, in which a temperature change $t-t_{ref}$ results in no change of shear angles, the only result being a change of volume of the element. The elastic strain tensor is linearly proportional to the stress tensor σ_{ij} as

$$\varepsilon_{ij}^M = \frac{1}{2G}\left(\sigma_{ij} - \frac{\nu}{1+\nu}\sigma_{kk}\delta_{ij}\right), \tag{2.2.3}$$

where G is shear modulus, ν is the Poisson's ratio. Eq. (2.2.3) is known as the constitutive law of linear elasticity or Hooke's law. The constitutive equation of linear thermoelasticity is

$$\varepsilon_{ij} = \frac{1}{2G}\left(\sigma_{ij} - \frac{\nu}{1+\nu}\sigma_{kk}\delta_{ij}\right) + \alpha\left(t_{abs} - t_{ref}\right)\delta_{ij}, \tag{2.2.4}$$

for the stress tensor we get

$$\sigma_{ij} = 2G\left[\varepsilon_{ij} + \frac{\nu}{1-2\nu}\left(\varepsilon_{kk} - \frac{1+\nu}{\nu}\alpha\left(t_{abs} - t_{ref}\right)\right)\delta_{ij}\right]. \tag{2.2.5}$$

Let us consider an elastic body with body force **B**. The motion equation can be expressed as

$$\sigma_{ij,j} + B_i = \rho\ddot{u}_i\,, \tag{2.2.6}$$

where the mass density is denoted by ρ, $\ddot{u}_i$ is the acceleration vector. The equilibrium equations $(\ddot{u}_i = 0)$ for O*xyz* Cartesian coordinate system are

$$\begin{aligned}
&\frac{\partial\sigma_x}{\partial x} + \frac{\partial\tau_{xy}}{\partial y} + \frac{\partial\tau_{xz}}{\partial z} + B_x = 0,\\
&\frac{\partial\tau_{yx}}{\partial x} + \frac{\partial\sigma_y}{\partial y} + \frac{\partial\tau_{yz}}{\partial z} + B_y = 0,\\
&\frac{\partial\tau_{zx}}{\partial x} + \frac{\partial\tau_{zy}}{\partial y} + \frac{\partial\sigma_z}{\partial z} + B_z = 0.
\end{aligned} \tag{2.2.7}$$

In O*rφz* cylindrical and O*rφϑ* spherical coordinate systems the equilibrium equations can be written as

$$\begin{aligned}
&\frac{\partial\sigma_r}{\partial r} + \frac{1}{r}\frac{\partial\tau_{r\varphi}}{\partial\varphi} + \frac{\partial\tau_{rz}}{\partial z} + \frac{1}{r}\left(\sigma_r - \sigma_\varphi\right) + B_r = 0,\\
&\frac{\partial\tau_{\varphi r}}{\partial r} + \frac{1}{r}\frac{\partial\sigma_\varphi}{\partial\varphi} + \frac{\partial\tau_{\varphi z}}{\partial z} + \frac{2}{r}\tau_{r\varphi} + B_\varphi = 0,\\
&\frac{\partial\tau_{zr}}{\partial r} + \frac{1}{r}\frac{\partial\tau_{z\varphi}}{\partial\varphi} + \frac{\partial\sigma_z}{\partial z} + \frac{1}{r}\tau_{rz} + B_z = 0,
\end{aligned} \tag{2.2.8}$$

and

$$\begin{aligned}
&\frac{\partial\sigma_r}{\partial r} + \frac{1}{r}\frac{\partial\tau_{r\vartheta}}{\partial\vartheta} + \frac{1}{r\sin\vartheta}\frac{\partial\tau_{r\varphi}}{\partial\varphi} + \frac{1}{r}\left(2\sigma_r - \sigma_\vartheta - \sigma_\varphi + \tau_{r\vartheta}\cos\vartheta\right) + B_r = 0,\\
&\frac{\partial\tau_{\vartheta r}}{\partial r} + \frac{1}{r}\frac{\partial\sigma_\vartheta}{\partial\vartheta} + \frac{1}{r\sin\vartheta}\frac{\partial\tau_{\vartheta\varphi}}{\partial\varphi} + \frac{1}{r}\left[\left(\sigma_\vartheta - \sigma_\varphi\right)\cos\vartheta + 3\tau_{r\vartheta}\right] + B_\vartheta = 0,\\
&\frac{\partial\tau_{\varphi r}}{\partial r} + \frac{1}{r}\frac{\partial\tau_{\varphi\vartheta}}{\partial\vartheta} + \frac{1}{r\sin\vartheta}\frac{\partial\sigma_\varphi}{\partial\varphi} + \frac{1}{r}\left(2\tau_{\vartheta\varphi}\cos\vartheta + 3\tau_{r\varphi}\right) + B_\varphi = 0.
\end{aligned} \tag{2.2.9}$$

2.3. Complementary energy

The practical solution of many structural problems is often obtained by one of various energy methods. The complementary energy is valid for finite strain and material nonlinearity. For small-strain problems this method is very effective, however for finite strains where the stresses couple with the displacements the complementary energy methods are difficult to use [51], [52].

The strain energy per unit volume can be expressed as

$$U_0' = \frac{1}{2}\left(\varepsilon_x\sigma_x + \varepsilon_y\sigma_y + \varepsilon_z\sigma_z + \gamma_{xy}\tau_{xy} + \gamma_{yz}\tau_{yz} + \gamma_{xz}\tau_{xz}\right), \tag{2.3.1}$$

with Hooke's law we get

$$U_0' = \frac{1}{2E}\left(\sigma_x^2 + \sigma_y^2 + \sigma_z^2\right) + \frac{1}{2G}\left(\tau_{xy}^2 + \tau_{xz}^2 + \tau_{yz}^2\right) - \frac{\nu}{E}\left(\sigma_x\sigma_y + \sigma_z\sigma_y + \sigma_x\sigma_z\right). \tag{2.3.2}$$

The complementary energy per unit volume U_0 for thermoelastic problems can be expressed as

$$U_0 = U_0' + \alpha T\left(\sigma_x + \sigma_y + \sigma_z\right), \tag{2.3.3}$$

then the total complementary energy can be determined as

$$\tilde{\Pi}_c\left(\sigma_x, \sigma_y, \sigma_z, \tau_{xy}, \tau_{xz}, \tau_{zy}\right) = \int_V U_0 \mathrm{d}V\,. \tag{2.3.4}$$

From U_0 we get the stress and strain components as

$$\varepsilon_x = \frac{\partial U_0}{\partial \sigma_x}, \varepsilon_y = \frac{\partial U_0}{\partial \sigma_y}, \varepsilon_z = \frac{\partial U_0}{\partial \sigma_z}, \gamma_{xy} = \frac{\partial U_0}{\partial \tau_{xy}}, \gamma_{xz} = \frac{\partial U_0}{\partial \tau_{xz}}, \gamma_{yz} = \frac{\partial U_0}{\partial \tau_{yz}}. \tag{2.3.5}$$

According to Eq. (2.3.4) the complementary energy can be expressed as

$$\tilde{\Pi}_c = \int_V \left\{ \frac{1}{2E}\left[\sigma_x^2 + \sigma_y^2 + \sigma_z^2 - 2\nu\left(\sigma_x\sigma_y + \sigma_y\sigma_z + \sigma_z\sigma_x\right) + 2(1+\nu)(\tau_{xy}^2 + \tau_{yz}^2 + \tau_{zx}^2)\right] + \alpha T(\sigma_x + \sigma_y + \sigma_z)\right\} \mathrm{d}V\,, \tag{2.3.6}$$

assuming that there are no prescribed surface displacements or the prescribed surface displacements vanish. The theorem of minimum of complementary energy states that among all the sets of admissible stresses σ_x, σ_y, σ_z, τ_{xy}, τ_{xy}, τ_{xy} which satisfy all the equilibrium equations and the prescribed stress boundary conditions, the set of actual stress components makes the functional $\tilde{\Pi}_c\left(\sigma_x, \sigma_y, \sigma_z, \tau_{xy}, \tau_{xz}, \tau_{zy}\right)$ an absolute minimum [51], [52].

2.4. Functions of the material properties

Within the functionally graded material the volume fraction of the constituent materials gradually varies in the gradiation direction thus the effective properties of FGMs change along this direction. Since functionally graded structures are most commonly used in high temperature environment where significant changes in mechanical properties of the constituent materials are to be expected [53], [54], it is essential to take into consideration this temperature-dependency for accurate prediction of the mechanical response. Thus, the effective Young's modulus E_f, Poisson's ratio ν_f, coefficient of linear thermal expansion α_f and thermal conductivity λ_f are assumed to be temperature-dependent.

There are several method to calculate these effective properties, such as the Mori–Tanaka scheme [55] for regions of the graded microstructure which have a well-defined continuous matrix and a discontinuous particulate phase or the self-consistent method [53] which assumes that each reinforcement inclusion is embedded in a continuum material and does not distinguish between matrix and reinforcement phases.

In many cases the effective material parameters can be expressed as a nonlinear functions of the temperature field [53], [56]:

$$M(T) = P_0(P_{-1}T^{-1} + 1 + P_1T + P_2T^2 + P_3T^3). \tag{2.4.1}$$

In Eq. (2.4.1) $M(T)$ denotes the function of the considered effective material property (E, ν, α and λ), P_0, P_{-1}, P_1, P_2 and P_3 are material dependent coefficients of temperature T [K]. Using these results we can present functions for the temperature- and position-dependent functionally graded material properties of disks, spherical bodies and plates [53]:

$$\begin{gathered} M_f(r,T) = \left[M_1(T) - M_2(T)\right]\left[K\right]^m + M_2(T), \\ \text{where for example: } K^{Sphere}(r) = \frac{r-a}{b-a}, \text{ or } K^{Plate}(z) = \frac{2z-h}{2h}, \end{gathered} \tag{2.4.2}$$

furthermore, indices 1 and 2 denote the constituent materials, mostly metal and ceramic components, a and b denote the inner and outer radii of the spherical body, h is the thickness of the plate, z is the thickness coordinate and m is the volume fraction of the FGM. The effect of the power index m is shown in Fig. 2.2 in the case of two constituent materials.

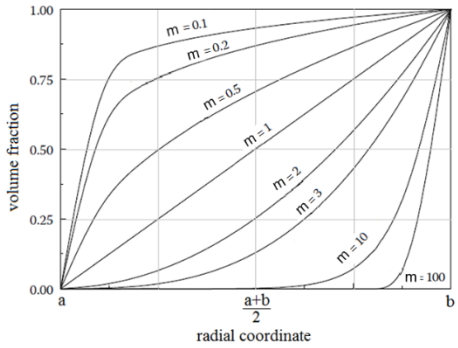

Figure 2.2. The effect of the power index m to the volume fraction.

2.5. Piezoelectric material behaviour

A piezoelectric material responds to an electric potential gradient by straining, while stress causes an electric potential gradient in the material. This means that the piezoelectric effect is the coupling of stress and electric field in these materials. Lets define an electric enthalpy function H as [57], [58]

$$H(\mathbf{E},\boldsymbol{\varepsilon}) = \frac{1}{2}C_{ijkl}\varepsilon_{ij}\varepsilon_{kl} - \frac{1}{2}\beta_{ij}E_iE_j - e_{ijk}\varepsilon_{ij}E_k, \tag{2.5.1}$$

where the relations of the strain tensor $\boldsymbol{\varepsilon}$ and the electric tensor $\mathbf{E}$ to the displacement field u and electric potential ϕ are

$$\varepsilon_{ij} = \frac{1}{2}\left(u_{i,j} + u_{j,i}\right), \quad E_i = -\phi_{,i}, \tag{2.5.2}$$

and the constitutive equations ,in the so-called e-form, can be derived from the electric enthalpy as

$$\sigma_{ij} = \frac{\partial H}{\partial \varepsilon_{ij}} = C_{ijkl}\varepsilon_{kl} - e_{kij}E_k,$$
$$D_i = \frac{\partial H}{\partial E_i} = e_{ijk}\varepsilon_{jk} + B_{ij}E_j. \qquad (2.5.3)$$

In these last terms the notation C_{ijkl} denotes the material stiffness measured by constant electric field, e_{ijk} are piezoelectric constants and $B_{ij} = \beta_{ij}^{-1}$ are the dielectric constants. Furthermore the coupled equations for a piezoelectric linear medium can be expressed in *g*-form as

$$\varepsilon_{ij} = S_{ijkl}\sigma_{kl} + g_{mij}D_m, \qquad (2.5.4)$$
$$E_i = -g_{ijk}\sigma_{jk} + \beta_{ij}D_j, \qquad (2.5.5)$$

where S_{ijkl} are the material compliances defined at zero electrical displacement and g_{ijk} are piezoelectric constants. It is useful to introduce the compressed notation [58] for these quantities. Due to the material symmetry, these equations take shorter forms.

3. Thermoelastic problems of layered composite and functionally graded spherical pressure vessels

In this chapter analytical solutions are presented for four cases of thermoelastic problems of spherical bodies. We consider one-dimensional thermoelastic problems of spherical bodies made from laminated composite and functionally graded materials which are subjected to axisymmetric thermal and mechanical loads on the inner and outer boundary surfaces. The hollow spherical body is subjected to unidirectional steady-state heat conduction with third- and first kind thermal and stress boundary conditions on the boundary surfaces. For multilayered spherical pressure vessels two analytical solutions are formulated. These methods can be used to determine the displacements and stress field of functionally graded spherical pressure vessels with arbitrary radial coordinate and temperature-dependent material properties. Further analytical solutions are derived for two cases of functionally graded materials. In the first case the material parameters are special functions of the radial coordinate -except the Poisson's ratio- and additionally the coefficient of linear thermal expansion is temperature-dependent. In the second case an analytical solution is derived via stress functions when the material properties are specific power-law functions of the radial coordinate. The analytical solutions presented in this chapter will be used to verify the accuracy of the developed numerical methods.

3.1. Multilayered spherical bodies

This section investigates a one-dimensional thermoelastic problem of a hollow layered spherical body. The geometry of the spherical body can be seen in Fig. 3.1, where the inner radius of the sphere is R_1, the outer radius is R_{n+1} and n is the number of layers. The layers of the spherical structural component are assumed to be perfectly bonded and made of homogeneous, isotropic materials, furthermore a spherical coordinate system O$r\varphi\vartheta$ is used.

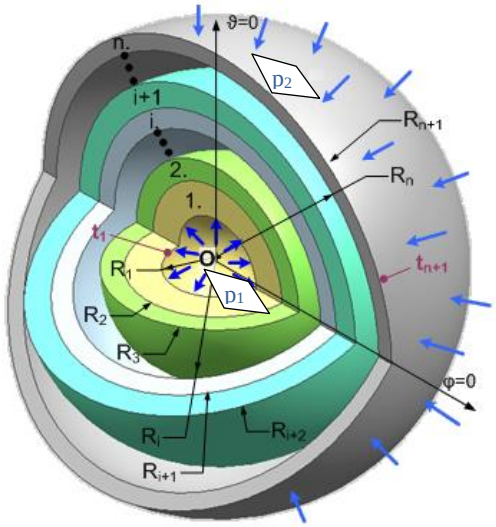

Figure 3.1. The three-dimensional sketch of the hollow layered sphere.

Thermal boundary conditions of first kind are prescribed on the inner and outer spherical surfaces. These temperature values are given, they are assumed to be constant, non-time-

dependent and denoted by t_1 and t_{n+1}. It follows that the temperature field is the function of the radial coordinate $T=T(r)$. The uniformly distributed mechanical loading exerted on the inner boundary surface is denoted by $p_1=-f_1$, as we can see in Fig. 3.2, while $-g_n=p_2$ is the pressure which acts on the outer curved boundary surface.

It is assumed that the radial stresses, the heatflow and the temperature are all continuous functions of the radial coordinate. Our aim is to determine the displacement field and normal stresses within the spherical component.

At first we deal with the determination of the temperature field $T=T(r)=t_{abs}(r)-t_{ref}$. Figure 3.2 shows the cross section and the loadings of the i-th layer.

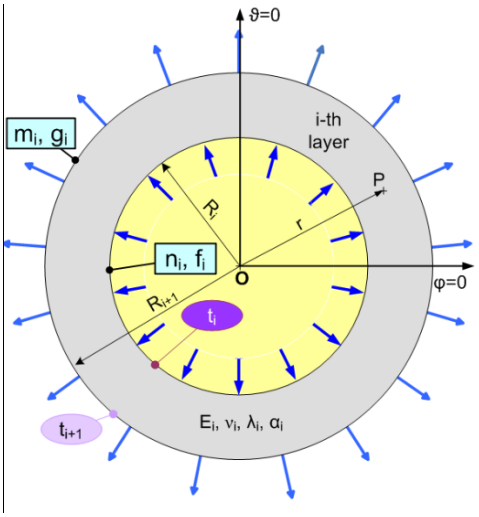

Figure 3.2. The cross section of the i-th layer of the sphere.

We assume that the temperature field is a continuous function of the radial coordinate thus we have from the equation of heat conduction [59, 60]

$$t_{i+1}=T_i(R_{i+1})=T_{i+1}(R_{i+1}),\quad T_i(r)=t_i-(t_{i+1}-t_i)(1-\frac{R_i}{r})\frac{R_{i+1}}{R_i-R_{i+1}},\ R_i\le r\le R_{i+1},\ i=1,2,...,n,\ (3.1.1)$$

where the temperature field of the i-th spherical layer is denoted by $T_i(r)$. We consider the case when the radial heatflow is constant, the temperatures of the inner and outer boundary surfaces are given:

$$q_i(r)=\lambda_i(t_{i+1}-t_i)\frac{R_iR_{i+1}}{R_{i+1}-R_i}\frac{1}{r^2},\quad i=1,...,n, \qquad (3.1.2)$$

$$q_i(R_{i+1})=q_{i+1}(R_{i+1}),\ i=1,...,n-1, \qquad (3.1.3)$$

where λ_i is the thermal conductivity. The surface temperature of the adjacent layers are equal therefore we get the following equations [59]:

$$\left(-\lambda_i\frac{R_iR_{i+1}}{R_{i+1}-R_i}\right)t_i+\left(\lambda_i\frac{R_iR_{i+1}}{R_{i+1}-R_i}+\lambda_{i+1}\frac{R_{i+1}R_{i+2}}{R_{i+2}-R_{i+1}}\right)t_{i+1}+\left(-\lambda_{i+1}\frac{R_{i+1}R_{i+2}}{R_{i+2}-R_{i+1}}\right)t_{i+2}=0. \quad (3.1.4)$$

From Eqs. (2.1.19) and (2.2.4) the radial and tangential normal strains ε_r, ε_φ and the stress-strain relations of a homogeneous sphere in one-dimensional problems can be presented as [52], [60]:

$$\varepsilon_r = \frac{\partial u}{\partial r}, \quad \varepsilon_\varphi = \varepsilon_\vartheta = \frac{u}{r}, \tag{3.1.5}$$

$$\sigma_r(r) = \frac{E}{(1+\nu)(1-2\nu)}\Big[(1-\nu)\varepsilon_r + 2\nu\varepsilon_\varphi - (1+\nu)\alpha T(r)\Big], \tag{3.1.6}$$

$$\sigma_\varphi(r) = \sigma_\vartheta(r) = \frac{E}{(1+\nu)(1-2\nu)}\Big[\nu\varepsilon_r + \varepsilon_\varphi - (1+\nu)\alpha T(r)\Big], \tag{3.1.7}$$

where $u=u(r)$ is the radial displacement field, ν is the Poisson's ratio, E is the Young modulus, α is the coefficient of linear thermal expansion, $\sigma_r(r)$ is the radial normal stress and $\sigma_\varphi(r)$ is the tangential normal stress of the spherical body. According to the Navier equation, let the displacement field for the i-th layer of the multilayered body be defined as

$$u_i(r) = C_i r + \frac{D_i}{r^2} + U_i(r), \tag{3.1.8}$$

where C_i and D_i are integration constants, $U_i(r)$ has the following form [52] ,[60]:

$$U_i(r) = \frac{1+\nu_i}{1-\nu_i}\alpha_i \frac{1}{r^2}\int_{R_i}^{r} T(\rho)\rho^2 \mathrm{d}\rho, \quad i = 1,...,n. \tag{3.1.9}$$

With the combination of Eqs. (3.1.5), (3.1.6), (3.1.8) and (3.1.9) the expression of the radial stress for the i-th layer can be calculated as

$$\sigma_{ri}(r) = C_i \frac{E_i}{1-2\nu} - D_i \frac{2E_i}{1+\nu_i}\frac{1}{r^3} + S_i(r), \tag{3.1.10}$$

$$S_i(r) = \frac{-2\alpha_i E_i}{1-\nu_i}\frac{1}{r^3}\int_{R_i}^{r} T(\rho)\rho^2 \mathrm{d}\rho, \; i = 1,...,n, \tag{3.1.11}$$

and the tangential normal stress is

$$\sigma_{\varphi i}(r) = C_i \frac{E_i}{1-2\nu_i} - D_i \frac{E_i}{1+\nu_i}\frac{1}{r^3} - \frac{E_i\alpha_i T(r)}{1-\nu_i} + \frac{E_i\alpha_i}{1-\nu_i}\frac{1}{r^3}\int_{R_i}^{r} T(\rho)\rho^2 \mathrm{d}\rho, i = 1,...,n. \tag{3.1.12}$$

The following values of the displacement field and radial stresses will be used for the equations of the i-th layer:

$$u_i(R_i) = n_i, \quad u_i(R_{i+1}) = m_i, \quad \sigma_{ri}(R_i) = f_i, \quad \sigma_{ri}(R_{i+1}) = g_i. \tag{3.1.13}$$

Using Eqs. (3.1.13), the unknown integration constants of Eqs. (3.1.8-3.1.12) can be calculated as

$$C_i = k_{1i}m_i + k_{2i}f_i - k_{1i}U_i(R_i) - k_{2i}S_i(R_i), \tag{3.1.14}$$

$$D_i = k_{3i}m_i - k_{4i}f_i - k_{3i}U_i(R_i) + k_{4i}S_i(R_i), \tag{3.1.15}$$

where

$$k_{1i} = \frac{2}{3R_i}\frac{1-2\nu_i}{1-\nu_i}, \; k_{2i} = \frac{(1-2\nu_i)(1+\nu_i)}{3E_i(1-\nu_i)}, \; k_{3i} = \frac{R_i^2}{3}\frac{1+\nu_i}{1-\nu_i}, \; k_{4i} = R_i^3 k_{2i}, \; i = 1,...,n. \tag{3.1.16}$$

From Eqs. (3.1.14-3.1.16) and (3.1.8-3.1.11) the expressions of the radial normal stress and radial displacement for the i-th layer can be obtained:

$$\sigma_{ri}(r) = K_{1i}(r)m_i + K_{2i}(r)\,f_i + K_{3i}(r)U_i(R_i) + K_{4i}(r)S_i(R_i) + S_i(r), \tag{3.1.17}$$

$$u_{ri}(r) = L_{1i}(r)m_i + L_{2i}(r)\,f_i + L_{3i}(r)U_i(R_i) + L_{4i}(r)S_i(R_i) + U_i(r), \tag{3.1.18}$$

where

$$\begin{aligned} K_{1i}(r) &= \frac{E_i}{1-2\nu_i}k_{1i} - \frac{1}{r^3}\frac{2E_i}{1+\nu_i}k_{3i},\ K_{2i}(r) = \frac{E_i}{1-2\nu_i}k_{2i} + \frac{1}{r^3}\frac{2E_i}{1+\nu_i}k_{4i}, \\ K_{3i}(r) &= -\frac{E_i}{1-2\nu_i}k_{1i} + \frac{1}{r^3}\frac{2E_i}{1+\nu_i}k_{3i},\ K_{4i}(r) = -\frac{E_i}{1-2\nu_i}k_{2i} - \frac{1}{r^3}\frac{2E_i}{1+\nu_i}k_{4i}, \end{aligned} \tag{3.1.19}$$

$$L_{1i}(r) = rk_{1i} + \frac{k_{3i}}{r^2}, L_{2i}(r) = rk_{2i} - \frac{k_{4i}}{r^2}, L_{3i}(r) = -rk_{1i} - \frac{k_{3i}}{r^2}, L_{4i}(r) = -rk_{2i} + \frac{k_{4i}}{r^2}. \tag{3.1.20}$$

For the *i*-th layer of the spherical body the following matrix equation can be derived:

$$\begin{aligned} \begin{bmatrix} f_i \\ g_i \end{bmatrix} &= \begin{bmatrix} -\dfrac{L_{1i}(R_{i+1})}{L_{2i}(R_{i+1})} & \dfrac{1}{L_{2i}(R_{i+1})} \\ K_{1i}(R_{i+1}) - K_{2i}(R_{i+1})\dfrac{L_{1i}(R_{i+1})}{L_{2i}(R_{i+1})} & \dfrac{K_{2i}(R_{i+1})}{L_{2i}(R_{i+1})} \end{bmatrix}\begin{bmatrix} m_i \\ n_i \end{bmatrix} + \begin{bmatrix} -\dfrac{1}{L_{2i}(R_{i+1})} & 0 \\ -\dfrac{K_{2i}(R_{i+1})}{L_{2i}(R_{i+1})} & 1 \end{bmatrix}\begin{bmatrix} U_i(R_{i+1}) \\ S_i(R_{i+1}) \end{bmatrix} \\ &+ \begin{bmatrix} -\dfrac{L_{3i}(R_{i+1})}{L_{2i}(R_{i+1})} & -\dfrac{L_{4i}(R_{i+1})}{L_{2i}(R_{i+1})} \\ K_{3i}(R_{i+1}) - K_{2i}(R_{i+1})\dfrac{L_{3i}(R_{i+1})}{L_{2i}(R_{i+1})} & K_{4i}(R_{i+1}) - K_{2i}(R_{i+1})\dfrac{L_{4i}(R_{i+1})}{L_{2i}(R_{i+1})} \end{bmatrix}\begin{bmatrix} U_i(R_i) \\ S_i(R_i) \end{bmatrix} \end{aligned} \tag{3.1.21}$$

$$\begin{bmatrix} f_i \\ g_i \end{bmatrix} = \begin{bmatrix} G_{11}^i & G_{12}^i \\ G_{21}^i & G_{22}^i \end{bmatrix}\begin{bmatrix} m_i \\ n_i \end{bmatrix} + \begin{bmatrix} h_1^i \\ h_2^i \end{bmatrix}. \tag{3.1.22}$$

By the whole multilayered spherical body the following notations and fitting conditions will be used for the discrete values:

$$u_i(R_{i+1}) = u_{i+1}(R_{i+1}) = u_{i+1},\ \ \sigma_{ri}(R_{i+1}) = \sigma_{ri+1}(R_{i+1}) \to g_i = f_{i+1},\ \ i = 1,...,n-1, \tag{3.1.23}$$

furthermore f_1 and g_n are given. For the whole geometry the next system of equations can be derived for the displacement values u_i as basic variables:

$$\begin{bmatrix} -p_1 \\ 0 \\ 0 \\ \vdots \\ -p_2 \end{bmatrix} = \begin{bmatrix} G_{11}^1 & G_{12}^1 & 0 & 0 & 0 & \cdots & 0 \\ G_{21}^1 & G_{22}^1 - G_{11}^2 & -G_{13}^2 & 0 & 0 & \cdots & 0 \\ 0 & G_{21}^2 & G_{22}^2 - G_{11}^3 & -G_{12}^3 & 0 & \cdots & 0 \\ \vdots & & & & \ddots & & \vdots \\ 0 & 0 & 0 & \cdots & 0 & G_{21}^n & G_{22}^n \end{bmatrix}\begin{bmatrix} u_1 \\ u_2 \\ u_3 \\ \vdots \\ u_{n+1} \end{bmatrix} + \begin{bmatrix} h_1^1 \\ h_2^1 - h_1^2 \\ h_2^2 - h_1^3 \\ \vdots \\ h_2^n \end{bmatrix}, \tag{3.1.24}$$

$$\mathbf{f} = \mathbf{G}\cdot\mathbf{u} + \mathbf{h}. \tag{3.1.25}$$

From Eqs. (3.1.24) and (3.1.25) the unknown displacement values u_i ($i=1,...,n+1$) can be calculated, and then, using Eq. (3.1.17-3.1.21) the radial normal stresses can be evaluated.

3.2. Multilayered model of spherical bodies with temperature-dependent material properties

This section presents an analytical solution for the axisymmetric thermoelastic problem of multilayered composite spherical bodies under combined mechanical and thermal loads -similarly to Section 3.1, furthermore this method can be used as a numerical method to approximate the thermoelastic problem of functionally graded spherical vessels with a thermomechanical problem of multilayered spherical bodies (Fig. 3.3) where the temperature dependency of the material parameters is taken into account.

The constant pressure is denoted by p_2 which acts on the outer curved boundary surface while the uniformly distributed mechanical loading exerted on the inner surface is denoted by p_1. The layers are perfectly bonded, which means that the radial stresses and displacement, the heatflow and the temperature are all continuous functions of the radial coordinate r, furthermore the material properties are position- and temperature-dependent.

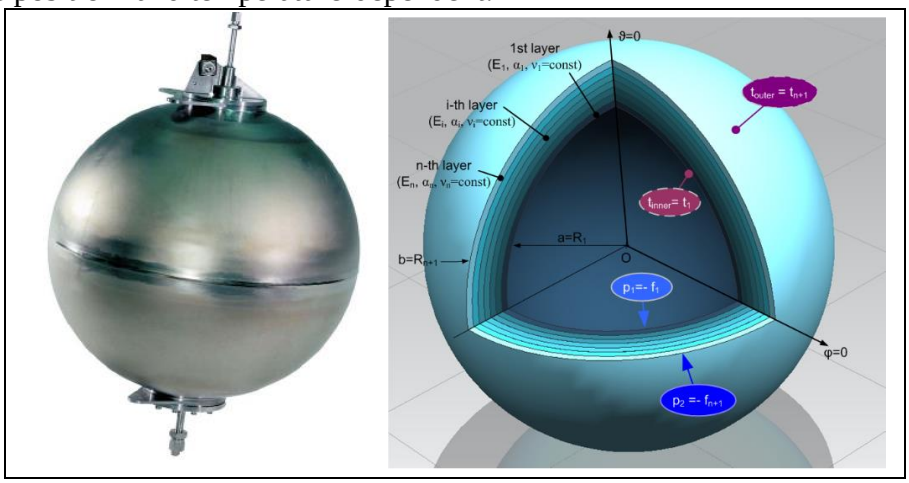

Figure 3.3. The multilayered model.

In this model the layers are made of isotropic homogeneous materials and are perfectly bonded, the material properties are constants within the layers but varying radially between them. The more layers are considered the more accurate the computations are, by FGMs $n\rightarrow\infty$.

Both the boundary conditions and the field equations [52], [60] are linear therefore the superposition principle can be used. This means that we can add the stresses and displacements caused by mechanical loads to the thermal stresses and displacements in order to solve this coupled problem. A spherical coordinate system $Or\varphi\vartheta$ is used for our models.

3.2.1. Approximation of the material properties

We need to approximate the material properties and compute their discrete values for the different homogeneous layers. When the material parameters are arbitrary functions of the radial coordinate, the material properties for the i-th layer are calculated in our current model as (Fig. 3.4)

$$R_{mi}=\frac{R_i+R_{i+1}}{2}, E_i=E(r=R_{mi}),\ \nu_i=\nu(r=R_{mi}), \alpha_i=\alpha(r=R_{mi}), \lambda_i=\lambda(r=R_{mi}), i=1,\ldots,n. \quad (3.2.1)$$

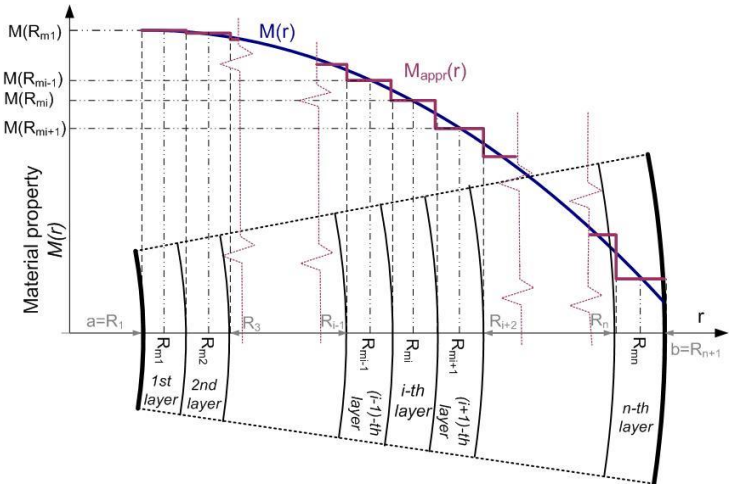

Figure 3.4. The approximation for the functions of the material properties.

In case of radial coordinate- and temperature-dependent material properties $E(r,T(r))$, $\alpha(r,T(r))$ and $\nu(r,T(r))$, the computation of their discrete values for the different quasi-homogeneous layers of the multilayered spherical model require another formulae. We can assign the following material property values for the spherical layers:

$$t_{mi} = T(r = R_{mi}), E_i = E(r = R_{mi}, T = t_{mi}),\ \nu_i = \nu(r = R_{mi}, T = t_{mi}), \alpha_i = \alpha(r = R_{mi}, T = t_{mi}). \qquad (3.2.2)$$

This means that we will approximate the arbitrary functions of the functionally graded material parameters with multi-stepped functions. To build the approximation function from the n step we can use for example the *Heaviside* function. Figure 3.5 indicates the sketch of the i-th layer of the multilayered spherical body. The constant mechanical loads exerted on the inner and outer surfaces of the i-th layer are denoted by f_i and f_{i+1}, respectively. The temperatures on the boundary surfaces are t_i and t_{i+1}.

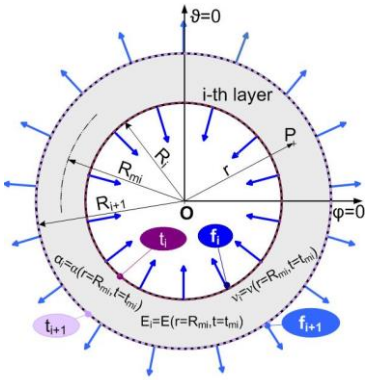

Figure 3.5. The sketch of the i-th layer with the mechanical and thermal loadings.

3.2.2. Determination of the temperature field

In this subsection two cases will be investigated. These models can be used to approximate the temperature field in a radially graded spherical body. At first, the thermal conductivity depends only on the radial coordinate and there are prescribed thermal boundary condition of the third kind at the inner and outer surfaces, in our second problem thermal boundary conditions of the first kind are considered but the material parameters depend on the temperature and radial coordinate.

An analytical solution for the temperature field can be derived when the distribution of the thermal conductivity has special form. An example can be found in [27, 28] for power-law function dependent thermal conductivity.

Case 1. When the thermal conductivity of the functionally graded sphere depends only on the radial coordinate, the temperature dependency is negligible, the differential equation for the temperature field and its solution have the following forms:

$$\frac{1}{r^2}\frac{\mathrm{d}}{\mathrm{d}r}\left[\lambda(r)\cdot r^2\frac{\mathrm{d}T(r)}{\mathrm{d}r}\right]=0,\ T(r)=A+B\int_a^r\frac{1}{\rho^2\lambda(\rho)}\mathrm{d}\rho. \tag{3.2.3}$$

Using the equations of the thermal boundary conditions of third kind on the inner and outer surfaces we get the unknown constants of Eq. (3.2.3):

$$B=\frac{\gamma_1\gamma_2(t_{e2}-t_{e1})}{\gamma_1\lambda(b)D_{I,b}+\gamma_1\gamma_2I_{ab}+\gamma_2\lambda(a)D_{I,a}},\ A=\frac{t_{e1}\gamma_1\lambda(b)D_{I,b}+t_{e1}\gamma_1\gamma_2I_{ab}+t_{e2}\gamma_2\lambda(a)D_{I,a}}{\gamma_1\lambda(b)D_{I,b}+\gamma_1\gamma_2I_{ab}+\gamma_2\lambda(a)D_{I,a}}, \tag{3.2.4}$$

where γ_1 and γ_2 are the heat transfer coefficients of the inner and outer curved boundary surfaces, t_{e1} and t_{e2} are the temperatures of the surrounding environment, furthermore

$$\begin{aligned}D_{I,b}&=\frac{\mathrm{d}}{\mathrm{d}r}\left[\int_a^r\left(\frac{1}{\rho^2\lambda(\rho)}\right)\mathrm{d}\rho\right]\mathrm{d}r\Big|_{r=b},\\ D_{I,a}&=\frac{\mathrm{d}}{\mathrm{d}r}\left[\int_a^r\left(\frac{1}{\rho^2\lambda(\rho)}\right)\mathrm{d}\rho\right]\mathrm{d}r\Big|_{r=a},\ I_{ab}=\int_a^b\left(\frac{1}{\rho^2\lambda(\rho)}\right)\mathrm{d}\rho.\end{aligned} \tag{3.2.5}$$

We will approximate the temperature field of the FGM sphere using the multilayered method in order to avoid the integration in Eqs. (3.2.5). We will consider a layered spherical body with n layer and each of them has its own temperature field $T_i(r)$. The first and the n-th layer have mixed thermal boundary conditions (of first kind and third kind) on the inner and outer surfaces.

$$T_1(R_2)=t_2,\ \lambda(R_1)\frac{\mathrm{d}T_1(r)}{\mathrm{d}r}\Big|_{r=R_1}=-\gamma_1(t_{e1}-t_1), \tag{3.2.6}$$

$$T_n(R_n)=t_n,\ \lambda(R_{n+1})\frac{\mathrm{d}T_n(r)}{\mathrm{d}r}\Big|_{r=R_{n+1}}=\gamma_2(t_{e2}-t_{n+1}). \tag{3.2.7}$$

The other layers have thermal boundary conditions of the first kind on both spherical surfaces. Using the previously presented boundary conditions we get the temperature fields for the different layers as

$$T_1(r)=\frac{-\lambda_1t_2R_2+t_{e1}R_1^2\gamma_1-\gamma_1t_2R_1R_2}{-\lambda_1R_2+\gamma_1R_1^2-\gamma_1R_1R_2}+\frac{\gamma_1R_2R_1^2(t_2-t_{e1})}{-\lambda_1R_2+\gamma_1R_1^2-\gamma_1R_1R_2}\frac{1}{r}, \tag{3.2.8}$$

$$T_n(r)=\frac{-\lambda_nt_nR_n-t_{e2}R_{n+1}^2\gamma_2+\gamma_2t_nR_{n+1}R_n}{-\lambda_nR_n-\gamma_2R_{n+1}^2+\gamma_2R_{n+1}R_n}+\frac{\gamma_2R_nR_{n+1}^2(t_{e2}-t_n)}{-\lambda_nR_n-\gamma_2R_{n+1}^2+\gamma_2R_{n+1}R_n}\frac{1}{r}, \tag{3.2.9}$$

$$T_i(r)=t_i-(t_{i+1}-t_i)(1-\frac{R_i}{r})\frac{R_{i+1}}{R_i-R_{i+1}},\quad i=2,...,n. \tag{3.2.10}$$

We assume that the radial heatflow is constant and the surface temperatures of the osculant layers are equal.

$$t_{i+1}=T_i(R_{i+1})=T_{i+1}(R_{i+1}),\ i=1,...,n,\ q_i(R_{i+1})=q_{i+1}(R_{i+1}),\ i=1,...,n-1, \tag{3.2.11}$$

$$q_1(r)=\frac{\lambda_1 R_2\gamma_1 R_1^2(t_{e1}-t_2)}{-\lambda_1 R_2+\gamma_1 R_1^2-\gamma_1 R_1 R_2}\frac{1}{r^2}=q_{n-1}(r)=\frac{\lambda_n R_n\gamma_2 R_{n+1}^2(t_n-t_{e2})}{-\lambda_n R_n-\gamma_2 R_{n+1}^2+\gamma_2 R_{n+1}R_n}\frac{1}{r^2}, \quad (3.2.12)$$

$$q_1(r)=q_{n-1}(r)=q_i(r)=\lambda_i(t_{i+1}-t_i)\frac{R_i R_{i+1}}{R_{i+1}-R_i}\frac{1}{r^2}, \ \ i=2,...,n-2. \quad (3.2.13)$$

The unknown boundary temperatures of the spherical layers can be calculated from Eqs. (3.2.12) and (3.2.13). Substituting these values into Eqs. (3.2.8-3.2.10) then summarizing the results we get the temperature field of multilayered vessel.

Case 2. Then that case will be investigated when the thermal conductivity $\lambda(T,r)$ is temperature- and radial coordinate-dependent. We will approximate the temperature field of the functionally graded sphere for a temperature field of a multilayered spherical body with *n* quasi-homogeneous layers whose thermal conductivities depend only on temperature.

$$\lambda_i(T)=\lambda(r=R_{mi},T), \qquad i=1,...,n. \quad (3.2.14)$$

For this case the nonlinear differential equation for the temperature field of the *i*-th layer $T_i(r)$ has the following form:

$$\frac{1}{r^2}\frac{\mathrm{d}}{\mathrm{d}r}\left[\lambda_i(T(r))\cdot r^2\frac{\mathrm{d}T_i(r)}{\mathrm{d}r}\right]=0, \quad R_i\le r\le R_{i+1}, \ i=1,...,n. \quad (3.2.15)$$

Using the Kirchoff integral transformation, this problem becomes linear

$$\theta_i=\int_0^{T_i}\lambda_i(\vartheta)\mathrm{d}\vartheta, \quad \frac{1}{r^2}\frac{\mathrm{d}}{\mathrm{d}r}\left[r^2\frac{\mathrm{d}\theta_i}{\mathrm{d}r}\right]=0. \quad (3.2.16)$$

From the thermal boundary conditions of first kind, the solution for the temperature field within the *i*-th layer can be derived in the following implicit form:

$$\int_{t_i}^{T_i}\lambda_i(\vartheta)\mathrm{d}\vartheta=\int_{t_i}^{t_{i+1}}\lambda_i(\vartheta)\mathrm{d}\vartheta\frac{R_{i+1}}{R_i-R_{i-1}}\left(\frac{R_i}{r}-1\right), \ i=1,...,n. \quad (3.2.17)$$

We assume that the surface temperatures t_i of the osculant layers are equal and the radial heatflow *q* is constant

$$\left[\lambda_i(T_i(r))\frac{\mathrm{d}T_i(r)}{\mathrm{d}r}\right]_{r=R_{i+1}}=q_i(R_{i+1})=q_{i+1}(R_{i+1})=\left[\lambda_{i+1}(T_{i+1}(r))\frac{\mathrm{d}T_{i+1}(r)}{\mathrm{d}r}\right]_{r=R_{i+1}}, i=1,...,n-1. \quad (3.2.18)$$

After some manipulations of Eqs (3.2.16-3.2.18) the unknown t_i (i=2, ...,n) boundary temperatures of the layers can be calculated from the following system of equations

$$const=\int_{t_i}^{t_{i+1}}\lambda_i(\vartheta)\mathrm{d}\vartheta\frac{R_{i+1}R_i}{R_i-R_{i-1}}\to t_i, \ \ i=2,...,n, \quad (3.2.19)$$

moreover temperatures t_1 and t_{n+1} are given. In the next step instead of using Eq (3.2.17) to compute the function of the temperature we will fit a curve or curves -for example with the least squares method- to the temperature values t_i in order to make the further calculations (especially the integrations) easier and faster. The recommended approximation function is

$$T_{appr}(r) = \theta_{-2} r^{-2} + \theta_{-1} r^{-1} + \theta_0 + \theta_1 r + \theta_2 r^2 . \qquad (3.2.20)$$

In order to make the approximation more accurate more polynomial curves can be used to build the approximated temperature function. After the determination of the temperature field, the temperatures in the middle of the different layers are calculated for the approximation function of the material parameters according to Eq. (3.2.2).

3.2.3. Thermal part of the problem

In the next steps the calculations will be split into two parts, then the superposition principle will be used to solve the problem. In the first case the *i*-th layer is under thermal loading (t_i, t_{i+1}) and has the previously calculated steady-state temperature field, the stresses on the boundary surfaces ($f_i = f_{i+1}=0$) of the layers have zero value. The $u_i^T(r)$ thermal radial displacement and the $\sigma_{ir}^T(r)$, $\sigma_{i\varphi}^T(r)$, $\sigma_{i\vartheta}^T(r)$ thermal stresses have the following forms [52]:

$$u_i^T(r) = \frac{1+\nu_i}{1-\nu_i}\alpha_i \left[\frac{1}{r^2}\int_{R_1}^{r} r^2 T_i(r)\mathrm{d}r + \frac{2(1-2\nu_i)}{1+\nu_i}\frac{r}{R_{i+1}^3 - R_i^3}\int_{R_1}^{R_2} r^2 T_i(r)\mathrm{d}r + \frac{R_i^3}{R_{i+1}^3 - R_i^3}\frac{1}{r^2}\int_{R_1}^{R_2} r^2 T_i(r)\mathrm{d}r \right], \qquad (3.2.21)$$

$$\sigma_{ir}^T(r) = \frac{\alpha_i E_i}{1-\nu_i}\left[\frac{2}{r^3}\frac{r^3 - R_i^3}{R_{i+1}^3 - R_i^3}\int_{R_1}^{R_2} r^2 T_i(r)\mathrm{d}r - \frac{2}{r^3}\int_{R_1}^{r} r^2 T_i(r)\mathrm{d}r \right], \qquad (3.2.22)$$

$$\sigma_{i\varphi}^T(r) = \sigma_{i\vartheta}^T(r) = \frac{\alpha_i E_i}{1-\nu_i}\left[\frac{1}{r^3}\frac{2r^3 + R_i^3}{R_{i+1}^3 - R_i^3}\int_{R_1}^{R_2} r^2 T_i(r)\mathrm{d}r + \frac{1}{r^3}\int_{R_1}^{r} r^2 T_i(r)\mathrm{d}r - T_i(r) \right], i = 1,\ldots,n . \qquad (3.2.23)$$

where $T_i(r)$ is the function of temperature difference (compared to a t_{ref} reference temperature) of the *i*-th layer. Because of the approximation of the temperature field Eq. (3.2.20), the integrals of Eqs. (3.2.21-3.2.23) contain fourth degree polinomials which can be easly calculated.

3.2.4. Mechanical part of the problem

In the second case it is assumed that the inner and outer boundary surfaces of the *i*-th spherical layer are under constant mechanical loading (f_i and f_{i+1}) without the thermal loads. The differential equation for the radial displacement field $u_i^M(r)$ can be derived from the equilibrium equations. The solution of this equation and the normal stresses –according to -Eqs. (2.2.3-2.2.5)- have the following forms [52], [60]:

$$u_i^M(r) = A_i r + \frac{B_i}{r^2}, \qquad (3.2.24)$$

$$\sigma_{ir}^M(r) = 2G_i\left(\frac{1+\nu_i}{1-2\nu_i}A_i - \frac{2}{r^3}B_i \right), \sigma_{i\vartheta}^M(r) = \sigma_{i\varphi}^M(r) = 2G_i\left(\frac{1+\nu_i}{1-2\nu_i}A_i + \frac{1}{r^3}B_i \right), i = 1,\ldots,n . \qquad (3.2.25)$$

The unknown parameters A_i and B_i (i=1,...,n) can be determined from the equations of the boundary conditions ($\sigma_{ir}^M(R_i)=f_i$, $\sigma_{ir}^M(R_{i+1})=f_{i+1}$) and they can be used to derive the expressions of the normal stresses.

$$A_i = \frac{(1-2\nu_i)(R_{i+1}^3 f_{i+1} - R_i^3 f_i)}{2G_i(1+\nu_i)(R_{i+1}^3 - R_i^3)},\ B_i = \frac{R_{i+1}^3 R_i^3 (f_{i+1} - f_i)}{4G_i(R_{i+1}^3 - R_i^3)}, \tag{3.2.26}$$

$$\sigma_{ir}^M(r) = \frac{R_{i+1}^3 f_{i+1} - R_i^3 f_i}{R_{i+1}^3 - R_i^3} - \frac{R_{i+1}^3 R_i^3 (f_{i+1} - f_i)}{R_{i+1}^3 - R_i^3}\frac{1}{r^3}, \tag{3.2.27}$$

$$\sigma_{i\varphi}^M(r) = \frac{R_{i+1}^3 f_{i+1} - R_i^3 f_i}{R_{i+1}^3 - R_i^3} - \frac{R_{i+1}^3 R_i^3 (f_i - f_{i+1})}{2(R_{i+1}^3 - R_i^3)}\frac{1}{r^3},\ i = 1,\ldots,n. \tag{3.2.28}$$

3.2.5. Application of the superposition principle

The superposition principle can be utilized for this problem, because both the previously used field equations and boundary conditions are linear. This means that we can add the stresses and displacements caused by mechanical loads -Eqs. (3.2.24-3.2.28)- to the thermal stresses and displacements -Eqs.(3.2.21-3.2.23)- in order to solve this problem. For the computation of the radial displacement, radial and tangential stresses the following equations are used:

$$u_i(r) = u_i^T(r) + u_i^M(r),\ \sigma_{ir}(r) = \sigma_{ir}^T(r) + \sigma_{ir}^M(r),\ \sigma_{i\varphi}(r) = \sigma_{i\varphi}^T(r) + \sigma_{i\varphi}^M(r),\quad i = 1,\ldots,n. \tag{3.2.29}$$

The unknown parameters f_i (i=2,...,n) in the equations of $u_i^M(r)$, $\sigma_{ir}^M(r)$, $\sigma_{i\varphi}^M(r)$ can be calculated from the following equations

$$u_i(R_{i+1}) = u_{i+1}(R_{i+1}),\ i = 1,\ldots,n-1, \tag{3.2.30}$$

which ensure the continuity of the radial displacement field furthermore f_1 and f_{n+1} are given.

$$\sigma_{1r}(R_1) = f_1 = -p_1,\ \sigma_{nr}(R_{n+1}) = f_{n+1} = -p_2. \tag{3.2.31}$$

The system of equations (3.2.30) has the following form:

$$a_i f_i + b_i f_{i+1} + c_i f_{i+2} = u_{i+1}^T(R_{i+1}) - u_i^T(R_{i+1}),\ i = 2,\ldots,n-1, \tag{3.2.32}$$

where the constants a_i, b_i and c_i are

$$a_i = \frac{3R_i^3 R_{i+1}}{4G_i(R_{i+1}^3 - R_i^3)}\frac{(1-\nu_i)}{(1+\nu_i)}, \tag{3.2.33}$$

$$b_i = -\frac{R_{i+1}}{2G_{i+1}\left(R_{i+2}^3 - R_{i+2}^3\right)}\left[\frac{(1-2\nu_{i+1})}{(1+\nu_{i+1})}R_{i+1}^3 + \frac{R_{i+3}^3}{2}\right] - \frac{R_{i+1}}{2G_i\left(R_{i+1}^3 - R_i^3\right)}\left[\frac{(1-2\nu_i)}{(1+\nu_i)}R_{i+1}^3 + \frac{R_i^3}{2}\right], \tag{3.2.34}$$

$$c_i = \frac{3R_{i+2}^3 R_{i+1}}{4G_{i+1}(R_{i+2}^3 - R_{i+1}^3)}\frac{(1-\nu_{i+1})}{(1+\nu_{i+1})},\quad i = 2,\ldots,n-1. \tag{3.2.35}$$

Using the previously determined f_i parameters and Eqs. (3.2.29) the radial displacement and the normal stresses of the multilayered spherical body can be evaluated.

3.2.6. Improvements in the accuracy of the multilayered approach

(*a*) By our multilayered model, the curve of the tangential normal stress may contain significant steps, but the stress values in the middle of each layer have good accuracy as we will see in Example 4. The radial quantities are accurate at the boundary of the layers. Thus an approximate curve can be fitted to these points to increase the accuracy and the convergence of the method, for this we can use the previously mentioned least squares method. For example the recommended form of the approximation for materials presented in Section 2.4 is

$$\sigma_{\varphi-appr}(r) = F_{-m}r^{-m} + F_{-3m/4}r^{-3m/4} + F_{-m/2}r^{-m/2} + F_{-m/4}r^{-m/4} + F_0 + F_{m/4}r^{m/4} + \\ + F_{m/2}r^{m/2} + F_{3m/4}r^{3m/4} + F_m r^m + F_{m+1}r^{m+1}, \quad (3.2.36)$$

which form can be useful for power indices about $0.5<m<150$. For smaller values of m we can compute the floor functions of the exponents in Eq. (3.2.36).

(*b*) Alternatively we can use the following expressions for the calculation of the discretized material property values:

$$t_{mi} = \frac{\int_{R_i}^{R_{i+1}} T(\rho)d\rho}{R_{i+1}-R_i}, E_i = \frac{\int_{R_i}^{R_{i+1}} E(\rho,T=t_{mi})d\rho}{R_{i+1}-R_i}, \alpha_i = \frac{\int_{R_i}^{R_{i+1}} \alpha(\rho,T=t_{mi})d\rho}{R_{i+1}-R_i}, \nu_i = \frac{\int_{R_i}^{R_{i+1}} \nu_i(\rho,T=t_{mi})d\rho}{R_{i+1}-R_i}. \quad (3.2.37)$$

(*c*) It is recommended to use partitions according to the value of the power index m by choosing the radii R_i (i=1,…,n+1) properly. It is essential by large or small values of m, when the effective material parameters change drastically in a small section of the body as we can see in Section 2.4. For example the following simple method can be utilized to determine the boundary of the layers when the distribution of the different material properties M, which denotes the quantities E, α, ν, λ, etc., is described by similar functions

$$M_{iv} = \frac{M(R_{n+1})-M(R_1)}{n}, \quad M(R_1)+(i-1)M_{iv} = M(R_i) \quad \rightarrow \quad R_i, \quad (i=1,...,n+1), \quad (3.2.38)$$

although it is recommended to further partition the thickest layer, for example when the relation between the radii of the first and second thickest layers is R_{i+1}-R_i>10(R_{j+1}-R_j).

(*d*) When the thermal loading is dominant, the accuracy of the calculations can be improved by using power-law material functions for the different layers instead of the initial constant values. The form of the approximate power function is

$$M_i(r,T=t_{mi}) = M_{0i}\left(\frac{r}{R_i}\right)^{m_{Mi}}, \; M_{0i} = M(R_i), \; m_{Mi} = \log_{\frac{R_{i+1}}{R_i}}\left(\frac{M(R_{i+1},T=t_{mi})}{M_{0i}}\right), \quad (3.2.39)$$

and the equations are

$$u_i^T(r) = \frac{1+\nu_i}{1-\nu_i}\alpha_{0i}\frac{1}{R_i^{m_{\alpha_i}}}\left\{\frac{1}{r^2}\int_{R_1}^{r} r^2T_i(r)\mathrm{d}r + \left[\frac{2(1-2\nu_i)}{1+\nu_i}\frac{r}{R_{i+1}^3-R_i^3} + \frac{R_i^3}{R_{i+1}^3-R_i^3}\frac{1}{r^2}\right]\int_{R_1}^{R_2} r^2T_i(r)\mathrm{d}r\right\}, \quad (3.2.40)$$

$$\sigma_{ir}^T(r) = \frac{\alpha_i E_i a^{-m}}{1-\nu_i}\left[\frac{2}{r^3}\frac{r^3-R_i^3}{R_{i+1}^3-R_i^3}\int_{R_1}^{R_2} r^{m+2}T_i(r)\mathrm{d}r - \frac{2}{r^3}\int_{R_1}^{r} r^{m+2}T_i(r)\mathrm{d}r\right], \; i=1,...,n, \quad (3.2.41)$$

$$\sigma_{i\varphi}^{T}(r)=\sigma_{i\vartheta}^{T}(r)=\frac{\alpha_i E_i}{1-\nu_i}\left[\frac{a^{-m}}{r^3}\frac{2r^3+R_i^3}{R_{i+1}^3-R_i^3}\int_{R_1}^{R_2} r^{m+2}T_i(r)\mathrm{d}r+\frac{a^{-m}}{r^3}\int_{R_1}^{r} r^{m+2}T_i(r)\mathrm{d}r-\frac{r^m}{a^m}T_i(r)\right]. \quad (3.2.42)$$

(e) We can go further and approximate the problem of radially graded spheres with a layered spherical body in which the material properties of the different layers are certain power-law functions of the radial coordinate. The approximation of the material properties is presented in Eq. (3.2.39), the steps of the model are presented in Section 3.1.

3.3. Analytical solution for a temperature-dependent functionally graded material

An analytical solution is developed for the case when the Poisson's ratio is constant, the distribution of the Young modulus is assumed to be described with a power-law along the radial coordinate [52], [28], the coefficient of linear thermal expansion specifically depends on the temperature and radial coordinate and the temperature field has the following form:

$$E(r)=P_1\left(\frac{r}{a}\right)^{m_E},\ \alpha(r,T(r))=(P_2+P_3T(r))\left(\frac{r}{a}\right)^{m_\alpha},\ a\le r\le b, \quad (3.3.1)$$

$$T(r)=H_1-\frac{H_2}{r},\ \text{if}\ \lambda=\text{const.}:\ H_1=t_{inner}-(t_{outer}-t_{inner})\frac{b}{a-b},\ H_2=(t_{outer}-t_{inner})\frac{ab}{a-b}, \quad (3.3.2)$$

where P_1, P_2, P_3, m_E and m_α are material parameters. The mechanical loads are constant pressures p_1 and p_2 which act on the boundary surfaces ($r= a$ and $r= b$).

3.3.1 Formulation of the analytical solution

Based on the investigated temperature field, the strain-displacement and the stress-strain relations for spherical bodies –from Eq. (2.2.5)- can be expressed as

$$\sigma_r(r)=\frac{E(r)}{(1-2\nu)(1+\nu)}\left[(1-\nu)\varepsilon_r+2\nu\varepsilon_\varphi-(1+\nu)\overline{\alpha}(r,T(r))\right],\ \overline{\alpha}(r,T)=\frac{1}{T}\int_0^T\alpha(r,\rho)\mathrm{d}\rho, \quad (3.3.3)$$

$$\sigma_\vartheta(r)=\sigma_\varphi(r)=\frac{E(r)}{(1-2\nu)(1+\nu)}\left[\nu\varepsilon_r+\varepsilon_\varphi-(1+\nu)\overline{\alpha}(r,T(r))\right]. \quad (3.3.4)$$

The time-independence of the functions involved separates the analysis of the temperature field from that of the elastic field, therefore the problem becomes uncoupled, which means that $\alpha(r,T)\rightarrow\alpha(r)$ and Eqs. (3.1.6-3.1.7) are valid. From the equilibrium equation, the following differential equation can be derived for the radial displacement u:

$$(1-\nu)\frac{\mathrm{d}^2u}{\mathrm{d}r^2}+(m_E+2)\frac{(1-\nu)}{r}\frac{\mathrm{d}u}{\mathrm{d}r}+2\left[\nu(m_E+1)-1\right]\frac{u}{r^2}=A_1r^{m_\alpha-1}+A_2r^{m_\alpha-2}+A_1r^{m_\alpha-3}, \quad (3.3.5)$$

where the constants A_1, A_2 and A_3 are

$$A_1 = \frac{1+\nu}{a^{m_\alpha}}(-m_E - m_\alpha)H_1(P_2 + P_3H_1), \tag{3.3.6}$$

$$A_2 = \frac{1+\nu}{a^{m_\alpha}}(m_E + m_\alpha - 1)H_2(P_2 + 2P_3H_1), \tag{3.3.7}$$

$$A_3 = \frac{1+\nu}{a^{m_\alpha}}(-m_E - m_\alpha + 2)P_3H_2^2. \tag{3.3.8}$$

The solution of differential equation (3.3.5) is

$$u(r) = C_1 r^{\lambda_1} + C_2 r^{\lambda_2} + \frac{G_1 r^{m_\alpha+1} + G_2 r^{m_\alpha} + G_3 r^{m_\alpha-1}}{G_4}, \tag{3.3.9}$$

where C_1 and C_2 are unknown constants of integration and the following notations are introduced:

$$\lambda_1 = \frac{1}{2}\left(-(m_E+1) + \sqrt{m_E^2 + 9 + 2m_E\frac{1-6\nu+5\nu^2}{(\nu-1)^2}}\right), \tag{3.3.10}$$

$$\lambda_2 = \frac{1}{2}\left(-(m_E+1) - \sqrt{m_E^2 + 9 + 2m_E\frac{1-6\nu+5\nu^2}{(\nu-1)^2}}\right), \tag{3.3.11}$$

$$G_1 = A_1\begin{Bmatrix} 2\nu\left[\nu(m_E(3m_E+5)+2) - m_E(m_E+6) - 4\right] + m_\alpha^3(\nu-1)^2(2m_E+m_\alpha) + 2(m_E+2) + \\ +m_\alpha(\nu-1)\left[m_\alpha(m_E(1-m_E)+5+\nu(m_E(m_E-5)-5) - m_E(5\nu(m_E+1)-5-m_E)\right] \end{Bmatrix}, \tag{3.3.12}$$

$$G_2 = A_2\begin{Bmatrix} m_\alpha^3(\nu-1)^2(m_\alpha+2m_E+2) + m_E\left[m_E(2\nu-1)-2\right] + m_E\nu^2(3m_E+2) + \\ +m_\alpha(\nu-1)\left[-4m_E(m_E+1) + m_\alpha(\nu(m_E(m_E-2)-5) - m_E(m_E+2)+5)\right] \end{Bmatrix}, \tag{3.3.13}$$

$$G_3 = A_3\begin{Bmatrix} m_\alpha^3(\nu-1)^2(m_\alpha+2m_E+4) + 2m_E\left[\nu^2(m_E+1) + m_E\nu - 1\right] + m_\alpha(\nu-1)\cdot \\ \cdot\left[m_\alpha(\nu(m_E+m_E^2+1) - m_E^2 - 5m_E - 1) - (\nu(m_E+1)(3m_E+6) - m_E + m_E^2 - 6)\right] \end{Bmatrix}, \tag{3.3.14}$$

$$G_4 = \left[m_\alpha(\nu-1)(m_\alpha+m_E+3) - m_E(\nu+1)\right]\left[(\nu-1)(m_\alpha(m_\alpha+m_E-1)-2) + m_E(1-3\nu)\right]\cdot \\ \cdot\left[(\nu-1)(m_\alpha(m_\alpha+m_E+1)-2) - 2m_E\nu\right]. \tag{3.3.15}$$

The radial stress takes the form

$$\sigma_r(r) = C_1S_1r^{\lambda_1+m_E-1} + C_2S_2r^{\lambda_2+m_E-1} + S_0r^{m_\alpha+m_E} + S_{-1}r^{m_\alpha+m_E-1} + S_{-2}r^{m_\alpha+m_E-2}, \tag{3.3.16}$$

in the last term we used the following simplifications

$$S_1 = Z\left[(1-\nu)\lambda_1 + 2\nu\right],\ \ S_2 = Z\left[(1-\nu)\lambda_2 + 2\nu\right],\ Z = \frac{P_1}{a^{m_E}(1-2\nu)(1+\nu)}, \tag{3.3.17}$$

$$S_0 = Z\left\{\frac{G_1}{G_4}\left[(1-\nu)(m_\alpha+1)+2\nu\right] - \frac{H_1(1+\nu)(P_2+P_3H_1)}{a^{m_\alpha}}\right\}, \tag{3.3.18}$$

$$S_{-1} = Z\left\{\frac{G_2}{G_4}\left[(1-\nu)m_\alpha+2\nu\right] + \frac{H_2(1+\nu)(P_2+2P_3H_1)}{a^{m_\alpha}}\right\}, \tag{3.3.19}$$

$$S_{-2} = Z\left\{\frac{G_3}{G_4}\left[(1-\nu)(m_\alpha-1)+2\nu\right] - \frac{H_2^2(1+\nu)P_3}{a^{m_\alpha}}\right\}. \tag{3.3.20}$$

The unknown constants C_1, C_2 can be obtained from the stress boundary conditions:

$$\sigma_r(a) = -p_1, \quad \sigma_r(b) = -p_2, \tag{3.3.21}$$

$$C_1 = \frac{b^{\lambda_2+m_E-1}c_a - a^{\lambda_2+m_E-1}c_b}{S_1\left(a^{\lambda_2+m_E-1}b^{\lambda_1+m_E-1} - a^{\lambda_1+m_E-1}b^{\lambda_2+m_E-1}\right)}, C_2 = \frac{a^{\lambda_1+m_E-1}c_b - b^{\lambda_1+m_E-1}c_a}{S_2\left(a^{\lambda_2+m_E-1}b^{\lambda_1+m_E-1} - a^{\lambda_1+m_E-1}b^{\lambda_2+m_E-1}\right)}, \tag{3.3.22}$$

$$c_a = a^{m_\alpha+m_E}\left(S_0 + S_{-1}a^{-1} + S_{-2}a^{-2}\right) + p_1, \quad c_b = b^{m_\alpha+m_E}\left(S_0 + S_{-1}b^{-1} + S_{-2}b^{-2}\right) + p_2. \tag{3.3.23}$$

3.3.2. Analytical solution for the temperature field

An analytical solution is derived to check the accuracy of the developed method for the temperature field in Section 3.2. The thermal conductivity is temperature- and coordinate-dependent and can be expressed as

$$\lambda(r,T(r)) = P_1 e^{P_2 T(r)}\left(\frac{r}{a}\right)^{m_\lambda}, \ a \le r \le b, \tag{3.3.24}$$

where P_1, P_2 and m_λ are material constants. After solving Eq. (3.2.15) the temperature field can be calculated and its constants can be evaluated from the thermal boundary conditions of the first kind:

$$T(r) = \frac{1}{P_2}\ln\left(\frac{P_2 C_1}{(m_\lambda+1)}\frac{r^{-m_\lambda-1}}{a^{-m_\lambda}} - P_2 C_1 C_2\right), \tag{3.3.25}$$

$$C_1 = \frac{ab(m+1)\left(e^{t_{outer}P_2} - e^{t_{inner}P_2}\right)}{P_2\left(a\left(\frac{b}{a}\right)^{-m_\lambda} - b\right)}, \ C_2 = \frac{be^{t_{outer}P_2} - ae^{t_{inner}P_2}\left(\frac{b}{a}\right)^{-m_\lambda}}{a(m+1)\left(e^{t_{outer}P_2} - e^{t_{inner}P_2}\right)b}. \tag{3.3.26}$$

3.4. Analytical solution with stress function

In this section an analytical solution will be elaborated for the previously presented thermoelastic problem of functionally graded spherical bodies using stress functions.
In this case the loading and the geometry can be seen in Fig. 3.6. The material properties of the radially graded material are given as

$$E(r) = E_0 r^{m_1}, \ \alpha = \alpha_0 r^{m_2}, \ \ \lambda = \lambda_0 r^{m_3}, \tag{3.4.1}$$

where E_0, α_0, λ_0, m_1, m_2 and m_3 are material constants, furthermore the Poisson's ratio ν is constant.

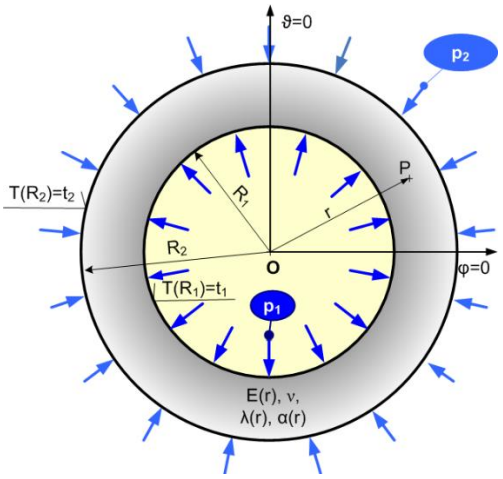

Figure 3.6. The sketch of the problem.

The radial stresses, the heatflow and the temperature field are all continuous functions of the radial coordinate. Our aim is to determine the displacement field and normal stresses within the spherical component.

The first step is the calculation of the temperature field when the thermal conductivity is prescribed by Eq. (3.4.1). For this problem the thermal boundary conditions of the first kind are

$$T(R_1) = t_1, \quad T(R_2) = t_2 = 0. \tag{3.4.2}$$

In this case the temperature difference field $T(r) = t - t_{ref}$ has the following form [59]:

$$T(r) = t_1 \left(1 - \frac{r^{-m_3-1} - R_1^{-m_3-1}}{R_2^{-m_3-1} - R_1^{-m_3-1}} \right), \quad R_1 \le r \le R_2. \tag{3.4.3}$$

The radial and tangential normal strains ε_r, $\varepsilon_\varphi = \varepsilon_\vartheta$ and the stress-strain relations for a spherical body can be formulated as in Eqs. (3.1.5-3.1.7) [52, 60]. According to Eqs. (2.2.9), the equilibrium equation in the radial direction of the spherical body has the following form

$$\frac{\mathrm{d}\sigma_r}{\mathrm{d}r} + \frac{2(\sigma_r - \sigma_\varphi)}{r} = 0, \quad R_1 \le r \le R_2. \tag{3.4.4}$$

We reformulate Eq. (3.4.4) in the next form

$$\frac{\mathrm{d}(r^2\sigma_r)}{\mathrm{d}r} = 2r\sigma_\varphi, \tag{3.4.5}$$

therefore the normal stresses can be expressed in terms of the stress function $V=V(r)$ as

$$\sigma_r = \frac{V}{r^2}, \qquad \sigma_\varphi = \frac{1}{2r}\frac{\mathrm{d}V}{\mathrm{d}r}, \quad R_1 \le r \le R_2. \tag{3.4.6}$$

After some manipulations from Eqs. (3.1.6), (3.1.7), (3.1.5) and (3.4.6) we can derive the next system of ordinary differential equations for the displacement field and the stress function

$$\frac{\mathrm{d}}{\mathrm{d}r}\begin{bmatrix} u \\ V \end{bmatrix} = \begin{bmatrix} -\dfrac{2\nu}{(1-\nu)}\dfrac{1}{r} & \dfrac{(1-2\nu)(1+\nu)}{(1-\nu)E}\dfrac{1}{r^2} \\ \dfrac{2E}{1-\nu} & \dfrac{2\nu}{1-\nu}\dfrac{1}{r} \end{bmatrix} \begin{bmatrix} u \\ V \end{bmatrix} + \begin{bmatrix} \dfrac{1+\nu}{1-\nu} \\ \dfrac{2E}{1-\nu}r \end{bmatrix} \alpha T. \tag{3.4.7}$$

Considering the functions of the material properties given by Eqs. (3.4.1) the final form for the system of differential equations can be expressed as:

$$\frac{\mathrm{d}}{\mathrm{d}r}\begin{bmatrix} u \\ V \end{bmatrix} = \begin{bmatrix} -\dfrac{2\nu}{(1-\nu)}\dfrac{1}{r} & \dfrac{(1-2\nu)(1+\nu)}{(1-\nu)E_0}\dfrac{1}{r^{m_1+2}} \\ \dfrac{2E_0 r^{m_1}}{1-\nu} & \dfrac{2\nu}{1-\nu}\dfrac{1}{r} \end{bmatrix}\begin{bmatrix} u \\ V \end{bmatrix} + \begin{bmatrix} \dfrac{1+\nu}{1-\nu} \\ \dfrac{2E_0}{1-\nu} r^{m_1+1} \end{bmatrix}\alpha_0 r^{m_2} T. \qquad (3.4.8)$$

The general solutions of the radial displacement field and the stress function are power functions of the radial coordinate. The homogeneous solutions are assumed to have the following forms:

$$u_h = C_1 r^{\lambda}, \qquad V_h = C_2 r^{\lambda+m_1+1}. \qquad (3.4.9)$$

Applying Eqs. (3.4.9) to Eqs. (3.4.8), we get the next system of linear equations for the constants C_1 and C_2

$$\begin{bmatrix} \lambda + \dfrac{2\nu}{(1-\nu)} & \dfrac{(1-2\nu)(1+\nu)}{(1-\nu)E_0} \\ -\dfrac{2E_0}{1-\nu} & (\lambda+m_1+1) - \dfrac{2\nu}{1-\nu} \end{bmatrix}\begin{bmatrix} C_1 \\ C_2 \end{bmatrix} = \begin{bmatrix} 0 \\ 0 \end{bmatrix}. \qquad (3.4.10)$$

From the solutions for the previously presented system of equations it follows that

$$u_h = \frac{(\lambda+m_1+1)(1-\nu)-2\nu}{2E_0} C_1 r^{\lambda_1} + \frac{(\lambda+m_1+1)(1-\nu)-2\nu}{2E_0} C_2 r^{\lambda_2}, \qquad (3.4.11)$$

$$V_h = C_1 r^{\lambda_1+m_1+1} + C_2 r^{\lambda_2+m_1+1}, \qquad (3.4.12)$$

$$\lambda_{1,2} = \frac{-1-m_1 \pm \sqrt{(m_1+1)^2 - 4A}}{2}, \; A = \frac{2\left[\nu(m_1+1)-1\right]}{1-\nu}, \qquad (3.4.13)$$

$$C_1 = \frac{(\lambda+m_1+1)(1-\nu)-2\nu}{2E_0} C_2. \qquad (3.4.14)$$

The following notations will be used for the computation of the particular solutions:

$$T_1 = t_1\left(1 + \frac{R_1^{-m_3-1}}{R_2^{-m_3-1} - R_1^{-m_3-1}}\right)\frac{\alpha_0}{1-\nu}, \; T_2 = \frac{t_1}{R_2^{-m_3-1} - R_1^{-m_3-1}}\frac{\alpha_0}{1-\nu}. \qquad (3.4.15)$$

The first particular solution is obtained by the next system of differential equations:

$$\frac{d}{dr}\begin{bmatrix} u \\ V \end{bmatrix} = \begin{bmatrix} -\dfrac{2\nu}{(1-\nu)}\dfrac{1}{r} & \dfrac{(1-2\nu)(1+\nu)}{(1-\nu)E_0}\dfrac{1}{r^{m_1+2}} \\ \dfrac{2E_0 r^{m_1}}{1-\nu} & \dfrac{2\nu}{1-\nu}\dfrac{1}{r} \end{bmatrix}\begin{bmatrix} u \\ V \end{bmatrix} + \begin{bmatrix} 1+\nu \\ 2E_0 r^{m_1+1} \end{bmatrix} T_1 r^{m_2}, \qquad (3.4.16)$$

$$u_{p1} = D_1 r^{m_2+1}, \qquad V_{p1} = D_2 r^{m_2+m_1+2}, \qquad (3.4.17)$$

and we have

$$D_1 = \frac{-(1+\nu)\left(m_1+m_2+2-\dfrac{2\nu}{1-\nu}\right)+\dfrac{2(1+\nu)(1-2\nu)}{1-\nu}}{\left(m_2+1+\dfrac{2\nu}{1-\nu}\right)\left(m_1+m_2+2-\dfrac{2\nu}{1-\nu}\right)-\dfrac{2(1+\nu)(1-2\nu)}{(1-\nu)^2}}T_1, \tag{3.4.18}$$

$$D_2 = \frac{-2E_0\left(m_1-m_3-\dfrac{2\nu}{1-\nu}\right)+\dfrac{2(1+\nu)E_0}{1-\nu}}{\left(m_2+1+\dfrac{2\nu}{1-\nu}\right)\left(m_1+m_2+2-\dfrac{2\nu}{1-\nu}\right)-\dfrac{2(1+\nu)(1-2\nu)}{(1-\nu)^2}}T_1. \tag{3.4.19}$$

The remaining particular solutions can be represented as

$$u_{p2} = F_1 r^{m_2-m_3}, \qquad V_{p2} = F_2 r^{m_2+m_1-m_3+1}, \tag{3.4.20}$$

$$F_1 = \frac{(1+\nu)\left(m_1+m_2-m_3+1-\dfrac{2\nu}{1-\nu}\right)-\dfrac{2(1+\nu)(1-2\nu)}{1-\nu}}{\left(m_2-m_3+\dfrac{2\nu}{1-\nu}\right)\left(m_1+m_2-m_3+1-\dfrac{2\nu}{1-\nu}\right)-\dfrac{2(1+\nu)(1-2\nu)}{(1-\nu)^2}}T_2, \tag{3.4.21}$$

$$F_2 = \frac{2E_0\left(m_2+1+\dfrac{2\nu}{1-\nu}\right)-\dfrac{2(1+\nu)E_0}{1-\nu}}{\left(m_2+1+\dfrac{2\nu}{1-\nu}\right)\left(m_1+m_2+2-\dfrac{2\nu}{1-\nu}\right)-\dfrac{2(1+\nu)(1-2\nu)}{(1-\nu)^2}}T_1. \tag{3.4.22}$$

The summarized form of the general solution for the displacement field and the stress function are as follows

$$u = \frac{(\lambda_1+m_1+1)(1-\nu)-2\nu}{2E_0}C_1 r^{\lambda_1} + \frac{(\lambda_2+m_1+1)(1-\nu)-2\nu}{2E_0}C_2 r^{\lambda_2} + \\ + D_1 r^{m_2+1} + F_1 r^{m_2-m_3}, \tag{3.4.23}$$

$$V = C_1 r^{\lambda_1+m_1+1} + C_2 r^{\lambda_2+m_1+1} + D_2 r^{m_2+m_1+2} + F_2 r^{m_2+m_1-m_3+1}. \tag{3.4.24}$$

In order to determine the unknown constants C_1 and C_2 the next stress boundary conditions will be used:

$$\frac{V(R_1)}{R_1^2} = -p_1, \quad \frac{V(R_2)}{R_2^2} = -p_2. \tag{3.4.25}$$

3.5. Numerical examples for layered composite sphere models

In this section numerical examples will be presented for our developed methods. The models will be compared to each other, to finite element solutions and to results obtained from the literature.

3.5.1. Example 1

In this subsection two numerical examples will be presented to check the accuracy of the temperature fields calculated from the previously presented methods of Subsection 3.2.2. We used the temperature equations of Subsection 3.3.2 and finite element simulations to verify the developed solutions. Furthermore, *Maple 15* mathematical software was used to create the program for the developed methods.

In the first numerical example the accuracy of the calculation for the temperature field is investigated when $\lambda=\lambda(r,T)$ and there are prescribed thermal boundary condition of first kind on the boundary surfaces of the spherical body. The following data were used to carry out the numerical computations for Eqs. (3.3.24):

$$a=0.04\text{m}, b=0.06\text{m}, P_1=10\frac{\text{W}}{\text{mK}}, P_2=1.34\cdot 10^{-3}\frac{1}{\text{K}}, m_\lambda=1.9, t_{ref}=273\text{K},\ t_{inner}=30\text{K},$$

$t_{outer}=500\text{K}$ and the approximation function of the temperature field has the form of Eq. (3.2.20), furthermore three cases with three different layer numbers (n_1=5, n_2=9, n_3=17) are compared to the analytical solution of Eqs. (3.3.25-3.3.26). Figure 3.7 shows the temperature function and the relative errors e_T of the approximations when

$$e_M(\%)=\left|\frac{M_{analytical}-M_{numerical}}{M_{analytical}}\right|\cdot 100,\quad M(r)=T(r),\ u(r),\ \sigma_r(r),\ \sigma_\varphi(r). \tag{3.5.1}$$

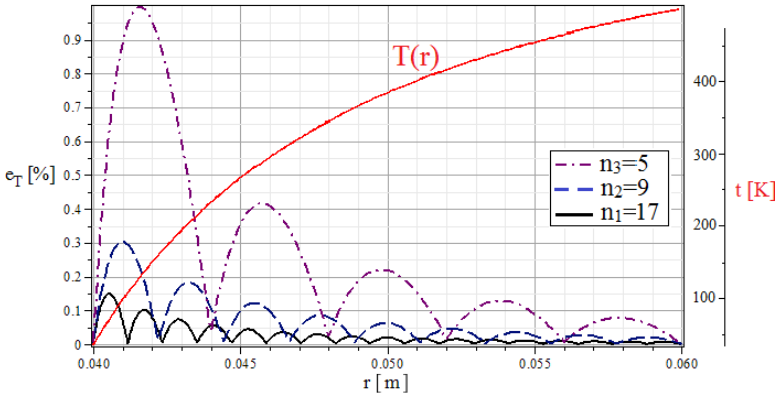

Figure 3.7. The temperature field and the relative errors of the model.

In Fig. 3.7 we can see that even in the case of 5 layers the maximum relative error is under 1%, furthermore the relative errors have minimums at the boundaries of the layers.

In the second numerical example the accuracy of the calculation for the temperature field presented in Subsection 3.2.2 is investigated when the thermal conductivity is power-law function of the radial coordinate and there are prescribed thermal boundary conditions of the third kind.

We consider two cases for the determination of the temperature difference function with two different layer numbers (n_1=4 and n_2=8). The parameters for this example, the function of the thermal conductivity are:

$$a=0.5\text{m}, b=0.65\text{m}, t_{ei}=298\text{K}, t_{eo}=773\text{K},\ h_i=12\frac{\text{W}}{\text{m}^2\text{K}}, h_o=32\frac{\text{W}}{\text{m}^2\text{K}}, \lambda_0=26\frac{\text{W}}{\text{mK}}, m_\lambda=2.5,$$

$$\lambda(r)=\lambda_0\left(\frac{r}{a}\right)^{m_\lambda}.$$

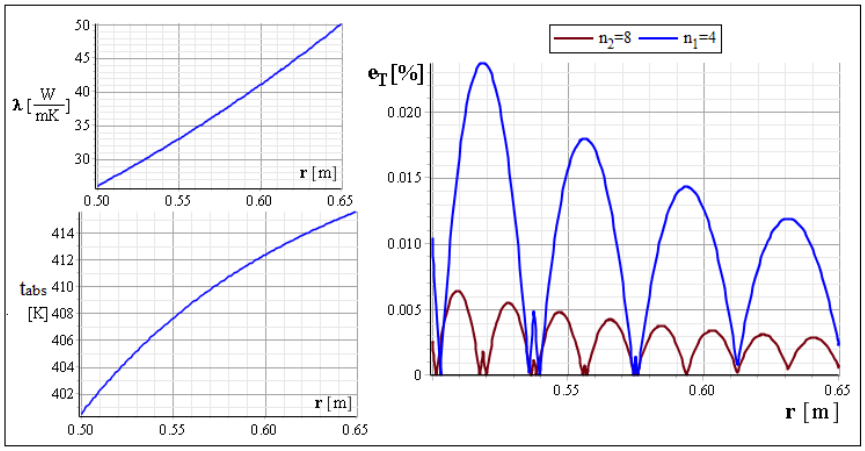

Figure 3.8. The relative errors of the multilayered method by power-law function of the thermal conductivity.

3.5.2. Example 2

We consider a three-layered spherical component for the numerical example of the analytical multilayered methods presented in Sections 3.1 and 3.2. The first and third layers are made of a thermal insulation material, while the material of the second one is steel. For the numerical computation the following data are used:

$$R_1 = 0.5\,\mathrm{m}, R_2 = 0.53\,\mathrm{m}, R_3 = 0.62\,\mathrm{m}, R_4 = 0.65\mathrm{m}, E_1 = E_3 = 320\,\mathrm{GPa}, E_2 = 211\mathrm{GPa},$$

$$\nu_1 = \nu_3 = 0,21, \nu_2 = 0,3, \lambda_1 = \lambda_3 = 4\frac{\mathrm{W}}{\mathrm{mK}}, \lambda_2 = 58\frac{\mathrm{W}}{\mathrm{mK}}, \alpha_1 = \alpha_3 = 7.4\cdot 10^{-6}\frac{1}{\mathrm{K}},$$

$$\alpha_2 = 12\cdot 10^{-6}\frac{1}{\mathrm{K}}, p_1 = 25\mathrm{MPa}, p_2 = 0\mathrm{MPa}, t_1 = 250\,^{\circ}\mathrm{C}, t_4 = 0^{\circ}\mathrm{C}.$$

The radial displacement and the normal stress fields obtained by the method presented in Section 3.1 can be seen in Figs. 3.9-3.11 and are denoted by blue dots (Method 1), while the results of Section 3.2 are illustrated by red solid lines (Method 2). The two developed methods lead to the same results.

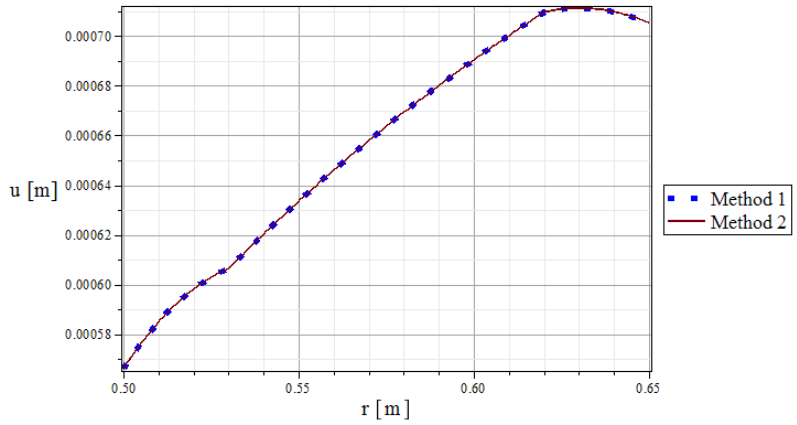

Figure 3.9. The plots of the displacement field in the three-layered sphere.

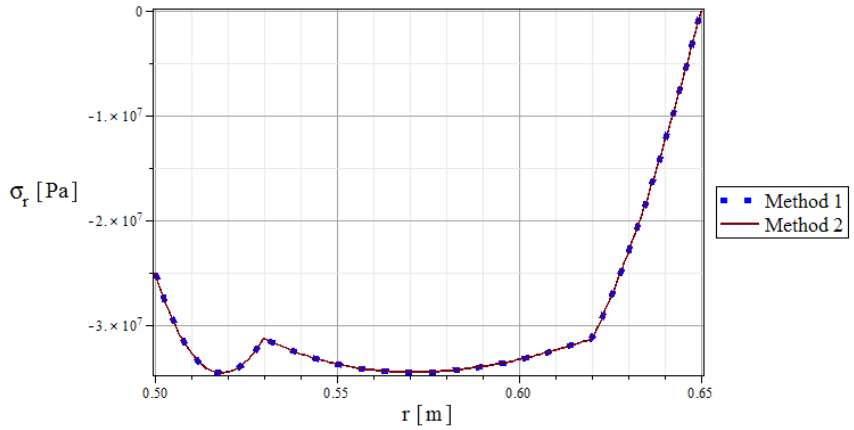

Figure 3.10. The radial stresses of the three-layered sphere.

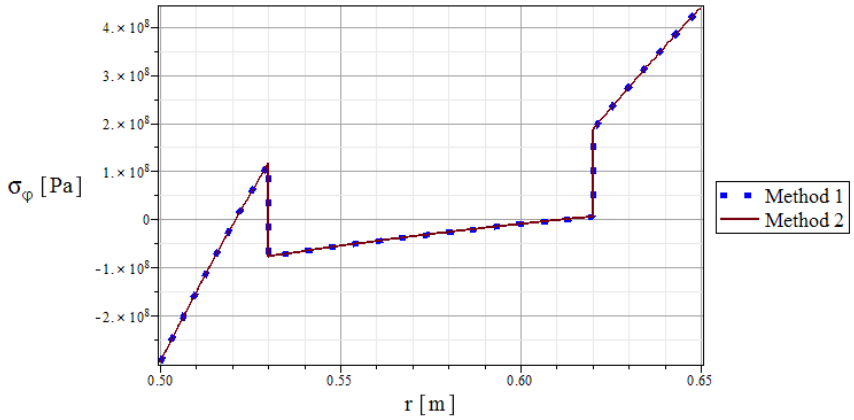

Figure 3.11. The tangential normal stresses of the three-layered sphere.

3.5.3. Example 3

As we have mentioned earlier the problem of a functionally graded spherical body can be solved with a model of layered spherical body which consist of homogeneous layers. In this example we verified our analytical method of Section 3.4, then we have tried to solve it with our multilayered approach when the temperature dependency is negligible. Furthermore an additional example will be presented to investigate the effect of the power index of the material properties described in Section 2.4.

The first analytical model was compared to the method presented in [27] and [28], we got the same results. In our current example this analytical solution [28] is compared to the models of Sections 3.1 and 3.2 in the case of power-law based material properties. The following data are used for the numerical computations:

$$a=0.04\text{m},\ b=0.06\text{m},\ t_{ei}=573\text{K},\ t_{eo}=298\text{K},\ h_i=h_o=10^8\frac{\text{W}}{\text{m}^2\text{K}},\ p_1=80\text{MPa},\ p_2=0\text{MPa},$$

$$\nu=0.3,\ \lambda_0=58\frac{\text{W}}{\text{mK}},\ E_0=2\cdot10^{11}\text{Pa},\ \alpha_0=1.2\cdot10^{-6}\frac{1}{\text{K}},\ m_\lambda=m_E=m_\alpha=m,$$

$$\lambda(r)=\lambda_0\left(\frac{r}{a}\right)^{m_\lambda},E(r)=E_0\left(\frac{r}{a}\right)^{m_E},\alpha(r)=\alpha_0\left(\frac{r}{a}\right)^{m_\alpha}.$$

Table 3.1. The comparison of the analytical solution and the multilayered approach, m=1.

m=1	Ana. value	Relative error (%)			An. value	Relative error (%)			Ana. value	relative error (%)		
r/a	***u(r)·10³***	n=4	n=8	n=32	**$-\sigma_r/p_1$**	n=4	n=8	n=32	**$-\sigma_\varphi/p_1$**	n=4	n=8	n=32
1	0.5187	0.231	0.058	0.003	1	$6\cdot10^{-8}$	0	0	0.1382	4.98	2.921	1.006
1.0875	0.5119	0.532	0.138	0.008	0.8077	0.209	0.056	0.004	0.3492	2.466	0.563	0.188
1.1875	0.5028	0.541	0.089	0.004	0.6010	0.138	0.024	0.001	0.5954	0.518	0.259	0.090
1.2875	0.4917	0.503	0.132	0.009	0.4033	0.025	0.004	.0001	0.8471	1.138	0.046	0.027
1.3875	0.4781	0.473	0.124	0.008	0.2115	0.107	0.071	0.005	1.1044	2.764	0.957	0.201
1.5	0.4597	0.498	0.125	0.008	0	$9\cdot10^{-7}$	0	0	1.4008	2.920	1.589	0.422

Tables 3.1 and 3.2 show the relative errors of the multilayered models by three different layer numbers (n=4, 8, 32). The results indicate that the approximation is accurate for the radial quantities, for the displacement field and stresses, for example when n=4 the maximum relative error is under 0.55%. For the determination of the normal stresses σ_φ and σ_ϑ finer partitioning is necessary because in some cases the errors can be significant especially at the curved boundary surfaces.

Table 3.2. The comparison of the analytical solution and the multilayered approach, m=-1.

m=-1	Ana. value	Relative error (%)			An. value	Relative error (%)			Ana. value	relative error (%)		
r/a	***u(r)·10³***	n=4	n=8	n=32	**$-\sigma_r/p_1$**	n=4	n=8	n=32	**$-\sigma_\varphi/p_1$**	n=4	n=8	n=32
1	0.6697	0.035	0.008	.00005	1	$9\cdot10^{-8}$	0	0	0.6777	0.783	0.597	0.192
1.0875	0.6497	0.271	0.071	0.004	0.7331	0.008	0.009	.0007	0.7668	0.325	0.208	0.034
1.1875	0.6231	0.281	0.037	0.002	0.4868	0.167	0.025	0.002	0.8119	0.221	0.266	0.179
1.2875	0.5948	0.256	0.068	0.003	0.2916	0.297	0.088	0.006	0.8241	1.663	0.307	0.093
1.3875	0.5664	0.244	0.064	0.003	0.1368	0.229	0.131	0.009	0.8189	3.267	1.211	0.287
1.5	0.5354	0.272	0.067	0.003	0	$9\cdot10^{-7}$	0	0	0.8023	3.776	1.924	0.487

The last example of this chapter investigates the effect of the power index m on the stress field. The material properties have the following forms:

$$\lambda(r)=\lambda_i+(\lambda_0-\lambda_i)\left(\frac{r-a}{b-a}\right)^{m_\lambda},\ E(r)=E_i+(E_0-E_i)\left(\frac{r-a}{b-a}\right)^{m_E},$$
$$\alpha(r)=\alpha_i+(\alpha_0-\alpha_i)\left(\frac{r-a}{b-a}\right)^{m_\alpha},\ \nu(r)=\nu_i+(\nu_0-\nu_i)\left(\frac{r-a}{b-a}\right)^{m_\nu}. \qquad (3.5.3)$$

$$a=0.55\text{m},b=0.7\text{m},t_{ei}=25\text{K},t_{eo}=350\text{K},\ p_1=40\text{MPa},\ p_2=0\text{MPa},h_i=10^8\frac{\text{W}}{\text{m}^2\text{K}},$$

$$h_o = 500\frac{\mathrm{W}}{\mathrm{m^2K}},\ \nu_o = 0.28,\ \lambda_0 = 20\frac{\mathrm{W}}{\mathrm{mK}},\ E_0 = 1.71\cdot 10^{11}\,\mathrm{Pa},\ \alpha_0 = 0.76\cdot 10^{-6}\frac{1}{K},$$

$$\nu_i = 0.336, \lambda_i = 58\frac{\mathrm{W}}{\mathrm{mK}}, E_i = 2.35\cdot 10^{11}\,\mathrm{Pa}, \alpha_i = 1.2\cdot 10^{-6}\frac{1}{\mathrm{K}}, m_\lambda = m_E = m_\alpha = m_\nu = m = 0.7.$$

The results are shown in Fig. 3.12 in three cases. The graphs of the combined loads are denoted by red solid lines, the green dash dot lines belong to the case when there are no thermal loading, the blue dash lines indicate the results for the thermal loads without mechanical loading. Figure 3.13. illustrates the effect of power index *m* on the equivalent stress field, where

$$\sigma_{eq-Mises} = \left|\sigma_\varphi - \sigma_r\right|. \tag{3.5.4}$$

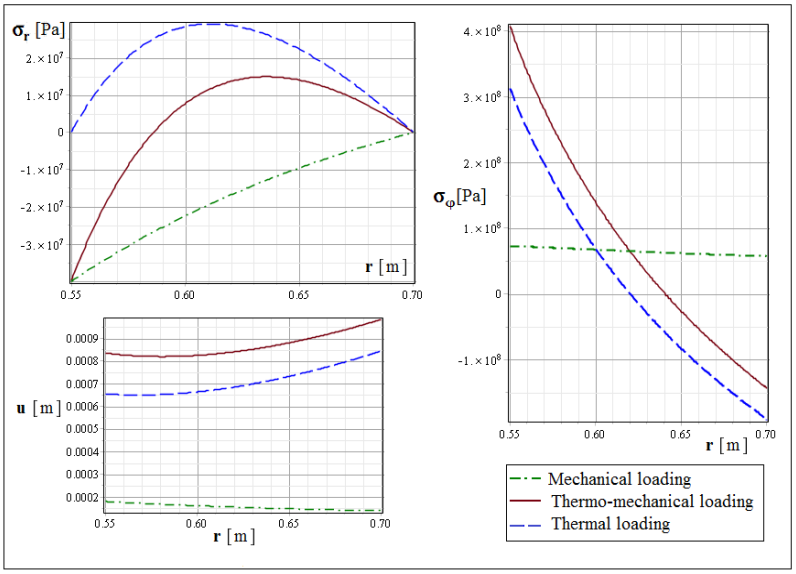

Figure 3.12. The results for the normal stresses and displacement field.

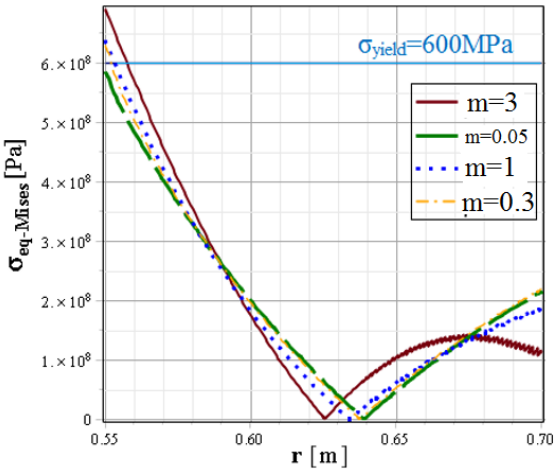

Figure 3.13. The effect of the power index m on the equivalent stresses.

4. Numerical solutions for the problems of functionally graded spherical bodies

In this chapter numerical methods are presented to deal with the thermoelastic problem of radially graded spherical bodies. An initial value problem and the previously developed multilayered models are applied to functionally graded materials when the material properties are arbitrary functions of the radial coordinate and the temperature field. Furthermore two special cases of radially graded spheres are investigated. A numerical model is presented to deal with the problem of functionally graded piezoelectric spherical parts. In the second case the equations are derived to calculate the normal stresses of incompressible functionally graded spheres.

4.1. Initial value problem of radially graded spheres with arbitrary material parameter distribution

A thermoelastic boundary value problem of a spherical body made from functionally graded materials with arbitrary gradient is analysed, where the material parameters are arbitrary smooth functions of the radial coordinate and temperature field, furthermore the steady-state temperature distribution is assumed to be arbitrary smooth function of the radial coordinate r (Subsection 3.2.2). A coupled system of ordinary differential equations containing the radial displacement and stress function is derived and used to get the distribution of normal stresses and radial displacements caused by combined axisymmetric mechanical and thermal loads. The geometry and the boundary conditions can be seen in Fig. 3.6.

The radial and tangential normal stresses in terms of stress function $V=V(r)$ can be represented as

$$\sigma_r = \frac{V}{r^2}, \qquad \sigma_\varphi = \frac{1}{2r}\frac{\mathrm{d}V}{\mathrm{d}r}, \quad R_1 \le r \le R_2. \tag{4.1.1}$$

After some manipulations from Eqs. (3.1.5-3.1.7) and (4.1.1) we can derive the next system of ordinary differential equations for the displacement field and the stress function

$$\begin{aligned}
\frac{\mathrm{d}u(r)}{\mathrm{d}r} &= -\frac{2\nu(r,T(r))}{(1-\nu(r,T(r)))}\frac{1}{r}u(r) + \frac{\big(1-2\nu(r,T(r))\big)\big(1+\nu(r,T(r))\big)}{\big(1-\nu(r,T(r))\big)E(r,T(r))}\frac{V(r)}{r^2} + \frac{1+\nu(r,T(r))}{1-\nu(r,T(r))}\alpha(r,T(r))T(r), \\
\frac{\mathrm{d}V(r)}{\mathrm{d}r} &= \frac{2E(r,T(r))}{1-\nu(r,T(r))}u(r) + \frac{2\nu(r,T(r))}{1-\nu(r,T(r))}\frac{V(r)}{r} + \frac{2E(r,T(r))}{1-\nu(r,T(r))}\alpha(r,T(r))T(r)r,
\end{aligned} \tag{4.1.2}$$

The validity of this statement comes from the fact, that in our time independent uncoupled problems, the temperature field can be obtained from the solution of the heat conduction equations as we have seen in Subsection 3.2.2. At first all material parameters are arbitrary smooth functions of the radial coordinate and temperature field, but the temperature field is given, which means that $M(r,T(r))\rightarrow M(r)$ and Eqs. (4.1.2) assume the form of Eqs. (3.4.7).

Our aim is the calculation of the initial values for the system of equations (4.1.2). The stress boundary conditions and its expressions in terms of the stress function $V=V(r)$ are as follows

$$\sigma_r(R_1) = -p_1, \quad \sigma_r(R_2) = -p_2, \tag{4.1.3}$$

$$V(R_1) = -p_1 R_1^2, \quad V(R_2) = -p_2 R_2^2. \tag{4.1.4}$$

In Eqs. (4.1.3), (4.1.4) p_1 and p_2 are known applied pressures at the inner and outer spherical boundary surfaces. Our aim is to transform the two-point boundary value problem formulated by Eqs. (4.1.2), (4.1.4) into an initial value problem. This step is required to the realization of the chosen numerical methods. To get the unknown initial displacement $u(R_1)$ we consider two solutions for system of equations (4.1.2) which are denoted by $[u_1(r), V_1(r)]$ and $[u_2(r), V_2(r)]$. These solutions have the next prescribed initial values:

$$u_1(R_1) = u_1 : \text{arbitrary value}, \tag{4.1.5}$$

$$V_1(R_1) = -p_1 R_1^2, \tag{4.1.6}$$

$$u_2(R_1) = u_2 : \text{arbitrary value, but } u_1 \neq u_2, \tag{4.1.7}$$

$$V_2(R_1) = -p_1 R_1^2. \tag{4.1.8}$$

To carry out the calculations and get $[u_1(r), V_1(r)]$ and $[u_2(r), V_2(r)]$, we can use for example the Runge-Kutta method. From these solutions the suitable value of $u(R_1)=u_3$ can be computed as

$$u_3 = u_1 + \frac{u_2 - u_1}{V_2(R_2) - V_1(R_2)}(-p_2 R_2^2 - V_1(R_2)). \tag{4.1.9}$$

The validity of this statement follows from the linearity of the considered thermoelastic boundary value problem. The solution of the thermoelastic boundary value problem is obtained from the numerical solution of system of equations (4.1.2) with the initial conditions

$$u(R_1) = u_3, \qquad V(R_1) = -p_1 R_1^2. \tag{4.1.10}$$

The stress field in this case can be obtained from the next equations

$$\sigma_r(r) = \frac{V(r)}{r^2}, \; \sigma_\varphi(r) = \frac{1}{2r}\frac{\mathrm{d}V}{\mathrm{d}r} = \frac{E}{1-\nu}\frac{u}{r} + \frac{\nu}{1-\nu}\frac{V(r)}{r^2} + \frac{E\alpha}{1-\nu}T(r). \tag{4.1.11}$$

4.2. Functionally graded piezoelectric spheres

In our next model a spherical body made from functionally graded materials with radial grading and polarization will be considered. The loads for this axisymmetric problem are constant mechanical loads denoted by p_1 and p_2 and electric potentials ϕ_1 and ϕ_2 on the inner and on the outer boundary surfaces, respectively. Our aim is to transform this problem into an initial value problem, then find a numerical method to solve it. The sketch of the problem can be seen in Fig. 4.1.

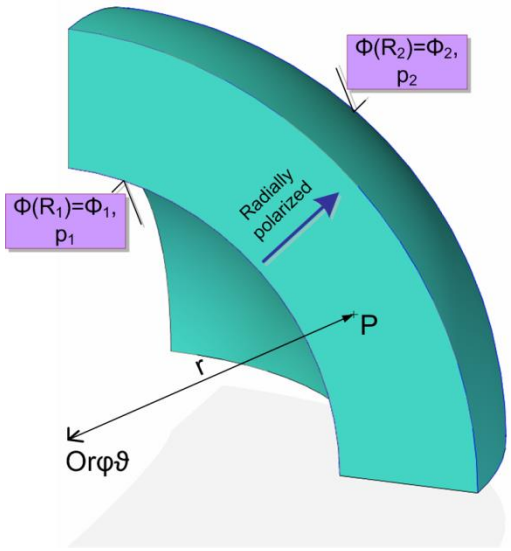

Figure 4.1. The sketch of the problem with the boundary conditions.

In spherical coordinate system the constitutive equations for radially polarized piezoelectric materials can be expressed as - according to Section 2.5 -

$$\varepsilon_\vartheta = \varepsilon_\varphi = \frac{u}{r} = \left(S_{11}+S_{12}\right)\sigma_\varphi + S_{13}\sigma_r + g_{31}D_r\,,\ \varepsilon_r = \frac{\mathrm{d}u}{\mathrm{d}r} = 2S_{13}\sigma_\varphi + S_{33}\sigma_r + g_{33}D_r\,, \quad (4.2.1)$$

$$E_r = -2g_{31}\sigma_\varphi - g_{33}\sigma_r + \beta_{33}D_r,\ R_1 \le r \le R_2\,, \quad (4.2.2)$$

where in these last terms the following expressions are introduced

$$D_r = \frac{D}{r^2}, \quad E_r = -\frac{\mathrm{d}\phi}{\mathrm{d}r}. \quad (4.2.3)$$

Here we note that D_r is obtained from the Gauss equation [57] which takes the form of

$$\frac{\mathrm{d}D_r}{\mathrm{d}r} + \frac{2}{r}D_r = 0, \quad (4.2.4)$$

furthermore in our current problem D is an unknown constant. We need to formulate the system of differential equations for the unknown stress-, electric potential-, radial displacement functions and electrical displacement. The combination of Eqs. (4.2.1-4.2.3) and (4.1.1) gives

$$\begin{aligned} \frac{\mathrm{d}V(r)}{\mathrm{d}r} &= \frac{\mathrm{d}}{\mathrm{d}r}\left(\sigma_r(r)r^2\right) = \frac{\mathrm{d}\sigma_r(r)}{\mathrm{d}r}r^2 + 2r\sigma_r(r), \\ \frac{\mathrm{d}V}{\mathrm{d}r} &= \frac{2}{S_{11}+S_{12}}u - \frac{2S_{13}}{S_{11}+S_{12}}\frac{V}{r} - \frac{2g_{31}}{S_{11}+S_{12}}\frac{D}{r}, \end{aligned} \quad (4.2.5)$$

$$\begin{aligned} \frac{\mathrm{d}u(r)}{\mathrm{d}r} &= 2S_{13}\left(\frac{1}{2r}\frac{\mathrm{d}V(r)}{\mathrm{d}r}\right) + S_{33}\left(\frac{V(r)}{r^2}\right) + g_{33}\left(\frac{D}{r^2}\right), \\ \frac{\mathrm{d}u}{\mathrm{d}r} &= \frac{2S_{13}}{S_{11}+S_{12}}\frac{u}{r} + \left(S_{33} - \frac{2S_{13}^2}{S_{11}+S_{12}}\right)\frac{V}{r^2} + \left(g_{33} - \frac{2S_{13}g_{31}}{S_{11}+S_{12}}\right)\frac{D}{r^2}, \end{aligned} \quad (4.2.6)$$

$$\begin{aligned}
\frac{\mathrm{d}\phi(r)}{\mathrm{d}r} &= -E_r(r) = 2g_{31}\left(\frac{1}{2r}\frac{\mathrm{d}V(r)}{\mathrm{d}r}\right) - g_{33}\left(\frac{V(r)}{r^2}\right) - \beta_{33}\left(\frac{D}{r^2}\right), \\
\frac{\mathrm{d}\phi}{\mathrm{d}r} &= \frac{2g_{31}}{S_{11}+S_{12}}\frac{u}{r} + \left(g_{33} - \frac{2g_{31}S_{13}}{S_{11}+S_{12}}\right)\frac{V}{r^2} - \left(\beta_{33} + \frac{2g_{31}^2}{S_{11}+S_{12}}\right)\frac{D}{r^2}.
\end{aligned} \tag{4.2.7}$$

This system of differential equations can be reformulate into a matrix equation:

$$\frac{\mathrm{d}}{\mathrm{d}r}\begin{bmatrix} V \\ u \\ \phi \end{bmatrix} = \begin{bmatrix} \dfrac{2}{S_{11}+S_{12}} & -\dfrac{2S_{13}}{S_{11}+S_{12}}\dfrac{1}{r} & -\dfrac{2g_{31}}{S_{11}+S_{12}}\dfrac{1}{r} \\ \dfrac{2S_{13}}{S_{11}+S_{12}}\dfrac{1}{r} & \left(S_{33} - \dfrac{2S_{13}^2}{S_{11}+S_{12}}\right)\dfrac{1}{r^2} & \left(g_{33} - \dfrac{2S_{13}g_{31}}{S_{11}+S_{12}}\right)\dfrac{1}{r^2} \\ \dfrac{2g_{31}}{S_{11}+S_{12}}\dfrac{1}{r} & \left(g_{33} - \dfrac{2g_{31}S_{13}}{S_{11}+S_{12}}\right)\dfrac{1}{r^2} & -\left(\beta_{33} + \dfrac{2g_{31}^2}{S_{11}+S_{12}}\right)\dfrac{1}{r^2} \end{bmatrix} \cdot \begin{bmatrix} u \\ V \\ D \end{bmatrix} \tag{4.2.8}$$

For our further investigation and numerical example, the following power-law functions will be used to describe the distribution of the material parameters

$$S_{11}(r) = S_{110}\left(\frac{r}{R_1}\right)^{m_1},\ S_{12}(r) = S_{120}\left(\frac{r}{R_1}\right)^{m_1},\ S_{13}(r) = S_{130}\left(\frac{r}{R_1}\right)^{m_1}, \tag{4.2.9}$$

$$S_0 = S_{110} + S_{120},\ \ S(r) = S_{11}(r) + S_{12}(r) = S_0\left(\frac{r}{R_1}\right)^{m_1}, \tag{4.2.10}$$

$$g_{31}(r) = g_{310}\left(\frac{r}{R_1}\right)^{m_2},\quad g_{33}(r) = g_{330}\left(\frac{r}{R_1}\right)^{m_2},\quad \beta_{33}(r) = \beta_{330}\left(\frac{r}{R_1}\right)^{m_3}. \tag{4.2.11}$$

Upon substituting these expressions into Eq. (4.2.8) we get

$$\frac{d}{dr}\begin{bmatrix} V \\ u \\ \phi \end{bmatrix} = \begin{bmatrix} \dfrac{2}{S_0}\left(\dfrac{r}{R_1}\right)^{-m_1} & -\dfrac{2S_{130}}{S_0}\dfrac{1}{r} & -\dfrac{g_{310}}{S_0}\left(\dfrac{r}{R_1}\right)^{m_2-m_1-1} \\ \dfrac{2S_{130}}{S_0}\dfrac{1}{r} & \left(S_{330} - \dfrac{2S_{130}^2}{S_0}\right)\left(\dfrac{r}{R_1}\right)^{m_1-2} & \left(g_{330} - \dfrac{2S_{130}g_{310}}{S_0}\right)\left(\dfrac{r}{R_1}\right)^{m_2-2} \\ \dfrac{g_{310}}{S_0}\left(\dfrac{r}{R_1}\right)^{m_2-m_1-1} & \left(g_{330} - \dfrac{2g_{310}S_{130}}{S_0}\right)\left(\dfrac{r}{R_1}\right)^{m_2-2} & -\left(\beta_{330}\left(\dfrac{r}{R_1}\right)^{m_3-2} + \dfrac{2g_{310}^2}{S_0}\right)\left(\dfrac{r}{R_1}\right)^{m_2-m_1-2} \end{bmatrix} \cdot \begin{bmatrix} u \\ V \\ D \end{bmatrix}. \tag{4.2.12}$$

The boundary conditions for this problem can be presented as

$$\begin{aligned}
V(R_1) &= -p_1R_1^2, \\
V(R_2) &= -p_2R_2^2, \\
\phi(R_1) &= \phi_1, \\
\phi(R_2) &= \phi_2.
\end{aligned} \tag{4.2.13}$$

Let the solution vector $\mathbf{X}(r)$ be defined as

$$\mathbf{X}(r)=\begin{bmatrix} u(r) \\ V(r) \\ \phi(r) \end{bmatrix}. \tag{4.2.14}$$

Four computations are required for the calculation of the solution. We need to solve the initial value problems of four cases with the following initial values (for example with Runge-Kutta method):

$$\mathbf{X}_i(r)=\begin{bmatrix} u_{ni}(r) \\ V_{ni}(r) \\ \phi_{ni}(r) \end{bmatrix}=\begin{bmatrix} X_{i1}(r) \\ X_{i2}(r) \\ X_{i3}(r) \end{bmatrix}, \quad (i=1,...,4), \tag{4.2.15}$$

where U_{ni}, V_{ni} and Φ_{ni} are numerical solutions of the different cases (i=1,…,4). Table 4.1. shows the recommended method to solve this initial value problem.

Table 4.1. The different initial value subproblems for the model.

Initial values	case 1		case 2		case 3		case 4	
	input	output	input	output	input	output	input	output
$u(R_1)$	1	$\mathbf{X}_1$	0	$\mathbf{X}_2$	0	$\mathbf{X}_3$	0	$\mathbf{X}_4$
$V(R_1)$	0		1		0		0	
$\phi(R_1)$	0		0		1		0	
D	0		0		0		1	

From the linearity of this problem it follows that

$$\mathbf{X}(r)=u(R_1)\begin{bmatrix} X_{11}(r) \\ X_{12}(r) \\ X_{13}(r) \end{bmatrix}+V(R_1)\begin{bmatrix} X_{21}(r) \\ X_{22}(r) \\ X_{23}(r) \end{bmatrix}+\phi(R_1)\begin{bmatrix} X_{31}(r) \\ X_{32}(r) \\ X_{33}(r) \end{bmatrix}+D\begin{bmatrix} X_{41}(r) \\ X_{42}(r) \\ X_{43}(r) \end{bmatrix} \tag{4.2.16}$$

After the manipulation of Eq. (4.2.16) we get the following system of equations:

$$V(R_2)=-p_2R_2^2=u(R_1)X_{12}+\left(-p_1R_1^2\right)X_{22}+\phi_1X_{32}+DX_{42}, \tag{4.2.17}$$

$$\phi_2=u(R_1)X_{13}+\left(-p_1R_1^2\right)X_{23}+\phi_1X_{33}+DX_{43}. \tag{4.2.18}$$

From this system of equations we can calculate the unknown values of $u(R_1)$ and D. The last step is the solution of the system of differential equation (4.2.12) with initial values [$u(R_1)$, V_1, ϕ_1, D].

4.3. Incompressible spherical bodies

A thick spherical vessel will be considered in $Or\varphi\vartheta$ spherical coordinate system as we can see in Fig. 4.2. The incompressible spherical body is radially graded, therefore the material properties are vary along the radial coordinate r. The thermal loading is a steady-state temperature difference field $T=T(r)$ and the mechanical loads p_1 and p_2 are constant pressures exerted on the inner and outer boundary surfaces.

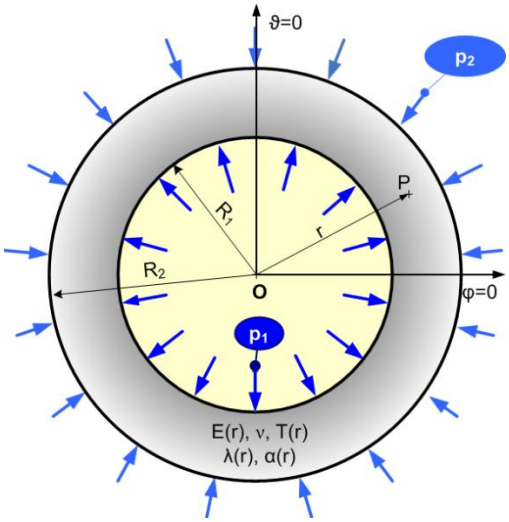

Figure 4.2. The sketch of the problem.

Our aim is to derive a method to calculate the displacement field and normal stresses within an incompressible spherical body.

In the case of incompressible materials the Poisson's ratio is ν=0.5 and the relation between the Young modulus and the shear modulus is E=3G. The stress-strain relations for these spherical bodies can be expressed as [52], [60]

$$\sigma_r = 2G\varepsilon_r^M + \sigma_0 = \frac{2}{3}E\varepsilon_r^M + \sigma_0, \tag{4.3.1}$$

$$\sigma_\vartheta = 2G\varepsilon_\vartheta^M + \sigma_0 = \frac{2}{3}E\varepsilon_\vartheta^M + \sigma_0, \tag{4.3.2}$$

$$\sigma_\varphi = 2G\varepsilon_\varphi^M + \sigma_0 = \frac{2}{3}E\varepsilon_\varphi^M + \sigma_0, \tag{4.3.3}$$

where σ_r, σ_φ, σ_ϑ are the normal stresses, $\varepsilon^M{}_r$, $\varepsilon^M{}_\varphi$, $\varepsilon^M{}_\vartheta$ denote the normal strains from mechanical loads, furthermore we have

$$\sigma_0 = \frac{1}{3}\left(\sigma_r + \sigma_\varphi + \sigma_\vartheta\right) = \frac{1}{3}\left(\sigma_r + 2\sigma_\varphi\right). \tag{4.3.4}$$

The normal strains can be written as the sum of its mechanical and thermal parts

$$\varepsilon_r(r) = \varepsilon_r^M(r) + \varepsilon_r^T(r) = \frac{\sigma_r(r) - \sigma_\varphi(r)}{E(r)} + \alpha(r)T(r), \tag{4.3.5}$$

$$\varepsilon_\varphi(r) = \varepsilon_\varphi^M(r) + \varepsilon_\varphi^T(r) = \frac{-\sigma_r(r) + \sigma_\varphi(r)}{2E(r)} + \alpha(r)T(r). \tag{4.3.6}$$

For the trace of the strain tensor the following relation can be written

$$\varepsilon = \varepsilon_r + \varepsilon_\varphi + \varepsilon_\vartheta = \varepsilon_r + 2\varepsilon_\varphi = 3\alpha T\ . \tag{4.3.7}$$

The displacement-strain relations of spherical bodies are

$$\varepsilon_r(r)=\frac{\mathrm{d}u(r)}{\mathrm{d}r},\quad \varepsilon_\varphi(r)=\varepsilon_\vartheta(r)=\frac{u(r)}{r}. \tag{4.3.8}$$

The combination of Eqs. (4.3.7-4.3.8) leads to

$$\varepsilon(r)=\frac{\mathrm{d}u(r)}{\mathrm{d}r}+2\frac{u(r)}{r}=\frac{1}{r^2}\frac{\mathrm{d}}{\mathrm{d}r}\left(u(r)r^2\right). \tag{4.3.9}$$

The solution of Eqs. (4.3.7), (4.3.9) gives the function of radial displacement field

$$u(r)=\frac{3\int_{R_1}^{r}\rho^2\alpha(\rho)T(\rho)\mathrm{d}\rho}{r^2}+\frac{C_1}{r^2}=3\frac{F_1(r)}{r^2}+\frac{C_1}{r^2}, \tag{4.3.10}$$

where the following notation is introduced

$$F_1(r)=\int_{R_1}^{r}\rho^2\alpha(\rho)T(\rho)\mathrm{d}\rho\,. \tag{4.3.11}$$

The substitution of Eq. (4.3.10) into the expressions of the normal strains Eqs. (4.3.5), (4.3.6) leads to the following formulae:

$$\varepsilon(r)=3\alpha(r)T(r)-6\frac{F_1(r)}{r^3}-2\frac{C_1}{r^3}, \tag{4.3.12}$$

$$\varepsilon_\varphi(r)=\varepsilon_\vartheta(r)=3\frac{F_1(r)}{r^3}+\frac{C_1}{r^3}. \tag{4.3.13}$$

In the case of hollow spherical bodies the equilibrium equation can be expressed -Eq. (2.2.9)- as

$$\frac{\mathrm{d}\sigma_r}{\mathrm{d}r}=2\frac{\sigma_\varphi-\sigma_r}{r}. \tag{4.3.14}$$

The combination of Eqs. (4.3.14) with Eqs. (4.3.1, 4.3.2, 4.3.12, 4.3.13) leads to

$$\frac{\mathrm{d}\sigma_r}{\mathrm{d}r}=2\left(6\frac{E(r)F_1(r)}{r^4}+2\frac{E(r)}{r^4}C_1-2\frac{E(r)\alpha(r)T(r)}{r}\right). \tag{4.3.15}$$

The solution of Eq. (4.3.15) gives the function of the radial normal stress

$$\sigma_r(r)=12\int_{R_1}^{r}\frac{E(\rho)F_1(\rho)}{\rho^4}\mathrm{d}\rho+4C_1\int_{R_1}^{r}\frac{E(\rho)}{\rho^4}\mathrm{d}\rho-4\int_{R_1}^{r}\frac{E(\rho)\alpha(\rho)T(\rho)}{\rho}\mathrm{d}\rho+C_2. \tag{4.3.16}$$

The unknown constants C_1 and C_2 can be calculated from the stress boundary conditions:

$$p_1=-\sigma_r(R_1),\quad p_2=-\sigma_r(R_2). \tag{4.3.17}$$

Form Eq. (4.3.17) it follows that

$$C_2=\sigma_r(R_1), \tag{4.3.18}$$

$$C_1 = \frac{\sigma_r(R_2) - \sigma_r(R_1) - 12\int_{R_1}^{R_2} \frac{E(\rho)F_1(\rho)}{\rho^4} + \frac{E(\rho)\alpha(\rho)T(\rho)}{3\rho}\mathrm{d}\rho}{4\int_{R_1}^{R_2} \frac{E(\rho)}{\rho^4}\mathrm{d}\rho}. \tag{4.3.19}$$

The tangential normal stresses can be calculated from Eqs. (4.3.14-4.3.16)

$$\sigma_\varphi(r) = \frac{1}{2} r \frac{\mathrm{d}\sigma_r}{\mathrm{d}r} + \sigma_r = \\ = 2E(r)\left(3\frac{F_1(r)}{r^3} + \frac{C_1}{r^3} - \alpha(r)T(r)\right) + C_2 + 4\int_{R_1}^{r} E(\rho)\left(3\frac{F_1(\rho)}{\rho^4} + \frac{C_1}{\rho^4} - \frac{\alpha(\rho)T(\rho)}{\rho}\right)\mathrm{d}\rho. \tag{4.3.20}$$

4.4. Numerical examples

In this section numerical calculations will be presented for the developed methods. In the first example the accuracy of the initial value method and the multilayered method is investigated. These models will be compared to the analytical solution derived in Section 3.3. In the next example these numerical methods will be checked by finite element simulations in the case of a metal-ceramic functionally graded material where the temperature dependency is taken into account. In the last two problems the results of the methods developed in Sections 4.2 and 4.3 will be presented and checked by FEM.

4.4.1. Example 4

In our first example the accuracy of the initial value method (Section 4.1) and multilayered method (Section 3.2) is investigated. The material parameters for the analytical solution presented in Section 3.3 and Eqs. (3.3.1), (3.3.2) are

$$a = 0.065\mathrm{m}, b = 0.08\mathrm{m}, P_1 = 198\mathrm{GPa}, P_2 = 10^{-8}\frac{1}{\mathrm{K}^2}, P_3 = 2\cdot 10^{-8}\frac{1}{\mathrm{K}}, m_\alpha = 1.9, m_E = 2,$$

$$\lambda = 58\frac{\mathrm{W}}{\mathrm{mK}}, t_{inner} = 450\mathrm{K}, t_{outer} = 20\mathrm{K}, t_{ref} = 273\mathrm{K}, p_1 = 20\mathrm{MPa}, p_2 = 0\mathrm{MPa}.$$

The results of the initial value method and the multilayered approach are compared to the exact solution. Figure 4.3 shows the graphs of the radial displacements for the investigated models. As for the multilayered method, the widths of the layers are equal, the material properties are computed according to the method described in Subsection 3.2.1. It is important to note, that the accuracy of this method can be improved when the widths of the layers are adjusted to the material functions. As regards of Fig. 4.3, even in the case of n=4 the relative error is under 1%.

The relative errors for the numerical models can be seen in Fig. 4.3. The initial value method has great accuracy according to Fig. 4.3, in our case the maximum error is $2.6\cdot 10^{-5}$ %. As for the multilayered method, the relative errors are minimal at the edge of the layers. If we want to further

improve the accuracy and speed of our method, we can get the displacement values at the boundaries of the layers and fit a curve with least squares method.

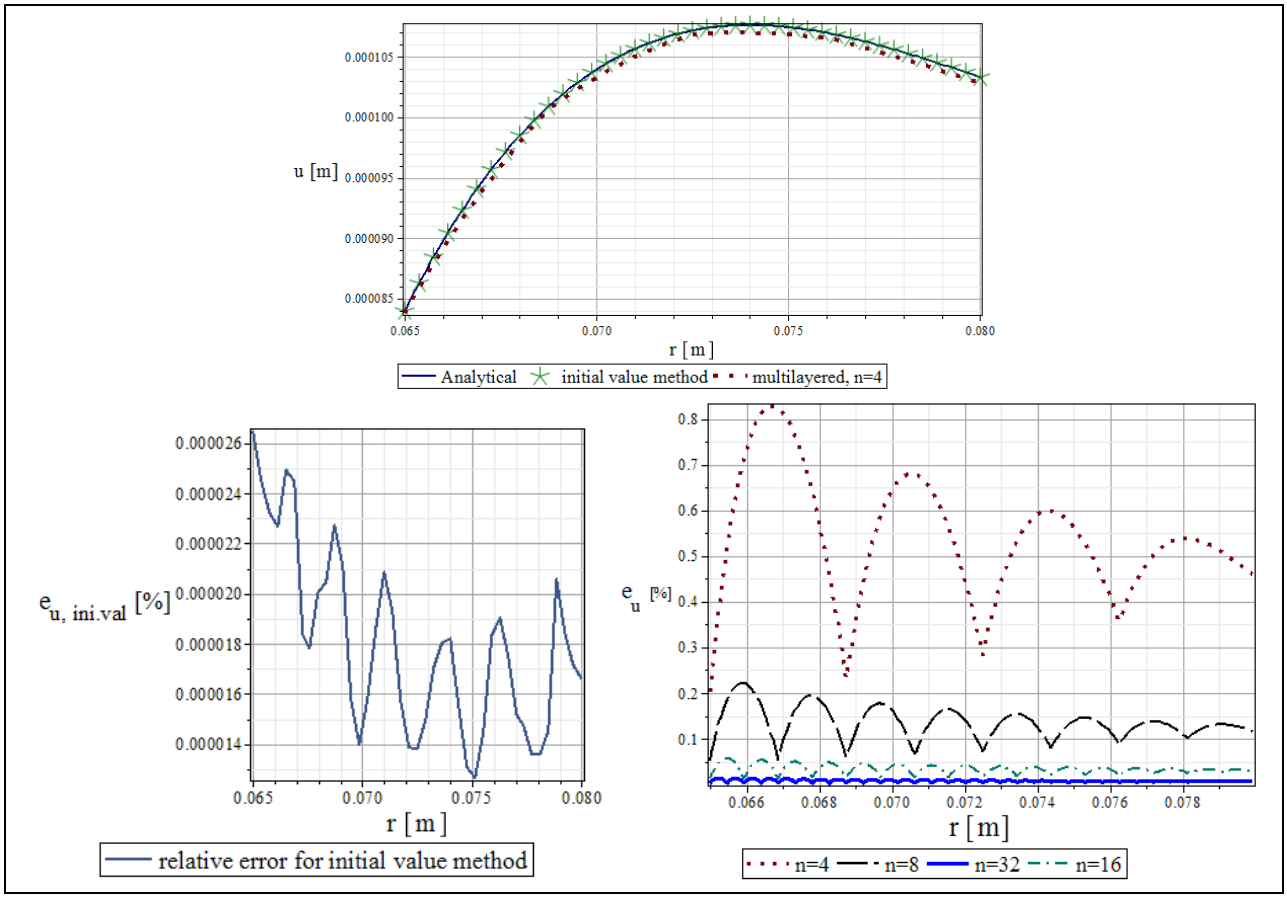

Figure 4.3. The plots and the relative errors for the displacement fields.

Figure 4.4 illustrates the radial normal stresses for the different methods.

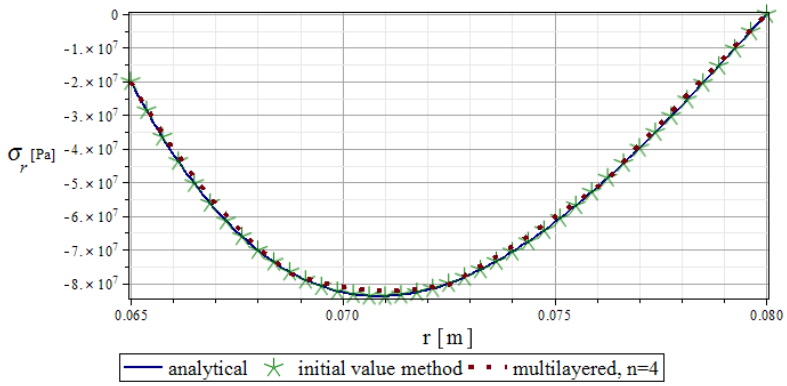

Figure 4.4. The graphs of the radial normal stresses.

The relative errors for the radial normal stresses can be seen in Fig. 4.5. The conclusions are the same as in the case of the displacement field.

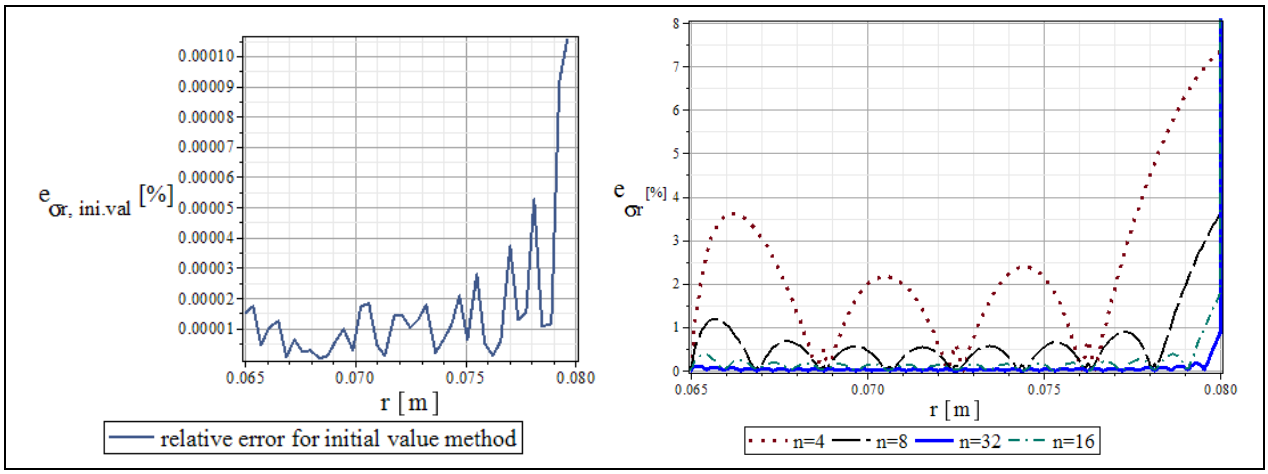

Figure 4.5. The relative errors of radial normal stresses.

Figures 4.6 and 4.7 show the results for the tangential normal stresses $\sigma_\varphi=\sigma_\vartheta$. The curve from Eqs. (3.2.28) is not continuous, but we can see that the values at the middle of the layers have good accuracy. With an approximation derived from Eq. (3.2.36) the accuracy can be greatly improved as we can see in Fig. 4.6: $\sigma_{\varphi-appr}(r) = F_{-2}r^{-2} + F_{-1}r^{-1} + F_0 + F_1 r + F_2 r^2 + F_3 r^3$

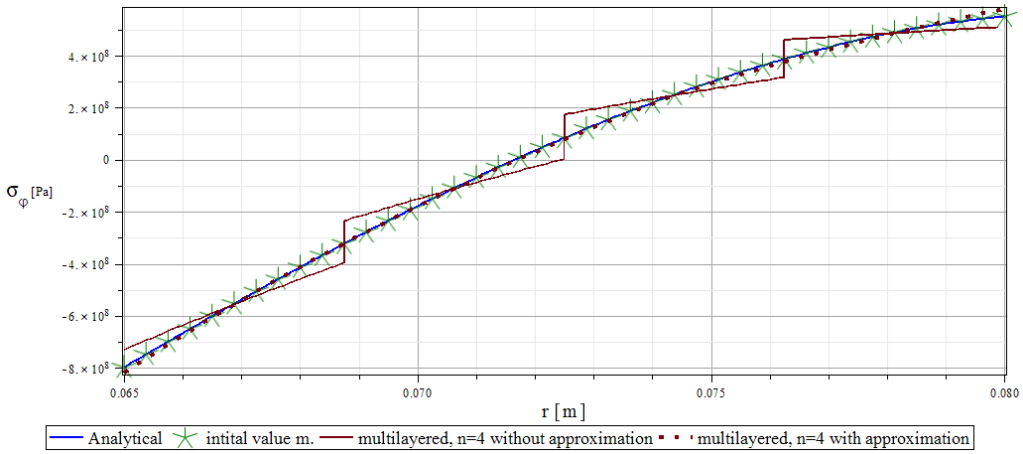

Figure 4.6. The graphs of the tangential normal stresses.

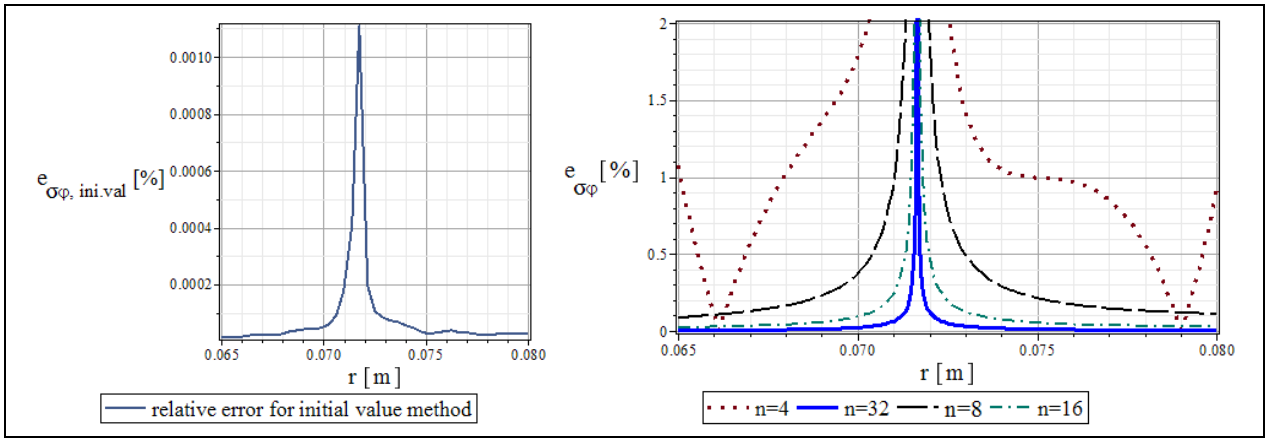

Figure 4.7. The relative errors for the tangential normal stresses.

With the approximation the relative errors can be decreased, and obviously the errors around the zero-beat of the tangential normal stress-function tend to infinity.

4.4.2. Example 5

In the second example a thermoelastic problem of a radially graded spherical pressure vessel with temperature-dependent material properties is investigated under axisymmetric thermal and mechanical loads. The results of the multilayered method presented in Sections 3.2 and the initial value method from Section 4.1 are compared to finite element simulation. The functions of the temperature-dependent functionally graded materials are described by Eqs. (2.4.1.) and (2.4.2). Table 4.2 shows the temperature coefficients of the steel – silicon nitride FGM. The other data of the radially graded spherical pressure vessel are:

$$d = 1\text{m}, h = 0.09\text{m}, t_{inner} = 420\text{K}, t_{outer} = 20\text{K}, p_1 = 150\text{MPa}, p_2 = 5\text{MPa}, m = 3.$$

Table 4.2. The material parameters for the investigated metal-ceramic FGM.

material property (M)	metal (stainless steel)				ceramic (silicon nitride)			
	P_{m0}	$P_{m1}(10^{-3})$	$P_{m2}(10^{-7})$	$P_{m3}(10^{-10})$	P_{c0}	$P_{c1}(10^{-3})$	$P_{c2}(10^{-7})$	$P_{c3}(10^{-11})$
λ(W/mK)	15.39	-1.264	20.92	-7.223	12.723	-1.032	5.466	-7.876
α (1/K)	$12.33\cdot10^{6}$	0.8086	0	0	$3.873\cdot10^{-6}$	0.9095	0	0
E (Pa)	$2.01\cdot10^{11}$	0.3079	-6.534	0	$3.484\cdot10^{11}$	-0.307	2.16	-8.946
ν (-)	0.3262	-0.1	3.797	0	0.24	0	0	0

The graphs of the material parameters at three temperature values and at three positions can be seen in Figs. 4.8-4.10.

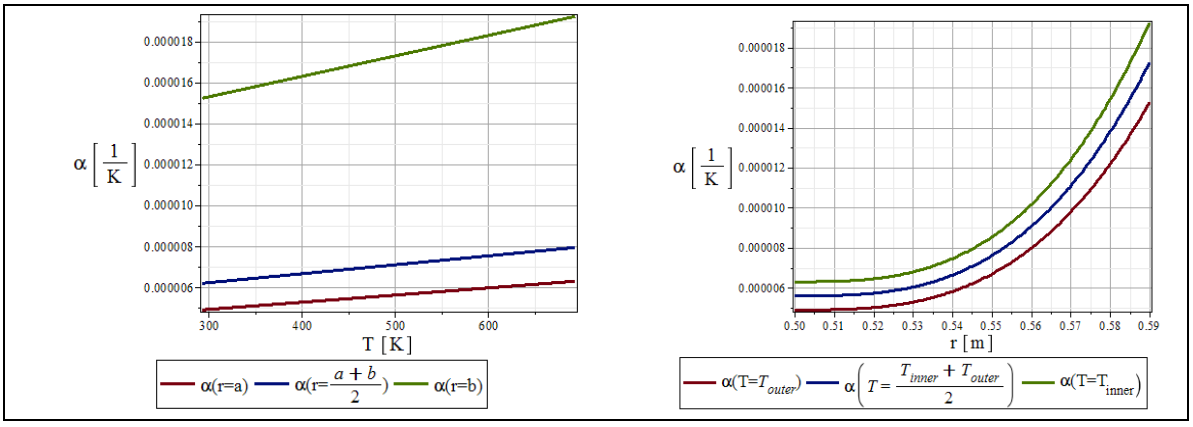

Figure 4.8. The curves of the temperature- and spatial- dependent coefficient of linear thermal expansion.

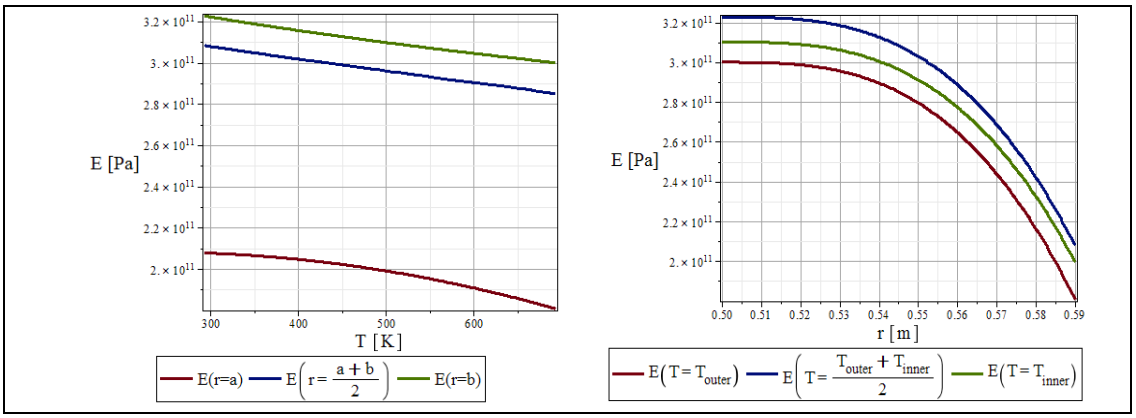

Figure 4.9. The curves of the temperature-dependent Young modulus of the steel – silicon nitrid FGM.

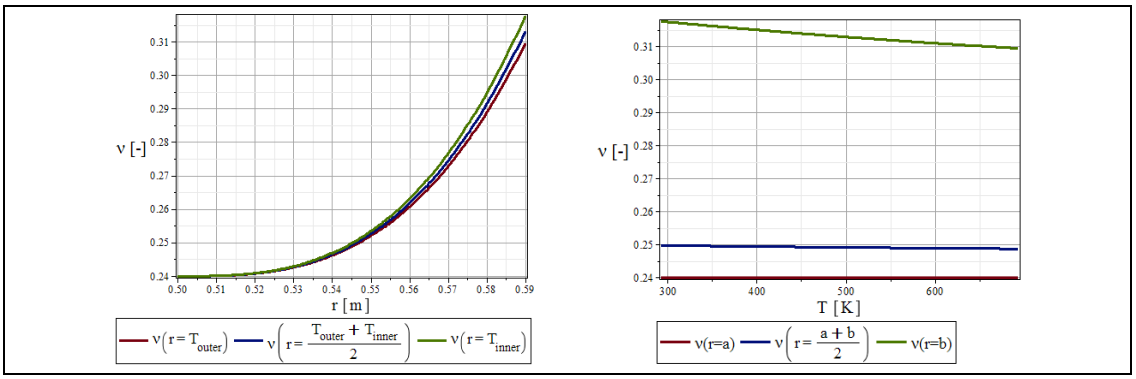

Figure 4.10. The graphs of the temperature- and spatial- dependent Poisson's ratio.

The numerical methods are compared to finite element models. The simulations were executed with Abaqus CAE finite element software. The problem is axisymmetric, so a quarter of the spherical vessel is modeled. The functionally graded sphere is modelled as a multilayered body. Due to the radial grading, the layers should be concentrical hollow spheres with *h/n* wall thickness and temperature-dependent properties. We allow the movement of the nodal points on the horizontal edge only in the horizontal direction, on the vertical edge only in the vertical direction as it is illustrated in Fig. 4.11. The mesh and the results for the displacement field are shown in Fig. 4.12.

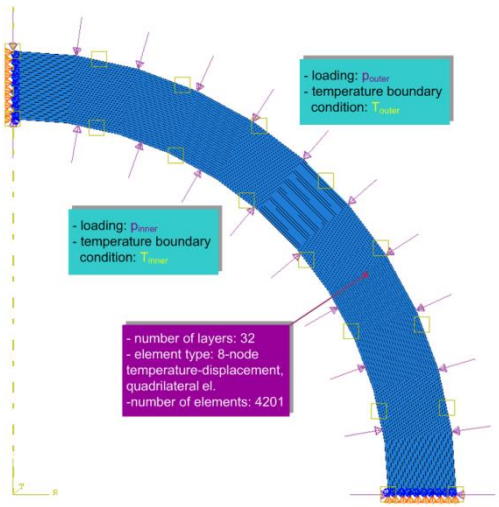

Figure 4.11. The finite element model of the sphere.

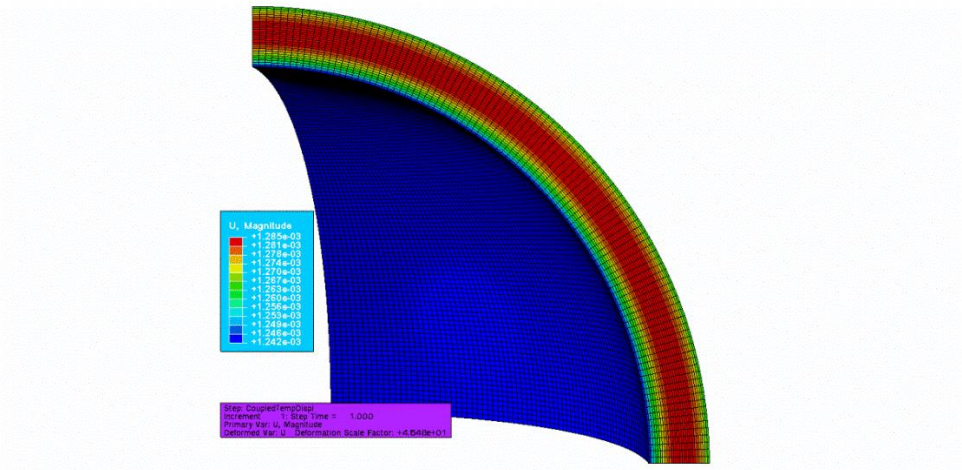

Figure 4.12. The mesh and the results of the FE simulation for the displacement field.

Figures 4.13-4.15 illustrate the graphs of the displacement fields and normal stresses for the finite element simulation, initial value method and the multilayered solutions by three different layer numbers. The results are in good agreement:

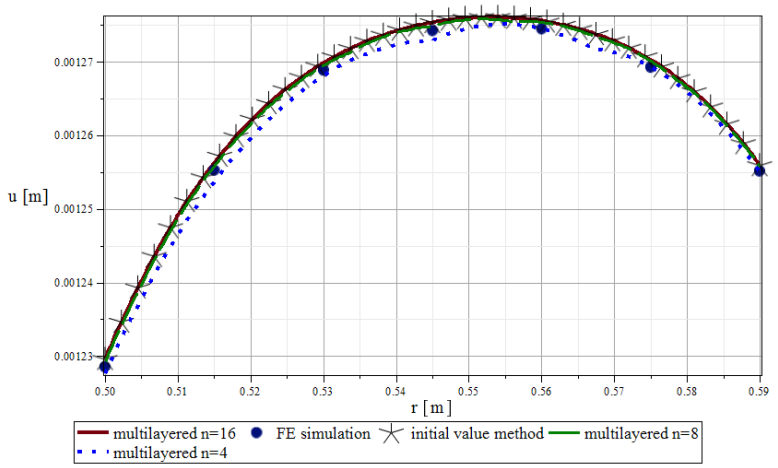

4.13. The graphs for the displacement fields.

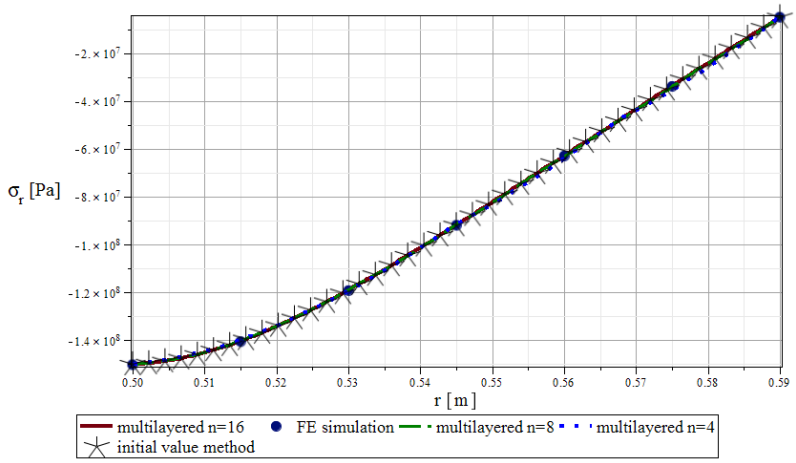

Figure 4.14. The graphs for the radial normal stresses.

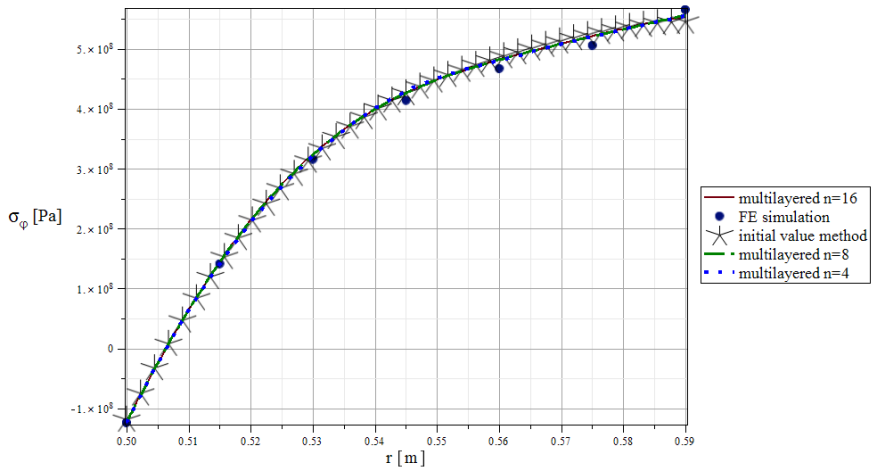

Figure 4.15. The graphs for the tangential normal stresses.

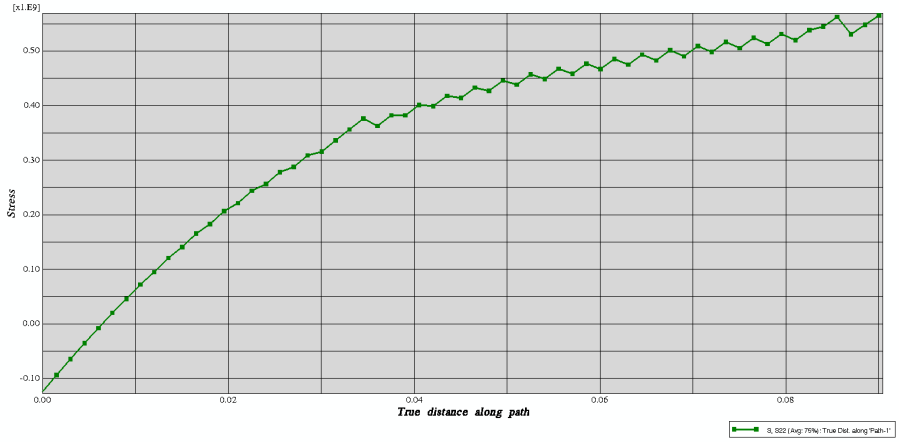

Figure 4.16. The result of the finite element simulation for the tangential normal stress.

In Figs. 4.16 and 4.17 the results of the finite element simulation are illustrated for the tangential normal stress and for the equivalent stress. The curves of these stresses fluctuate, generally at the boundary surfaces, which may lead to significant errors. In Fig 4.15, even by our multilayered method with *n*=4 layers and approximation, the solutions had high accuracy.

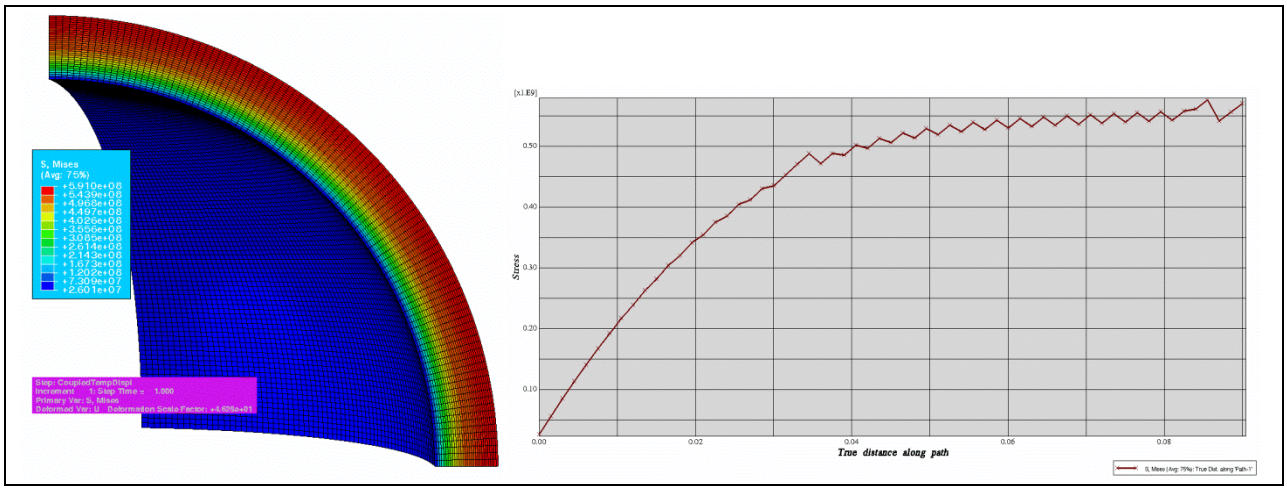

Figure 4.17. The equivalent stresses computed by the finite element software.

4.4.3. Example 6

In this subsection a problem of a thick-walled functionally graded piezoelectric spherical actuator is investigated. The method developed in Section 4.2 is compared to finite element solutions. The material at the inner radius of the sphere is Pzt-4 [57], [58] with the following parameters and data:

$$R_1 = 0.02\text{m},\ R_2 = 0.06\text{m},\ p_1 = 10\text{MPa},\ p_2 = 0\text{MPa},\ \phi_1 = -100\text{V},\ \phi_2 = 300\text{V},\ m_1 = m_2 = m_3 = m,$$

$$m = -2, S_0 = 5.552 \cdot 10^{-12}\,\text{Pa}, S_{130} = -2.1425 \cdot 10^{-12}\,\text{Pa},\ S_{330} = 8.0813 \cdot 10^{-12}\,\text{Pa},\ g_{310} = -0.010894 \frac{\text{m}^2}{\text{C}},$$

$$g_{330} = 0.025678 \frac{\text{m}^2}{\text{C}}, \beta_{330} = 8.9152 \cdot 10^7.$$

Figure 4.18 shows the finite element model for this example. The number of element rows are n=12. In Fig. 4.19 the comparison of the results of the finite element model and our method - Section 4.2- can be seen for the displacement field.

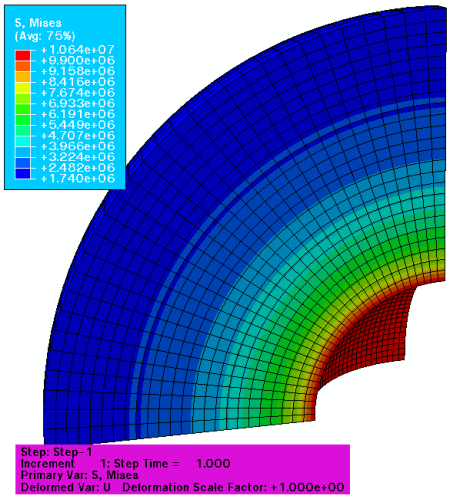

Figure 4.18. The finite element model for the piezoelectric problem.

The results show good agreement for the displacement field, but regarding of the radial normal stresses and electric potential the curves of the finite element simulation are fluctuating, as we can see in Figs. 4.20-4.22. According to Fig. 4.21, the worst results come from the tangential normal stresses –and for the equivalent stresses- of the finite element model. Our method produce more accurate solutions.

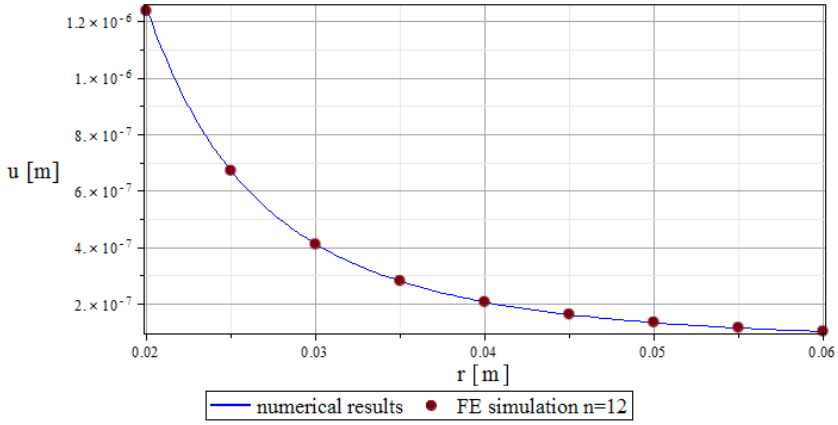

Figure 4.19. The graphs of the radial displacement field.

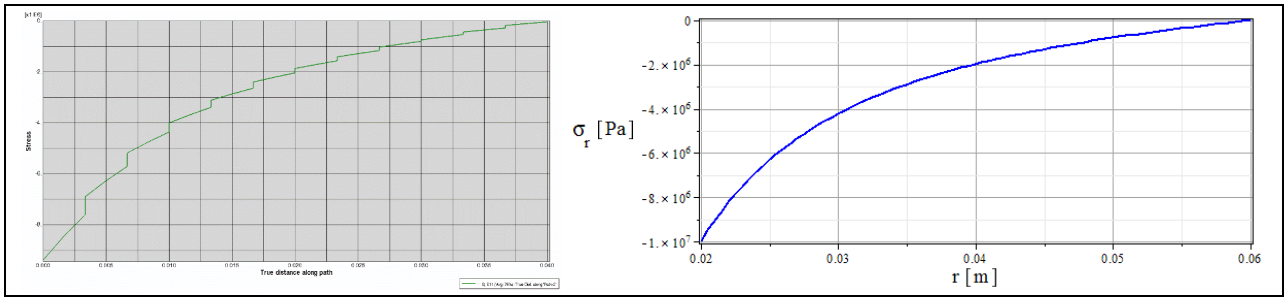

Figure 4.20. The results for the radial normal stresses (left: FE method, right: our numerical method).

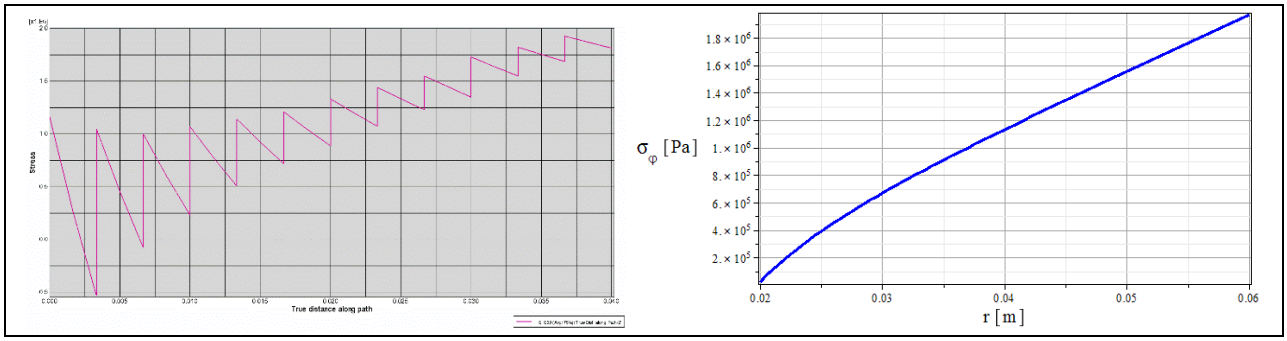

Figure 4.21. The graphs of the tangential normal stresses (left: FE method, right: our numerical method).

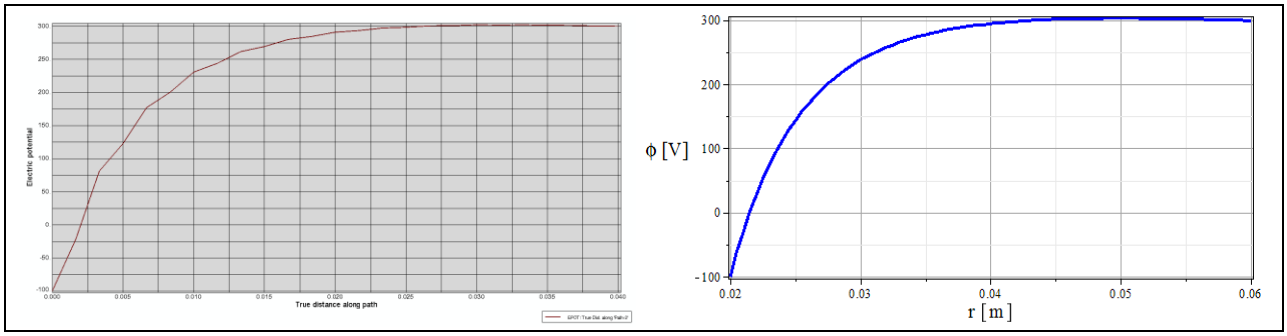

Figure 4.22. The graphs of the electric potential field (left: FE method, right: our numerical method).

4.4.4. Example 7

In this subsection a numerical example is presented for the problem of incompressible functionally graded sphere of Section 4.3. The following power-law functions will be used to describe the distribution of the material properties and temperature field within the radially graded sphere

$$\alpha(r)=\alpha_0\left(\frac{r}{R_1}\right)^{m_1},E(r)=E_0\left(\frac{r}{R_1}\right)^{m_2},\ T(r)=T_0 r^{m_3}, \tag{4.4.1}$$

and the other data are:

$$R_1=0.5\text{m},R_2=0.7\text{m},\alpha_0=1.2\cdot10^{-6}\frac{1}{\text{K}},E_0=210\text{GPa},T_0=1494\frac{\text{K}}{\text{m}^{m_3}},m_1=m_2=m,m_3=5.638,$$

$$p_1=30\text{MPa},\ p_2=0.$$

Figure 4.23 shows the curves of the radial normal stresses by three different values of power index m=(1, 0.2, 2). The tangential normal stresses can be seen in Fig. 4.24.

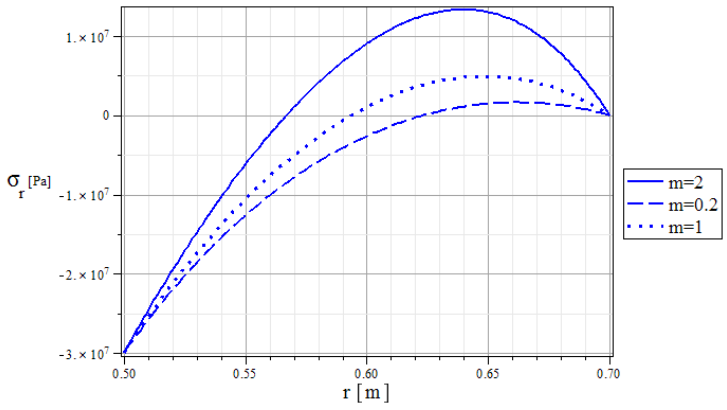

Figure 4.23. The plots of the radial normal stresses within the incompressible sphere.

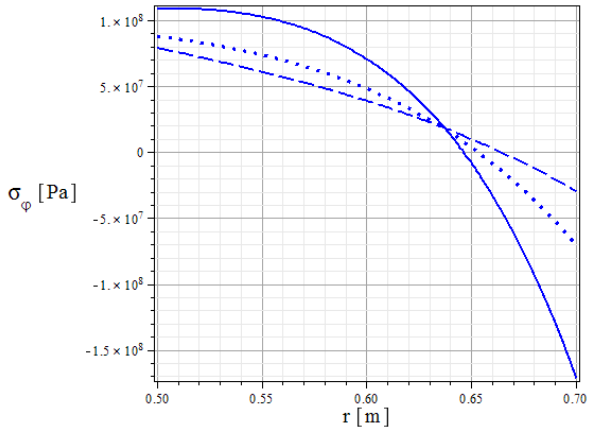

Figure 4.24. The plots of the tangential normal stresses within the incompressible sphere.

Next the solutions will be compared to finite element simulation. In the FE model the axisymmetric functionally graded sphere is modeled as a multilayered body with n=20

homogeneous spherical layers, as presented in [7]. In this case the displacement field can be seen in Fig. 4.25. The results for the normal stresses are identical to the previously presented plots.

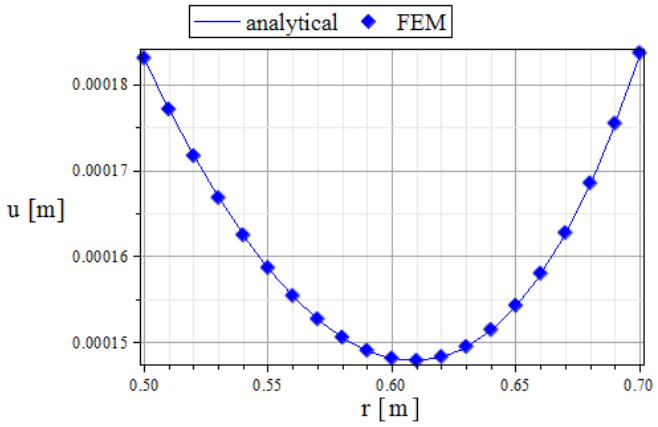

Figure 4.25. The comparison of the results for displacement field when m=2.

5. Thermoelastic problems of layered composite and functionally graded disks

In this chapter a few thermoelastic problems of thin functionally graded disks are investigated. At first the temperature fields will be presented in three cases with different boundary conditions and geometry. The next part is the determination of the displacements and stress field in rotating functionally graded and layered composite disks subjected to combined axisymmetric thermal and mechanical loads. Analytical solutions are presented for layered composite disks and for a radially graded disk where the material parameters follow a power-law distribution. Numerical solutions will be presented for radially graded disks made from functionally graded materials with arbitrary spatial and temperature-dependent parameters. The thickness of the disk in most cases will be arbitrary functions of the radial coordinate. Furthermore, numerical examples will be presented to compare the developed models to each other and to solutions obtained by finite element simulations.

Figure 5.1 shows the method which approximates the problem of functionally graded materials with multilayered approach similarly to the methods presented in the last two chapters. Cylindrical coordinate system *Orφz* will be used to solve these problems.

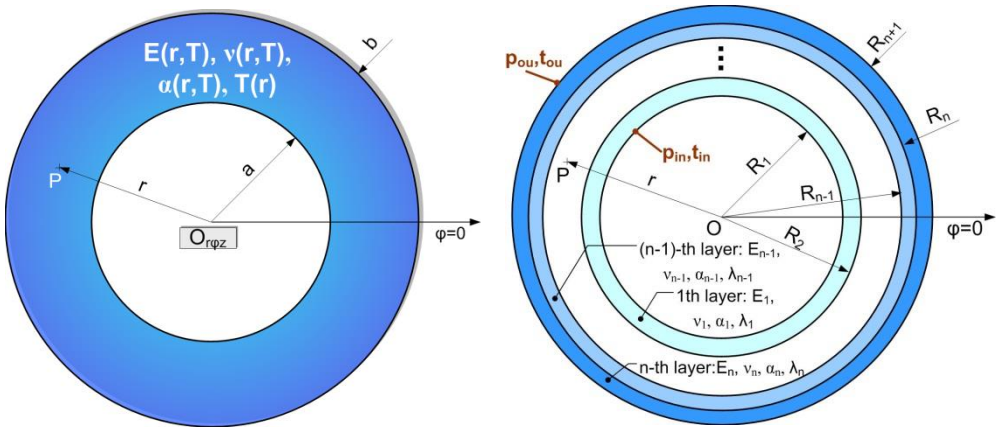

Figure 5.1. The functionally graded disk and its approximation with a multilayered model.

5.1. Temperature field in thin radially graded disks

In this section three cases will be investigated beside an analytical solution. In our first heat conduction problem a multilayered disk is investigated with thermal boundary conditions of the first kind on the cylindrical boundary surfaces and arbitrary convective heat transfer on the lower and upper plane boundary surfaces. In our second case the method of finite differences is used to solve the heat conduction problem of functionally graded disks with arbitrary thickness profile and boundary conditions of the third kind. The last method presents a solution for functionally graded disks with variable thickness and temperature-dependent material parameters using a multilayered approach.

5.1.1. Multilayered approach with Bessel functions

This subsection presents an analytical solution for the heat conduction problem of multilayered disks with constant thickness. Of course, this method can be used as a numerical approximate method for functionally graded materials and for arbitrary heat transfer coefficient where the parameters and the thickness profile are functions of the radial coordinate.

The temperatures of the cylindrical boundary surfaces are given, they are constant, non-time-dependent and denoted by t_1 and t_{n+1}, moreover there is symmetric convective heat exchange on the lower and upper plane boundary surfaces. It follows that the temperature field $T(r)$ is the function of the radial coordinate. Figure 5.2 illustrates the sketch of the heat conduction problem, where the heat transfer coefficient γ can be arbitrary functions of the radial coordinate. For radial coordinate-dependent thickness $h(r)$ and heat transfer, the parameters for the i-th layer can be computed as in Eqs. (3.2.1).

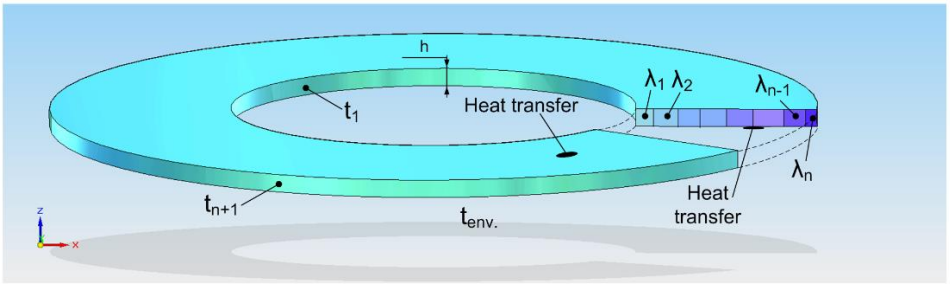

Figure 5.2. The sketch of heat conduction problem.

We assume that the temperature field T and the environmental temperature t_{env} is a continuous function of the radial coordinate. By the previously mentioned thermal boundary conditions the differential equation of the heat conduction in the layers has the following forms [59], [74]:

$$\nabla\left(t\mathbf{q}\right)+hT(r)=0, \qquad \frac{\mathrm{d}^2T}{\mathrm{d}r^2}+\frac{1}{r}\frac{\mathrm{d}T}{\mathrm{d}r}-p^2(T(r)-t_{env})=0\,, \tag{5.1.1}$$

where we have introduced the notation p as

$$p=\sqrt{\frac{2\gamma}{h\lambda}}\,,\ p_i=p(r=R_{mi}),\ h_i=h(r=R_{mi}),\text{etc.} \tag{5.1.2}$$

After solving Eq. (5.1.1), we get the temperature field of the i-th layer with the unknown constants of integration:

$$T_i(r)=C_iI_0(p_ir)+D_iK_0(p_ir)+t_{env}\,,\quad i=1,...,n. \tag{5.1.3}$$

Using the boundary conditions C_i and D_i can be evaluated, and with $t_{envi}=t_{env}(r=R_{mi})$ we have:

$$\begin{aligned}T_i(r)=&\frac{(t_i-t_{envi})K_0(p_iR_{i+1})-(t_{i+1}-t_{envi})K_0(p_iR_i)}{K_0(p_iR_{i+1})I_0(p_iR_i)-K_0(p_iR_i)I_0(p_iR_{i+1})}I_0(p_ir)+\\&+\frac{(-t_i-t_{envi})I_0(p_iR_{i+1})+(t_{i+1}-t_{envi})I_0(p_iR_i)}{K_0(p_iR_{i+1})I_0(p_iR_i)-K_0(p_iR_i)I_0(p_iR_{i+1})}K_0(p_ir)+t_{env}(r),\end{aligned} \tag{5.1.4}$$

where $I_0(x)$ and $K_0(x)$ are the Bessel functions of the first and second kind and of order zero [59]. We consider the case when the radial heatflow is constant, the temperatures of the inner and outer boundary surfaces are given. The surface temperatures of the adjacent layers are equal therefore we get the following equations for disks with constant thickness:

$$t_{i+1} = T_i(R_{i+1}) = T_{i+1}(R_{i+1}), \quad h_i q_i(R_{i+1}) = h_{i+1} q_{i+1}(R_{i+1}), \quad i = 1,\ldots,n-1, \tag{5.1.5}$$

$$q_i(r) = -\lambda_i p_i \frac{(t_i - t_{envi})K_0(p_i R_{i+1}) - (t_{i+1} - t_{envi})K_0(p_i R_i)}{K_0(p_i R_{i+1})I_0(p_i R_i) - K_0(p_i R_i)I_0(p_i R_{i+1})} I_1(p_i r) + \\ - \lambda_i p_i \frac{(-t_i - t_{envi})I_0(p_i R_{i+1}) + (t_{i+1} - t_{envi})I_0(p_i R_i)}{K_0(p_i R_{i+1})I_0(p_i R_i) - K_0(p_i R_i)I_0(p_i R_{i+1})} K_1(p_i r) \quad , \quad i = 1,\ldots,n, \tag{5.1.6}$$

where the thermal conductivity of the i-th layer λ_i is is calculated according to Eq. (3.2.1) in case of FGMs. The unknown temperature values of the boundary surfaces t_i can be calculated using the system of Eqs. (5.1.5-5.1.6).

5.1.2. Finite difference method

The sketch of this problem can be seen in Fig. 5.3. There are thermal boundary conditions of the third kind prescribed on the inner and outer cylindrical surfaces. γ_a and γ_b denote the heat transfer coefficients on the boundary surfaces, $t_{env,a}$ and $t_{env,b}$ are the environment temperatures at the inner and outer cylindrical surfaces, respectively. If $\gamma \to \infty$, then we have thermal boundary conditions of first kind on these surfaces. On the other two boundary surfaces the environmental temperatures are arbitrary functions of the radial coordinate, the heat transfer coefficient is coordinate and temperature-dependent.

The problem of the previously presented functionally graded disk will be solved based on the equations of the steady-state heat conduction. The approximate model can be seen in Fig. 5.4. The number of layers is n, the layers have constant thicknesses and the material properties are discretized. Furthermore it is assumed, that the layers are perfectly bonded.

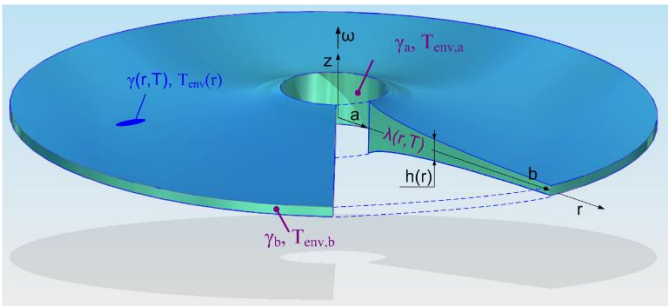

Figure 5.3. The disk with the thermal boundary conditions.

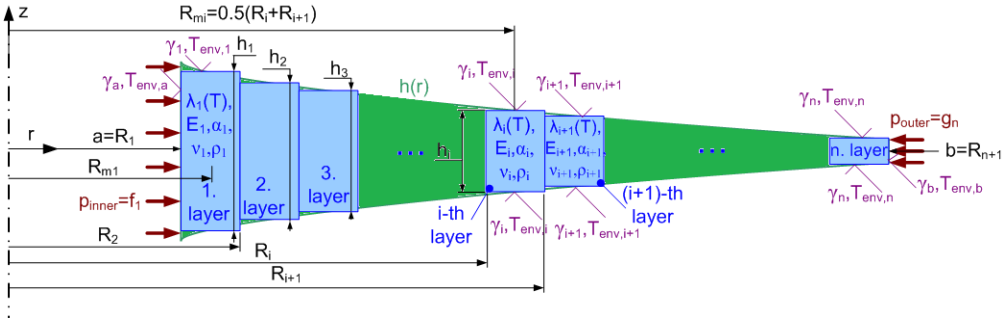

Figure. 5.4. The approximate model of the functionally graded disk.

The functionally graded disk is built from n layers with different $h_i>0$ uniform thickness (Fig. 5.4), the material parameters and the environmental temperature for the i-th layer can be discretized as

$$R_{mi}=\frac{R_i+R_{i+1}}{2},\lambda_i(T)=\lambda(r=R_{mi},T),\gamma_i=\gamma(r=R_{mi},T),$$
$$h_i=h(r=R_{mi}),t_{env,i}=T_{env}(r=R_{mi}),\ i=1,\ldots,n, \tag{5.1.7}$$

or using integral means similarly to Eqs. (3.2.1) and (3.2.2). For this case the nonlinear differential equation for the temperature field of the i-th layer ($T_i(r)$) has the following form [59]:

$$\frac{1}{r}\frac{\mathrm{d}}{\mathrm{d}r}\left(r\lambda_i(T_i(r))\frac{\mathrm{d}T_i(r)}{\mathrm{d}r}\right)-\frac{2\gamma_i(T_i(r))}{h_i}\left(T_i(r)-t_{env,i}\right)=0\,. \tag{5.1.8}$$

Finding the closed form analytical solution for Eq. (5.1.8) is very hard, therefore a numerical method will be utilized to solve this differential equation. The points of the temperature field will be calculated with the finite difference method. The nonlinear system of equations (with m points in each layer, the number of layers is n) for the whole model can be expressed as:

$$0=\frac{\lambda_i\left(T=t_{k+(i-1)n}\right)}{a+(i-1)d_m+k\Delta r}\frac{t_{k+(i-1)n}-t_{k+(i-1)n-1}}{\Delta r}+\frac{t_{k+(i-1)n}-t_{k+(i-1)n-1}}{\Delta r}\frac{\mathrm{d}\lambda_i\left(T=t_{k+(i-1)n}\right)}{\mathrm{d}r}+$$
$$+\frac{t_{k+(i-1)n+1}-2t_{k+(i-1)n}+t_{k+(i-1)n-1}}{\Delta r^2}\lambda_i\left(T=t_{k+(i-1)n}\right)-\frac{2\gamma_i(T=t_{k+(i-1)n})}{h_i}\left(t_{k+(i-1)n}-t_{env,i}\right), \tag{5.1.9}$$
$$d_m=\frac{b-a}{n},\ \Delta r=\frac{b-a}{nm},\quad i=1,\ldots,m,\ \text{while}\ k=1,\ldots,n-1.$$

If the thermal conductivity has the form of Eqs. (2.4.1) and (2.4.2) then we can get for the previous system of Eq. (5.1.9):

$$\lambda_i\left(T=t_{k+(i-1)n}\right)=L_{0,i}+L_{-1,i}t_{k+(i-1)n}^{-1}+L_{1,i}t_{k+(i-1)n}+L_{2,i}t_{k+(i-1)n}^2+L_{3,i}t_{k+(i-1)n}^3\,, \tag{5.1.10}$$

$$\frac{\mathrm{d}\lambda_i\left(T=t_{k+(i-1)n}\right)}{\mathrm{d}r}=\left(-L_{-1,i}t_{k+(i-1)n}^{-2}+L_{1,i}+2L_{2,i}t_{k+(i-1)n}+3L_{3,i}t_{k+(i-1)n}^2\right)\frac{t_{k+(i-1)n}-t_{k+(i-1)n-1}}{\Delta r}, \tag{5.1.11}$$

where

$$L_{-1,i}=\left(P_{-1}^{1}\lambda_0^1-P_{-1}^{2}\lambda_0^2\right)\cdot G(r=R_{mi})+P_{-1}^{2}\lambda_0^2,\ L_{0,i}=\left(\lambda_0^1-\lambda_0^2\right)\cdot G(r=R_{mi})+\lambda_0^2,$$
$$L_{1,i}=\left(P_1^1\lambda_0^1-P_1^2\lambda_0^2\right)\cdot G(r=R_{mi})+P_1^2\lambda_0^2, L_{2,i}=\left(P_2^1\lambda_0^1-P_2^2\lambda_0^2\right)\cdot G(r=R_{mi})+P_2^2\lambda_0^2, \quad (5.1.12)$$
$$L_{3,i}=\left(P_3^1\lambda_0^1-P_3^2\lambda_0^2\right)\cdot G(r=R_{mi})+P_3^2\lambda_0^2,$$

where λ_0^j (j=1,2: number of the constituent material) are material constants, constants P_l^j (j=1,2 and l = -1,0,1,2,3) are temperature coefficients. We assume that the surface temperatures of the adjacent layers are equal and the radial heatflow q is constant.

$$-h_i\lambda_i\left(T=t_{(i-1)n}\right)\frac{t_{(i-1)n+1}-t_{(i-1)n}}{\Delta r}=-h_{i-1}\lambda_{i-1}\left(T=t_{(i-1)n}\right)\frac{t_{(i-1)n}-t_{(i-1)n-1}}{\Delta r},\quad i=2,...,m. \quad (5.1.13)$$

From the thermal boundary conditions of the third kind it follows that

$$\frac{t_2-t_1}{\Delta r}-(t_1-t_{env,a})h_1(T=t_1)=0,\ \ \frac{t_{nm}-t_{nm-1}}{\Delta r}+(t_{nm}-t_{env,b})h_n(T=t_{nm})=0. \quad (5.1.14)$$

The points of the temperature field can be calculated from the solution of the nonlinear system of equations (5.1.9), (5.1.13) and (5.1.14). Then a polynomial curve will be fitted to these values (via least squares method), the recommended form for power-law distributions for smaller power index values (m<7) is:

$$T_{appr}=\vartheta_6 r^6+\vartheta_5 r^5+\vartheta_4 r^4+\vartheta_3 r^3+\vartheta_2 r^2+\vartheta_1 r+\vartheta_0+\vartheta_{-1}r^{-1}+\vartheta_{-2}r^{-2}+\vartheta_{-3}r^{-3}. \quad (5.1.15)$$

5.1.3. Temperature-dependent heat conduction equation

In this subsection a numerical method is presented to approximate the temperature field of radially graded disks –and cylinders- made from functionally graded materials with arbitrary spatial- and temperature-dependent thermal conductivity. A multilayered model is derived where the disks are made from homogeneous layers with arbitrary temperature-dependent materials as we saw in Subsection 3.2.2. The thermal boundary conditions are boundary conditions of the first kind t_1 and t_{n+1} on the inner and outer cylindrical surfaces. There are n layers, the thermal conductivity is arbitrary function of the temperature. Two cases will be investigated, the equations will be derived for disks with constant thickness and with arbitrary thickness profile $h(r)$. For each layer we have

$$\lambda_i(T)=\lambda(r=R_{mi},T), t_i=T_i(R_i)=T_{i-1}(R_i),\quad i=1,...,n. \quad (5.1.16)$$

For this case the nonlinear differential equation for the temperature field of the i-th layer $T_i(r)$ can be presented as:

$$\frac{1}{r}\frac{\mathrm{d}}{\mathrm{d}r}\left[\lambda_i(T(r))\cdot r\frac{\mathrm{d}T_i(r)}{\mathrm{d}r}\right]=0,\quad R_i\le r\le R_{i+1},\ i=1,...,n. \quad (5.1.17)$$

With the Kirchoff integral transformation this problem becomes linear

$$\theta=\int_0^{T_i}\lambda(\vartheta)\mathrm{d}\vartheta,\quad \frac{1}{r}\frac{\mathrm{d}}{\mathrm{d}r}\left[r\frac{\mathrm{d}\theta}{\mathrm{d}r}\right]=0. \quad (5.1.18)$$

With the solution of the previous differential equation we obtain $\Theta(r)$ and its boundary conditions

$$\theta_i(r) = C_{i1}\ln(r) + C_{i2},\quad \int_0^{t_i} \lambda_i(\vartheta)\mathrm{d}\vartheta = C_{i1}\ln(R_i) + C_{i2},\quad \int_0^{t_{i+1}} \lambda_{i+1}(\vartheta)\mathrm{d}\vartheta = C_{i1}\ln(R_{i+1}) + C_{i2}. \quad (5.1.19)$$

The solution for the temperature field within the *i*-th layer assumes the implicit forms

$$\theta_i(r) = \int_0^{T_i(r)} \lambda_i(\vartheta)\mathrm{d}\vartheta = \ln(r)\frac{R_i R_{i+1}}{R_{i+1}-R_i}\int_{t_i}^{t_{i+1}} \lambda_i(\vartheta)\mathrm{d}\vartheta + \int_0^{t_i} \lambda_i(\vartheta)\mathrm{d}\vartheta + \frac{R_{i+1}}{R_{i+1}-R_i}\int_{t_i}^{t_{i+1}} \lambda_i(\vartheta)\mathrm{d}\vartheta, \quad (5.1.20)$$

$$\int_{t_i}^{T_i(r)} \lambda_i(\vartheta)\mathrm{d}\vartheta = \frac{R_{i+1}}{R_{i+1}-R_i}\left(R_i\ln(r)+1\right)\int_{t_i}^{t_{i+1}} \lambda_i(\vartheta)\mathrm{d}\vartheta\ ,\ i=1,...,n\,. \quad (5.1.21)$$

In the case of disks with constant thickness, we assume that the surface temperatures t_i of the adjacent layers are equal and the radial heatflow q is – according to Fourier's law:

$$\left[\lambda_i \frac{\mathrm{d}T_i(r)}{\mathrm{d}r}\right]_{r=R_{i+1}} = q_i(R_{i+1}) = q_{i+1}(R_{i+1}) = \left[\lambda_{i+1}\frac{\mathrm{d}T_{i+1}(r)}{\mathrm{d}r}\right]_{r=R_{i+1}},\ i=1,...,n-1. \quad (5.1.22)$$

After the manipulation of Eqs (5.1.21-5.1.22) the unknown t_i (i=2, ...,n) boundary temperatures of the layers can be calculated from the following system of equations

$$\int_{t_{i+1}}^{t_{i+2}} \lambda_{i+1}(\vartheta)\mathrm{d}\vartheta\frac{R_{i+2}R_{i+1}}{R_{i+2}-R_{i+1}} = \int_{t_i}^{t_{i+1}} \lambda_i(\vartheta)\mathrm{d}\vartheta\frac{R_{i+1}R_i}{R_{i+1}-R_i} \to t_i,\ \ i=2,...,n, \quad (5.1.23)$$

moreover t_1 and t_{n+1} temperatures are given. Here it is recommended that instead of using Eqs. (5.1.20) and (5.1.21) to compute the function of the temperature we will fit a curve or curves -for example with the least squares method- to the temperature values t_i obtained by Eq. (5.1.23) in order to make the further calculations, especially the integrations easier and faster. The approximation function has the following form – in case of power-law distribution with $|m|<6$:

$$T_{appr}(r) = \theta_{-2}r^{-2} + \theta_{-1}r^{-1} + \theta_0 + \theta_1 r + \theta_2 r^2\,. \quad (5.1.24)$$

In order to make the approximation more accurate more polynomial curves can be used to build the approximated temperature function.

In the case when the disk has arbitrary $h(r)$ thickness, we will consider n layers with n different $h_i=h(r=R_{mi})>0$ values similarly to the method presented in Subsection 5.1.2.

$$\left[h_i\lambda_i\frac{\mathrm{d}T_i(r)}{\mathrm{d}r}\right]_{r=R_{i+1}} = \left[h_{i+1}\lambda_{i+1}\frac{\mathrm{d}T_{i+1}(r)}{\mathrm{d}r}\right]_{r=R_{i+1}}, \quad (5.1.25)$$

$$const. = \int_{t_i}^{t_{i+1}} \lambda_i(\vartheta)\mathrm{d}\vartheta\frac{R_{i+1}R_i}{R_{i+1}-R_i}h_i \to t_i \quad i=2,...,n. \quad (5.1.26)$$

The accuracy of this method is similar to the method presented in Subsection 3.2.2.

5.1.4. Analytical formulation when the temperature dependence is neglected

In this subsection it is assumed that the thermal conductivity depends on the radial coordinate and the temperature values are given at the inner and outer cylindrical boundary surfaces of the

functionally graded disk (t_1 and t_2, respectively) so we have the following thermal boundary conditions of first kind:

$$T(R_1) = t_1, \quad T(R_2) = t_2. \tag{5.1.27}$$

The steady-state temperature field -without internal heat sources- satisfies the next equation [59]

$$\frac{1}{r}\frac{\mathrm{d}}{\mathrm{d}r}\left[r\lambda(r)\frac{\mathrm{d}T}{\mathrm{d}r} \right] = 0, \;\; R_1 \le r \le R_2, \tag{5.1.28}$$

where the thermal conductivity of the functionally graded material $\lambda=\lambda(r)$ is arbitrary function of the radial coordinate r. The solution of Eq. (5.1.28) under the current boundary conditions gives the temperature distribution along the radial coordinate

$$T(r) = t_1 + \frac{t_2 - t_1}{\int\limits_{R_1}^{R_2} \frac{1}{\rho\lambda(\rho)}\mathrm{d}\rho} \int\limits_{R_1}^{r} \frac{1}{\rho\lambda(\rho)}\mathrm{d}\rho, \;\; R_1 \le r \le R_2. \tag{5.1.29}$$

5.2. Numerical solutions with multilayered approach

In this section the thermoelastic problems of rotating disks and cylinders will be solved with the superposition of two separated cases, a mechanical loading without thermal load, and a prescribed thermal load on the cylindrical boundary surfaces without mechanical loading. The method derived for thin functionally graded disks can be used as analytical solutions for layered composite disks with constant thickness.

5.2.1. Multilayered approach for thin functionally graded disks

In this subsection a numerical method is presented to determine the displacement field and thermal stresses in functionally graded rotating disks with arbitrary axisymmetric thickness profile $h(r)$. The model is similar to the one presented in Section 3.2 for spheres. The thermoelastic problem is split into two part, then the superposition principle is used to solve it.

The previously determined temperature field is the input of this method, the material parameters for each layer can be discretized as

$$\begin{gathered} E_i = E(r = R_{mi}, T = t_{mi}),\ \nu_i = \nu(r = R_{mi}, T = t_{mi}), \alpha_i = \alpha(r = R_{mi}, T = t_{mi}), \\ \rho_i = \rho(r = R_{mi}, T = t_{mi}), \;\; i = 1, \ldots, n, \end{gathered} \tag{5.2.1}$$

then we consider the case when the i-th layer is under thermal loading and has a steady-state temperature field. The stresses on the curved boundary surfaces of the layers have zero values.

The $u_i^T(r)$ thermal radial displacement and the $\sigma_{ir}^T(r)$, $\sigma_{i\varphi}^T(r)$ thermal stresses can be formulated as [52]:

$$u_i^T(r)=\frac{1+\nu_i}{r}\alpha_i\int_{R_i}^{r} rT_i(r)\mathrm{d}r+\frac{(1+\nu_i)R_i^2+(1-\nu_i)r^2}{r(R_{i+1}^2-R_i^2)}\alpha_i\int_{R_i}^{R_{i+1}} rT_i(r)\mathrm{d}r, \tag{5.2.2}$$

$$\sigma_{ir}^T(r)=-\frac{\alpha_i E_i}{r^2}\int_{R_i}^{r} rT_i(r)\mathrm{d}r+\frac{\alpha_i E_i}{R_{i+1}^2-R_i^2}\left(1-\frac{R_i^2}{r^2}\right)\int_{R_i}^{R_{i+1}} rT_i(r)\mathrm{d}r\,, \tag{5.2.3}$$

$$\sigma_{i\varphi}^T(r)=\frac{\alpha_i E_i}{r^2}\int_{R_i}^{r} rT_i(r)\mathrm{d}r-E_i\alpha_i T_i(r)+\frac{\alpha_i E_i}{R_{i+1}^2-R_i^2}\left(1+\frac{R_i^2}{r^2}\right)\int_{R_i}^{R_{i+1}} rT_i(r)\mathrm{d}r,\ i=1,\ldots,n. \tag{5.2.4}$$

In the previous expressions the index i refers to the i-th layer, the sketch of a layer with the loads is illustrated in Fig. 5.5.

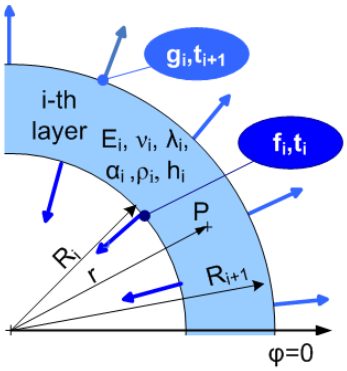

Figure 5.5. The cross section of a quarter of the i-th layer.

In the next step it is assumed that the inner and outer cylindrical boundary surfaces of the i-th layer are under constant mechanical loading $f_i=\sigma_{ir}^M(R_i)$ and $g_i=\sigma_{ir}^M(R_{i+1})$. The differential equation of the radial displacement field, derived from the equilibrium equation (Section 2.2):

$$\frac{\mathrm{d}\sigma_r}{\mathrm{d}r}+\frac{\sigma_r-\sigma_\varphi}{r}+\rho\omega^2 r=0, \tag{5.2.5}$$

$$\frac{\mathrm{d}^2u_i^M(r)}{\mathrm{d}r^2}+\frac{\mathrm{d}u_i^M(r)}{\mathrm{d}r}\frac{1}{r}-\frac{u_i^M(r)}{r^2}+K_i r=0\,, \tag{5.2.6}$$

where

$$K_i=\frac{(1-\nu_i^2)\rho_i\omega^2}{E_i}\,. \tag{5.2.7}$$

In the expression of K_i, ρ_i is the density of the i-th layer and ω is the angular velocity of the rotating disk. Furthermore the strain-displacement and stress-strain relations for homogeneous disks can be expressed (Section 2.2) as

$$\varepsilon_r=\frac{\mathrm{d}u}{\mathrm{d}r},\quad \varepsilon_\varphi=\frac{u}{r},$$
$$\sigma_r=\frac{E}{1-\nu^2}\left[\varepsilon_r+\nu\varepsilon_\varphi-\alpha(1+\nu)T\right],\quad \sigma_\varphi=\frac{E}{1-\nu^2}\left[\nu\varepsilon_r+\varepsilon_\varphi-\alpha(1+\nu)T\right]. \tag{5.2.8}$$

After solving Eq. (5.2.6) we get the following expressions for the displacement field and the normal stresses:

$$u_i^M(r) = C_i r + \frac{B_i}{r} - \frac{K_i}{8} r^3, \tag{5.2.9}$$

$$\sigma_{ir}^M(r) = \frac{E_i C_i}{1-\nu_i} - \frac{E_i B_i}{1+\nu_i}\frac{1}{r^2} - A_i r^2, \qquad A_i = \frac{E_i(3+\nu_i)K_i}{8(1-\nu_i^2)}, \tag{5.2.10}$$

$$\sigma_{i\vartheta}^M(r) = \sigma_{i\varphi}^M(r) = \frac{E_i C_i}{1-\nu_i} + \frac{E_i B_i}{1+\nu_i}\frac{1}{r^2} - A_i r^2, \; i = 1,\ldots,n. \tag{5.2.11}$$

Using the equations of the boundary conditions, the unknown parameters B_i and C_i can be determined as

$$B_i = \frac{(1+\nu_i)R_{i+1}^2 R_i^2 (A_i(R_i^2 - R_{i+1}^2) + f_i - g_i)}{E_i(R_i^2 - R_{i+1}^2)}, \tag{5.2.12}$$

$$C_i = \frac{(1-\nu_i)(A_i(R_{i+1}^4 - R_i^4) + R_{i+1}^2 g_i - R_i^2 f_i)}{E_i\left(R_i^2 - R_{i+1}^2\right)}. \tag{5.2.13}$$

The superposition principle can be utilized for this problem, because both the previously used field equations and boundary conditions are linear. This means that we can add the stresses and displacements caused by mechanical loads (5.2.8-5.2.13) to the thermal stresses and displacements (5.2.2-5.2.4) in order to solve this problem. For the computation of the radial displacement, radial and tangential stresses the following equations are used:

$$u_i(r) = u_i^T(r) + u_i^M(r), \tag{5.2.14}$$

$$\sigma_{ir}(r) = \sigma_{ir}^T(r) + \sigma_{ir}^M(r), \tag{5.2.15}$$

$$\sigma_{i\varphi}(r) = \sigma_{i\varphi}^T(r) + \sigma_{i\varphi}^M(r), \; i = 1,\ldots,n. \tag{5.2.16}$$

The unknown parameters f_i (i=2...n) and g_i (i=1...n-1) in the equations of $u_i^M(r)$, $\sigma_{ir}^M(r)$, $\sigma_{i\varphi}^M(r)$ can be calculated from the following equations

$$u_i(R_{i+1}) = u_{i+1}(R_{i+1}), \; i = 1,\ldots,n-1, \tag{5.2.17}$$

which ensure the continuity of the radial displacement field furthermore f_1 and f_{n+1} are given.

$$\sigma_{1r}(R_1) = f_1 = -p_{inner}, \; \sigma_{nr}(R_{n+1}) = g_n = -p_{outer}. \tag{5.2.18}$$

The system of equations (5.2.17) has the following form:

$$u_{i+1}^T(R_{i+1}) - u_i^T(R_{i+1}) =$$

$$\left[\frac{(1-\nu_i)(A_i(R_{i+1}^4 - R_i^4) + R_{i+1}^2 g_i - R_i^2 f_i)}{E_i\left(R_i^2 - R_{i+1}^2\right)} R_{i+1} + \frac{(1+\nu_i)R_{i+1}^2 R_i^2 (A_i(R_i^2 - R_{i+1}^2) + f_i - g_i)}{E_i(R_i^2 - R_{i+1}^2)R_{i+1}} - \frac{K_i}{8} R_{i+1}^3\right] -$$

$$-\left[\frac{(1-\nu_{i+1})(A_{i+1}(R_{i+2}^4 - R_{i+1}^4) + R_{i+2}^2 g_{i+1} - R_{i+1}^2 f_{i+1})}{E_{i+1}\left(R_{i+1}^2 - R_{i+2}^2\right)} R_{i+1} + \frac{(1+\nu_{i+1})R_{i+1}^2 R_{i+2}^2 (A_{i+1}(R_{i+1}^2 - R_{i+2}^2) + f_{i+1} - g_{i+1})}{E_{i+1}(R_{i+1}^2 - R_{i+2}^2)R_{i+1}} - \frac{K_{i+1}}{8} R_{i+1}^3\right],$$

$$h_i g_i = h_{i+1} f_{i+1}. \tag{5.2.19}$$

Using the previously determined parameters f_i and equations (5.2.14-5.2.16) the radial displacement and the normal stresses of the multilayered disk can be evaluated by summation. Because of the multilayered model the curve of the tangential normal stress may contain significant

steps, but the stress values in the middle of each layer have good accuracy (as we saw in Chapter 4). Thus an approximate curve can be fitted to these points (for example using the least squares method) to increase the accuracy and the convergence of the method. Furthermore the accuracy of the method can be improved according to Subsection 3.2.6.

5.2.2. Layered composite cylindrical bodies

In this subsection the method presented in Subsection 5.2.1 will be applied to layered cylinders where the homogeneous layers are only radially bonded -but not axially, for example in the case of tubes with additional layers made from thermal insulation materials. For this problem a cylindrical coordinate system $Or\varphi z$ will be used. The axisymmetric temperature field and mechanical loading do not depend on the axial coordinate z and on the tangential coordinate φ. To determine the thermal stresses, the equations of generalized plane strain will be used.

$$\sigma_{ir}^{T}(R_i)=\sigma_{ir}^{T}(R_{i+1})=0,\ \ N_i^{T}=2\pi\int_{R_i}^{R_{i+1}} r\sigma_{iz}^{T}(r)\mathrm{d}r=0,\ \ i=1,\ldots,n\,. \tag{5.2.20}$$

The $u_i{}^T(r)$ thermal radial displacement and the $\sigma_{ir}{}^T(r)$, $\sigma_{i\varphi}{}^T(r)$, $\sigma_{iz}{}^T(r)$ thermal normal stresses can be formulated as:

$$u_i^{T}(r)=\frac{1+\nu_i}{1-\nu_i}\alpha_i\left\{\frac{1}{r}\int_{R_i}^{r}\left[T(\rho)\rho\right]\mathrm{d}\rho+\left[\frac{1-3\nu}{1+\nu}r+\frac{R_i^2}{r}\right]\frac{1}{R_{i+1}^2-R_i^2}\int_{R_i}^{R_{i+1}}\left[T(\rho)\rho\right]\mathrm{d}\rho\right\}, \tag{5.2.21}$$

$$\sigma_{ir}^{T}(r)=\frac{2\alpha_i G_i(1+\nu_i)}{1-\nu_i}\left[-\frac{1}{r^2}\int_{R_i}^{r}\rho T(\rho)\mathrm{d}\rho+\frac{r^2-R_i^{\,2}}{r^2(R_{i+1}^2-R_i^2)}\int_{R_i}^{R_{i+1}}\rho T(\rho)\mathrm{d}\rho\right], \tag{5.2.22}$$

$$\sigma_{i\varphi}^{T}(r)=\frac{2\alpha_i G_i(1+\nu_i)}{1-\nu_i}\left[\frac{1}{r^2}\int_{R_i}^{r}\rho T(\rho)\mathrm{d}\rho+\frac{r^2+R_i^{\,2}}{r^2(R_{i+1}^2-R_i^2)}\int_{R_i}^{R_{i+1}}\rho T(\rho)\mathrm{d}\rho-T(r)\right], \tag{5.2.23}$$

$$\sigma_{iz}^{T}(r)=\frac{2\alpha_i G_i(1+\nu_i)}{1-\nu_i}\left[\frac{2}{R_{i+1}^2-R_i^2}\int_{R_i}^{R_{i+1}}\rho T(\rho)\mathrm{d}\rho-T(r)\right],\ i=1,\ldots,n\,. \tag{5.2.24}$$

The mechanical part of this problem has the following solutions:

$$u_i^{M}(r)=\frac{1}{2G_i}\left(\frac{1-\nu_i}{1+\nu_i}C_{i1}r+\frac{C_{i2}}{r}\right), \tag{5.2.25}$$

$$\sigma_{ir}^{M}=C_{i1}-\frac{C_{i2}}{r^2},\ \sigma_{i\varphi}^{M}=C_{i1}+\frac{C_{i2}}{r^2},\ \sigma_{iz}^{M}=0, \tag{5.2.26}$$

$$C_{i1}=\frac{f_{i+1}R_{i+1}^2-f_iR_i^2}{R_{i+1}^2-R_i^{\,2}},\quad C_{2i}=\frac{R_{i+1}^2R_i^2}{R_{i+1}^2-R_i^{\,2}}(f_{i+1}-f_i),\quad i=1,\ldots,n\,. \tag{5.2.27}$$

Applying the principle of superposition according to Eqs. (5.2.14-5.2.17) we get [68]

$$a_i f_i+b_i f_{i+1}+c_i f_{i+2}=u_{i+1}^{T}(R_{i+1})-u_i^{T}(R_{i+1}),\ i=2,\ldots,n-1, \tag{5.2.28}$$

$$a_i=-\frac{1}{G_i(1+\nu_i)}\frac{R_i^2R_{i+1}}{R_{i+1}^2-R_i^2}, \tag{5.2.29}$$

$$b_i = \frac{R_{i+1}}{2G_i\left(R_{i+1}^2 - R_i^2\right)}\left[\frac{(1-\nu_i)}{(1+\nu_i)}R_{i+1}^2 + R_i^2\right] + \frac{R_{i+1}}{2G_{i+1}}\left[\frac{(1-\nu_{i+1})}{(1+\nu_{i+1})}R_{i+1}^2 + R_{i+2}^2\right], \qquad (5.2.30)$$

$$c_i = -\frac{1}{G_{i+1}(1+\nu_{i+1})}\frac{R_{i+2}^2 R_{i+1}}{R_{i+2}^2 - R_{i+1}^2}, \quad i = 2,\ldots,n-1. \qquad (5.2.31)$$

5.3. The initial value problem of functionally graded disks

In the next model we investigate a thermoelastic problem of thin functionally graded disks whose material properties vary arbitrarily along the radial direction and are temperature-dependent. A numerical approach will be presented which is based on a coupled system of first order ordinary differential equations. The unknown functions of the system of linear differential equations are the radial displacement and the stress function. Two models will be derived, in the first case a radially graded disk is presented with constant thickness. The second model deals with the determination of displacements and stress field of rotating radially graded disks with arbitrary thickness $h(r)$.

5.3.1. Radially graded disks with constant thickness

In this subsection the system of differential equations of the radial displacement and stress function is derived for radially graded disks with constant thickness. After the numerical solution of this system of ordinary differential equation, the thermal stresses and radial displacement for arbitrary radial nonhomogeneity can be obtained.

We consider a functionally graded hollow circular disk as shown in Fig. 5.6. R_1 and R_2 denote the inner and outer radii of the disk.

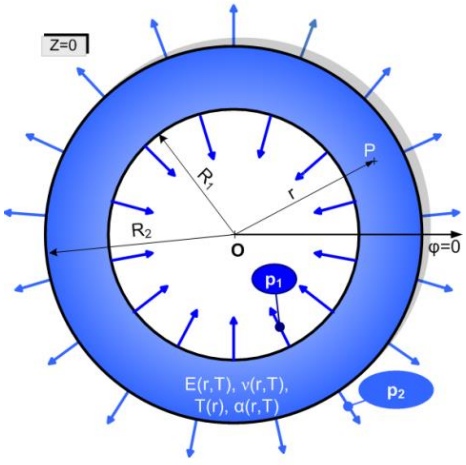

Figure 5.6. The hollow functionally graded disk with the mechanical and thermal loads.

The temperature field is denoted by $T=T(r)$ which is obtained from the solution of the steady-state heat conduction equation (Section 5.1). The strain-displacement and stress-strain relations are presented in Eqs. (5.2.8), where for this case the Young modulus E, the Poisson's ratio ν and the

coefficient of thermal expansion α depend on the radial coordinate r and on the temperature difference function T. In this time independent uncoupled problem the temperature field can be determined separately from the elastic problem, which means that for the material properties $M(r,T(r))\rightarrow M(r)$ is valid and the stress-strain and strain-stress relations assume the forms of

$$\begin{aligned}\sigma_r(r) &= \frac{E}{1-\nu^2}\left[\varepsilon_r + \nu\varepsilon_\varphi - \alpha(1+\nu)T(r)\right],\\ \sigma_\varphi(r) &= \frac{E}{1-\nu^2}\left[\nu\varepsilon_r + \varepsilon_\varphi - \alpha(1+\nu)T(r)\right],\end{aligned} \tag{5.3.1}$$

$$\begin{aligned}\varepsilon_r(r) &= \frac{1}{E}\left[\sigma_r - \nu\sigma_\varphi\right] + \alpha T(r),\\ \varepsilon_\varphi(r) &= \frac{1}{E}\left[\sigma_\varphi - \nu\sigma_r\right] + \alpha T(r).\end{aligned} \tag{5.3.2}$$

The equilibrium equation in radial direction - disregarding the body force and the inertia terms - is

$$\frac{\mathrm{d}\sigma_r}{\mathrm{d}r} + \frac{\sigma_r - \sigma_\varphi}{r} = 0, \quad R_1 \le r \le R_2. \tag{5.3.3}$$

The general solution of Eq. (5.3.3) in terms of stress function $V=V(r)$ can be represented as

$$\sigma_r = \frac{V}{r}, \qquad \sigma_\varphi = \frac{\mathrm{d}V}{\mathrm{d}r}, \quad R_1 \le r \le R_2. \tag{5.3.4}$$

After some manipulations from Eqs. (5.3.1-5.3.2) and (5.3.4) we can derive the next system of ordinary differential equations for the displacement field and the stress function

$$\frac{\mathrm{d}}{\mathrm{d}r}\begin{bmatrix}u(r)\\ V(r)\end{bmatrix} = \begin{bmatrix}-\dfrac{\nu(r,T)}{r} & \dfrac{1-\nu^2(r,T)}{rE(r,T)}\\ \dfrac{E(r,T)}{r} & \dfrac{\nu(r,T)}{r}\end{bmatrix}\cdot\begin{bmatrix}u(r)\\ V(r)\end{bmatrix} + \begin{bmatrix}1+\nu(r,T)\\ -E(r,T)\end{bmatrix}\alpha(r,T)T(r) \tag{5.3.5}$$

In Eqs. (5.3.5) all material properties depend arbitrarily on the radial coordinate and the temperature field.

5.3.2. Radially graded rotating disks with arbitrary thickness

In this subsection a rotating thin radially graded disk is investigated with constant angular velocity. The thickness of the structural component varies arbitrarily along the radial direction $h(r)>0$. In this case the equilibrium equation can be expressed as

$$\frac{\mathrm{d}}{\mathrm{d}r}\left(r\sigma_r(r)h(r)\right) - h(r)\sigma_\varphi(r) + h(r)\rho(r)\omega^2 r^2 = 0. \tag{5.3.6}$$

$$\frac{d\sigma_r}{dr} + \frac{\sigma_r - \sigma_\varphi}{r} + \frac{dh}{dr}\frac{1}{h}\sigma_r + \rho\omega^2 r = 0. \tag{5.3.7}$$

From Eq. (5.3.7) the normal stresses in terms of stress function $V(r)$ can be defined as

$$\sigma_r(r) = \frac{V(r)}{rh(r)}, \tag{5.3.8}$$

$$\sigma_\varphi(r) = \frac{\mathrm{d}V(r)}{\mathrm{d}r}\frac{1}{h(r)} + \omega^2\rho(r)r^2. \tag{5.3.9}$$

After lengthy manipulations the following system of ordinary differential equations can be derived for the displacement field and the stress function

$$\begin{aligned} \frac{\mathrm{d}u(r)}{\mathrm{d}r} &= \frac{1-\nu(r,T)^2}{h(r)E(r,T)}\frac{V(r)}{r} - \nu(r,T)\frac{u(r)}{r} + \alpha(r,T)\big[1+\nu(r,T)\big]T(r), \\ \frac{\mathrm{d}V(r)}{\mathrm{d}r} &= \nu(r,T)\frac{V(r)}{r} + h(r)E(r,T)\frac{u(r)}{r} - \alpha(r,T)T(r)h(r)E(r,T) - h(r)\rho(r)\omega^2 r^2. \end{aligned} \tag{5.3.10}$$

5.3.3. The solution of the initial value problem

The next step is the determination of the initial values for the system of Eqs. (5.3.5) and (5.3.10). The stress boundary conditions of the considered thermoelastic problem (Fig. 5.6) are

$$\sigma_r(R_1) = -p_1, \quad \sigma_r(R_2) = -p_2, \tag{5.3.11}$$

which can be expressed in terms of the stress function $V=V(r)$ when the thickness of the disk is constant such as

$$V(R_1) = -p_1R_1, \quad V(R_2) = -p_2R_2. \tag{5.3.12}$$

In the case of arbitrary $h(r)$ thickness we have

$$V(R_1) = -p_1R_1h_1, \quad V(R_2) = -p_2R_2h_2, \tag{5.3.13}$$

where $h(R_1)=h_1$ and $h(R_2)=h_2$.

We formulate an initial value problem for the coupled system of ordinary differential equations (5.3.5) and (5.3.10). To get the stresses and radial displacement for the considered thermoelastic problem, three numerical solutions will be used with three different initial values. The aim is to look for the suitable value of $u(R_1)$ which provides the validity of the prescribed boundary condition (5.3.12) and (5.3.13). At first we consider two solutions for system of equations (5.3.5) and (5.3.10) which are denoted by $[u_1(r), V_1(r)]$ and $[u_2(r), V_2(r)]$. These solutions have the next initial values:

$$u_1(R_1) = u_1 : \text{arbitrary value}, \tag{5.3.14}$$

$$V_1(R_1) = -p_1R_1, \text{when } h = \text{constant} \quad \text{and} \quad V_1(R_1) = -p_1R_1h_1, \text{ when } h = h(r), \tag{5.3.15}$$

$$u_2(R_1) = u_2 : \text{arbitrary value, but } u_1 \neq u_2, \tag{5.3.16}$$

$$V_2(R_1) = -p_1R_1, \text{when } h = \text{constant} \quad \text{and} \quad V_2(R_1) = -p_1R_1h_1, \text{ when } h = h(r), \tag{5.3.17}$$

By these solutions we compute u_3 as

$$u_3 = u_1 + \frac{u_2 - u_1}{V_2(R_2) - V_1(R_2)}(-p_2R_2 - V_1(R_2)), \text{ when } h \text{ is constant}, \tag{5.3.18}$$

$$u_3 = u_1 + \frac{u_2 - u_1}{V_2(R_2) - V_1(R_2)}(-p_2 R_2 h_2 - V_1(R_2)) \text{ when } h = h(r). \tag{5.3.19}$$

The solution of the thermoelastic boundary value problem formulated by Eqs. (5.3.1), (5.2.8) and (5.3.11) is obtained from the numerical solution of system of equations (5.3.5) and (5.3.10) with the initial conditions

$$u(R_1) = u_3, \qquad V(R_1) = -p_1 R_1 \quad \text{or} \quad V(R_1) = -p_1 R_1 h_1. \tag{5.3.20}$$

The validity of this statement follows from the linearity of the considered thermoelastic boundary value problem. The stress field can be obtained by Eqs. (5.3.4), (5.3.8) and (5.3.9).

5.4. An analytical solution of a radially graded disk

An analytical solution is developed for the case when the angular velocity is zero and the distributions of the material properties are assumed to be described with a power-law along the radial coordinate [69] as

$$E(r) = E_0 r^{m_1},\ \alpha(r) = \alpha_0 r^{m_2},\ \lambda(r) = \lambda_0 r^{m_3} \text{ and } \nu\text{=constant}. \tag{5.4.1}$$

The boundary conditions are steady-state first kind thermal (t_1 and t_2) and mechanical (p_1 and p_2) boundary conditions. The general solution of the following homogeneous system of ordinary differential equations

$$\frac{\mathrm{d}u_h}{\mathrm{d}r} + \frac{\nu}{r}u_h - \frac{1-\nu^2}{E_0 r^{m_1+1}}V_h = 0, \tag{5.4.2}$$

$$\frac{\mathrm{d}V_h}{\mathrm{d}r} - E_0 r^{m_1-1}u_h - \frac{\nu}{r}V_h = 0, \tag{5.4.3}$$

are as follows

$$u_h = \frac{\lambda_1 + m_1 - \nu}{E_0}C_1 r^{\lambda_1} + \frac{\lambda_2 + m_1 - \nu}{E_0}C_2 r^{\lambda_2}, \qquad V_h = C_1 r^{\lambda_1 + m_1} + C_2 r^{\lambda_2 + m_1}, \tag{5.4.4}$$

where

$$\lambda_{1,2} = \frac{-m_1 \pm \sqrt{m_1^2 - 4m_1\nu + 4}}{2}, \tag{5.4.5}$$

and C_1 and C_2 are arbitrary constants which can be obtained from the boundary condition Eq. (5.3.12). Here we note that

$$m_1^2 - 4m_1\nu + 4 = (m_1 - 2\nu)^2 + 4(1-\nu^2) > 0, \tag{5.4.6}$$

this means that λ_1 and λ_2 are real numbers because $0 \le \nu \le 0.5$. For simplicity it is assumed that t_2=0. In this case the temperature change is

$$T(r) = t_1 \frac{r^{-m_3} - R_2^{-m_3}}{R_1^{-m_3} - R_2^{-m_3}},\ R_1 \le r \le R_2. \tag{5.4.7}$$

Next, we seek a particular solution for the system of nonhomogeneous differential equations

$$\frac{\mathrm{d}u_p}{\mathrm{d}r}+\frac{\nu}{r}u_p-\frac{1-\nu^2}{E_0 r^{m_1+1}}V_p-\alpha_0 t_1(1+\nu)\frac{r^{m_2-m_3}-R_2^{-m_3}r^{m_2}}{R_1^{-m_3}-R_2^{-m_3}}=0, \tag{5.4.8}$$

$$\frac{\mathrm{d}V_p}{\mathrm{d}r}-E_0 r^{m_1-1}u_p-\frac{\nu}{r}V_p+\alpha_0 E_0 t_1\frac{r^{m_1+m_2-m_3}-R_2^{-m_3}r^{m_1+m_2}}{R_1^{-m_3}-R_2^{-m_3}}=0. \tag{5.4.9}$$

A simple computation shows that the particular solution for the the system of Eqs. (5.4.8), (5.4.9) is as follows

$$u_p=A_1 r^{m_2-m_3+1}+B_1 r^{m_2+1},\ V_p=A_2 r^{m_1+m_2-m_3+1}+B_2 r^{m_1+m_2+1}, \tag{5.4.10}$$

where the following notations are used:

$$A_1=\frac{\alpha_0 t_1\left[1-\nu^2-(1+\nu)(m_1+m_2-m_3-\nu+1)\right]}{(R_2^{-m_3}-R_1^{-m_3})\left[(m_2-m_3+\nu+1)(m_1+m_2-m_3-\nu+1)-1+\nu^2\right]}, \tag{5.4.11}$$

$$A_2=-\frac{\alpha_0 E_0 t_1(m_2-m_3)}{(R_2^{-m_3}-R_1^{-m_3})\left[(m_2-m_3+\nu+1)(m_1+m_2-m_3-\nu+1)-1+\nu^2\right]}, \tag{5.4.12}$$

$$B_1=-\frac{\alpha_0 t_1 R_2^{-m_3}\left[(m_1+m_2-\nu+1)(1+\nu)+1-\nu^2\right]}{(R_2^{-m_3}-R_1^{-m_3})\left[(m_2+\nu+1)(m_1+m_2-\nu+1)-1+\nu^2\right]}, \tag{5.4.13}$$

$$B_2=\frac{\alpha_0 E_0 t_1 R_2^{-m_3} m_2}{(R_1^{-m_3}-R_2^{-m_3})\left[(m_2+\nu+1)(m_1+m_2-\nu+1)-1+\nu^2\right]}. \tag{5.4.14}$$

The complete solution for the system of equations in the present case is

$$u(r)=u_h(r)+u_p(r),\quad V(r)=V_h(r)+V_p(r). \tag{5.4.15}$$

The constants C_1 and C_2 can be obtained from the stress boundary conditions as the solution of the following system of linear equations

$$C_1 R_1^{\lambda_1+m_1}+C_2 R_1^{\lambda_2+m_1}+A_2 R_1^{m_1+m_2-m_3+1}+B_2 R_1^{m_1+m_2+1}=-p_1 R_1, \tag{5.4.16}$$

$$C_1 R_2^{\lambda_1+m_1}+C_2 R_2^{\lambda_2+m_1}+A_2 R_2^{m_1+m_2-m_3+1}+B_2 R_2^{m_1+m_2+1}=-p_2 R_2. \tag{5.4.17}$$

Solution of system of equations (5.4.16-5.4.17) gives

$$C_1=-\frac{(p_1R_1+A_2R_1^{m_1+m_2-m_3+1}+B_2R_1^{m_1+m_2+1})R_2^{\lambda_2+m_2}}{R_1^{\lambda_1+m_1}R_2^{\lambda_2+m_2}-R_1^{\lambda_2+m_1}R_2^{\lambda_1+m_1}}+\frac{(p_2R_2+A_2R_2^{m_1+m_2-m_3+1}+B_2R_2^{m_1+m_2+1})R_1^{\lambda_2+m_1}}{R_1^{\lambda_1+m_1}R_2^{\lambda_2+m_2}-R_1^{\lambda_2+m_1}R_2^{\lambda_1+m_1}}, \tag{5.4.18}$$

$$C_2=\frac{(p_1R_1+A_2R_1^{m_1+m_2-m_3+1}+B_2R_1^{m_1+m_2+1})R_2^{\lambda_1+m_1}}{R_1^{\lambda_1+m_1}R_2^{\lambda_2+m_2}-R_1^{\lambda_2+m_1}R_2^{\lambda_1+m_1}}-\frac{(p_2R_2+A_2R_2^{m_1+m_2-m_3+1}+B_2R_2^{m_1+m_2+1})R_1^{\lambda_1+m_1}}{R_1^{\lambda_1+m_1}R_2^{\lambda_2+m_2}-R_1^{\lambda_2+m_1}R_2^{\lambda_1+m_1}}. \tag{5.4.19}$$

With Eqs. (5.4.18) and (5.4.19) we can get the radial displacement and normal stresses for ω=0 as

$$u(r)=\frac{\lambda_1+m_1-\nu}{E_0}C_1 r^{\lambda_1}+\frac{\lambda_2+m_1-\nu}{E_0}C_2 r^{\lambda_2}+A_1 r^{m_2-m_3+1}+B_1 r^{m_2+1}, \tag{5.4.20}$$

$$\sigma_r(r)=\frac{V(r)}{r}=C_1 r^{\lambda_1+m_1-1}+C_2 r^{\lambda_2+m_1-1}+A_2 r^{m_1+m_2-m_3}+B_2 r^{m_1+m_2}, \tag{5.4.21}$$

$$\begin{aligned}\sigma_\varphi(r)=\frac{\mathrm{d}V(r)}{\mathrm{d}r}&=C_1(\lambda_1+m_1)r^{\lambda_1+m_1-1}+C_2(\lambda_2+m_1)r^{\lambda_2+m_1-1}+\\&+A_2(m_1+m_2-m_3+1)r^{m_1+m_2-m_3}+B_2(m_1+m_2+1)r^{m_1+m_2}.\end{aligned} \tag{5.4.22}$$

5.5. Numerical examples

In this section numerical examples will be presented to the developed methods for the thermoelastic problems of radially graded disks. The methods will be compared to each other and to finite element simulations.

5.5.1. Example 8

In this example the initial value method will be verified with the analytical solution of Section 5.4. The material properties are prescribed as in Eqs. (5.4.1). The geometry, material parameters and loading of the radially graded disk are

$$R_1 = 1\,\mathrm{m},\ R_2 = 1.4\,\mathrm{m},\ m_1 = 3,\ m_2 = -2,\ m_3 = 1.5,\ \nu = 0.3,\ E_0 = 2\cdot 10^{11}\,\frac{\mathrm{N}}{\mathrm{m}^5},\ \alpha_0 = 1.2\cdot 10^{-6}\,\frac{1}{^{\circ}\mathrm{C}\mathrm{m}^3},$$

$$T(R_1) = 0\ ^{\circ}\mathrm{C},\ T(R_2) = 300\ ^{\circ}\mathrm{C},\ p_1 = 60\,\mathrm{MPa},\ p_2 = 5\mathrm{MPa}.$$

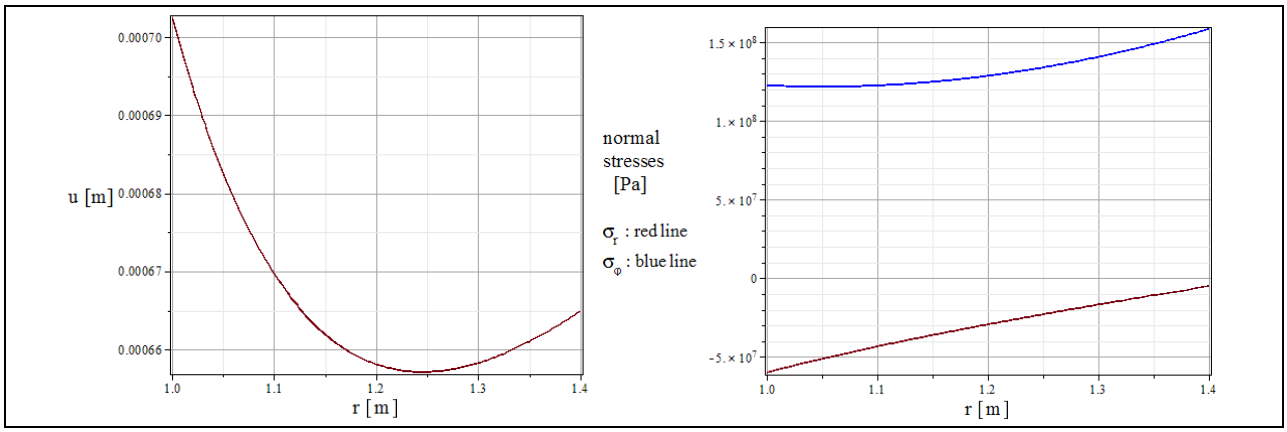

Figure 5.7. The radial displacement field and the normal stresses of the analytical solution.

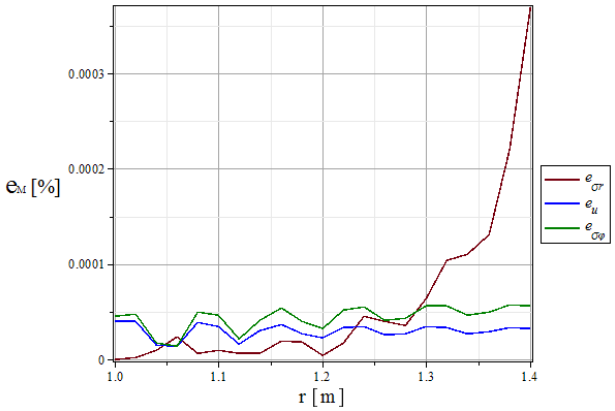

Figure 5.8. The relative errors of the initial value method compared to the analytical solutions.

The result of the comparison can be seen in Figs. 5.7 and 5.8. The developed initial value method has good accuracy.

5.5.2. Example 9

In this subsection the methods presented in Sections 5.3 and 5.2 will be investigated. The methods will be compared to each other in two cases. The properties of the material of the disks based on Eqs. (2.4.1) and (2.4.2) can be seen in Table 5.1 [8].

Table 5.1. Material properties of the functionally graded material of the disk.

Material Property (M_{eff})	material (1)				material (2)			
	P_{m0}	$P_{m1}(10^{-3})$	$P_{m2}(10^{-7})$	$P_{m3}(10^{-10})$	P_{c0}	$P_{c1}(10^{-3})$	$P_{c2}(10^{-7})$	$P_{c3}(10^{-11})$
λ(W/mK)	15.39	-2.364	20.92	-7.223	1.7	-0.1276	0.06648	-1
γ(W/m²K)	10	0	0	0	2	0	0	0
ρ(kg/m³)	7200	0.3079	-6.534	0	10^4	-0.307	2.16	-8.946
α (1/K)	$12.33\cdot10^{-6}$	0.8086	0	0	$3.873\cdot10^{-6}$	0.9095	0	0
E (Pa)	$2.01\cdot10^{11}$	0.3079	-6.534	0	$3.484\cdot10^{11}$	-0.307	2.16	-8.946
ν (-)	0.3262	-0.1	0.3797	0	0.24	0	0	0

We will consider a thin disk with constant thickness with the following geometry and loading:

$$R_1 = 10\,\text{mm},\ R_2 = 50\,\text{mm},\ m = 2, \omega = 0\frac{1}{\text{s}}, T(r) = 310.83 - \frac{0.027}{r^2}[\text{K}],\ p_1 = 60\,\text{MPa},\ p_2 = 5\text{MPa}.$$

Then the following disk will be investigated with thickness $h(r)$:

$$R_1 = 0.1\text{m},\ R_2 = 0.3\text{m},\ m = 0.1, p_1 = 60\,\text{MPa},\ p_2 = 0\text{Pa}, h(r) = 0.01 - 0.035r^2 - \frac{r^3}{100}[\text{m}],$$

$$\omega = 400\frac{1}{\text{s}}, T(r) = -\frac{8.56}{r} + 170 - 721r + 12298r^2 - 41305r^3 + 59657r^4\,[\text{K}].$$

The result for the multilayered method and the initial value method are shown in Figs. 5.9-5.11. Here we can see that the results are in good agreement. Furthermore the radial displacements computed via the multilayered model even by n=4 are fairly accurate (Fig. 5.9).

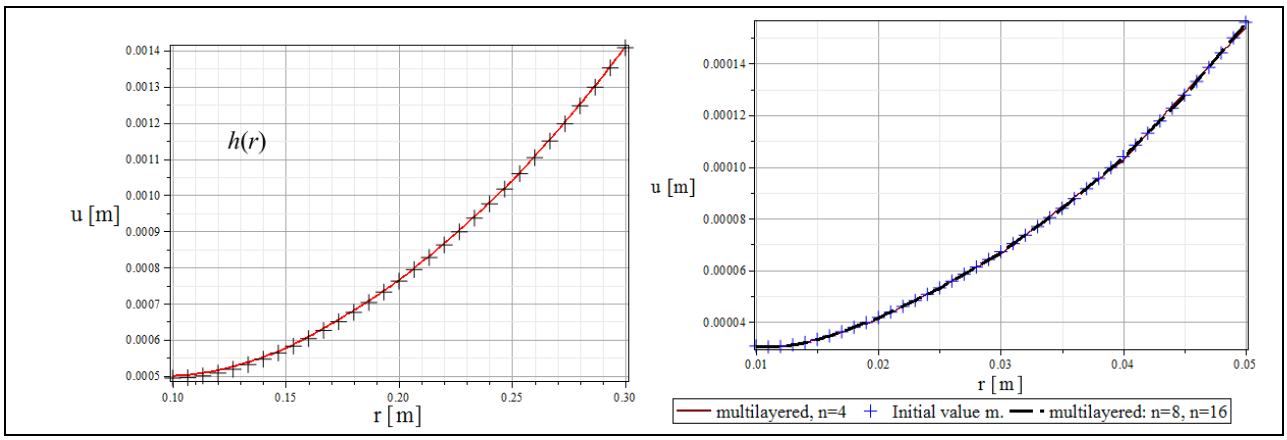

Figure 5.9. The graphs of the displacement fields.

In the case of disks with constant thickness the results for the radial normal stresses have good accuracy at the edge of the layers, the graphs of the tangential normal stresses are accurate at the middle of each layers (Figs. 5.10 and 5.11). The accuracy of this method can be improved with curve fitting to these points.

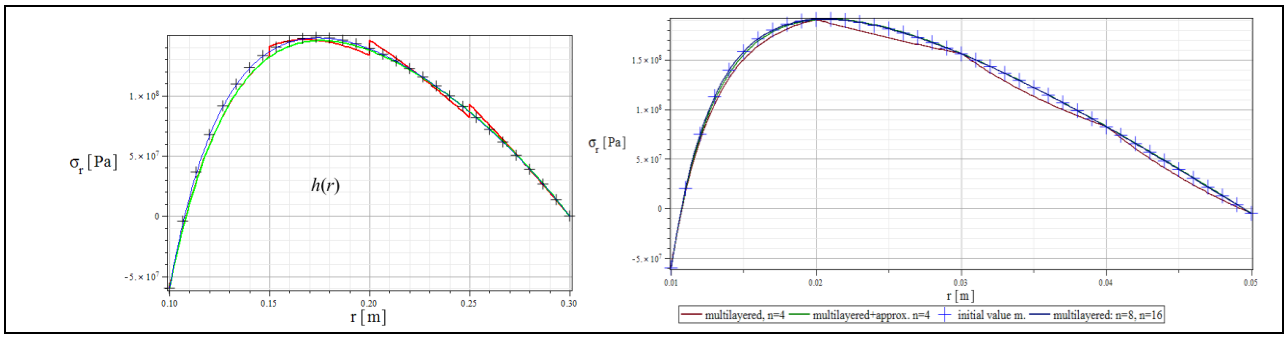

Figure 5.10. The graphs of the radial normal stresses.

The approximate function for the radial and tangential normal stresses have the following form in these cases:

$$\sigma_{appr}(r) = F_{-3}r^{-3} + F_{-2}r^{-2} + F_{-1}r^{-1} + F_0 + F_1 r + F_2 r^2 + F_3 r^3 + F_4 r^4 + F_5 r^5 . \qquad (5.5.1)$$

For the disk with thickness $h(r)$ the next function is used for the normal stresses (Figs. 5.10 and 5.11):

$$\sigma_{appr}(r) = F_{-1}r^{-1} + F_0 + F_1 r + F_2 r^2 + F_3 r^3 + F_4 r^4 + F_5 r^5 . \qquad (5.5.2)$$

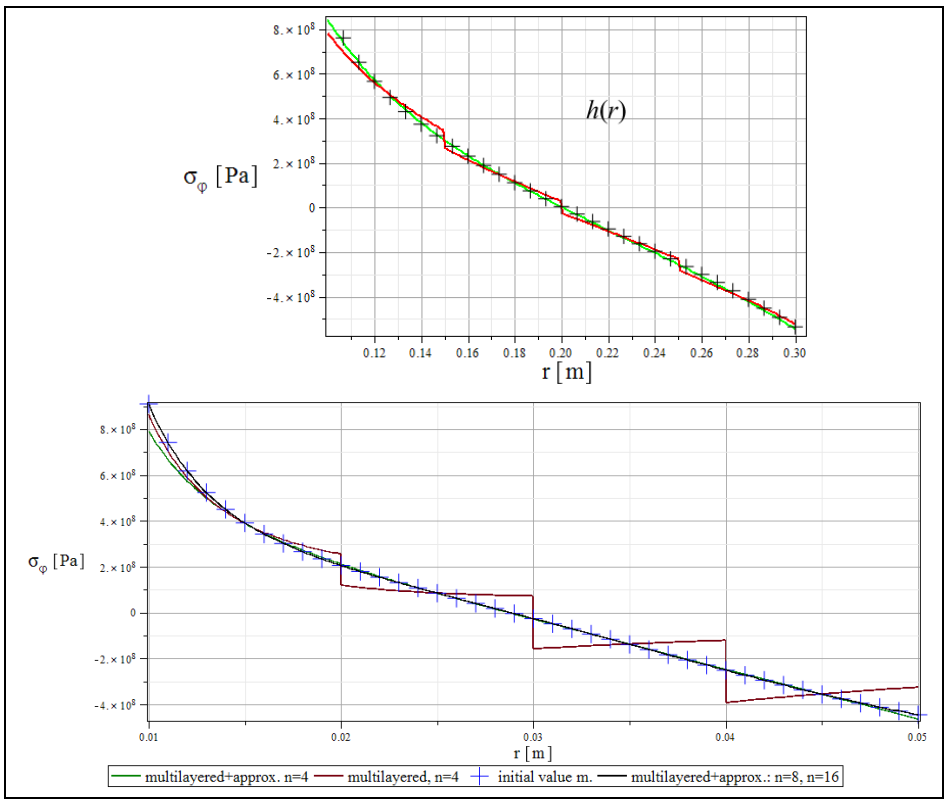

Figure 5.11. The graphs of the tangential normal stresses.

With these approximations we get a fast and relatively accurate methods to deal with this kind of problems of radially graded rotating disks. The accuracy of the multilayered approach can be further improved with partitioning according to the material change within the structural component - in our current case according to the power index m.

5.5.3. Example 10

In this subsection a numerical example is presented for rotating functionally graded disks with a prescribed $h=h(r)$ thickness and temperature-dependent material properties. The temperature field is determined by the method presented in Subsection 5.1.2. The displacement field and normal stresses are computed according to Section 5.2 and compared to results obtained by finite element simulation in Abaqus. The following numerical data will be used for the computations:

a=0.1m, b=0.3m, h=0.0115-0.025r [m], $T_{env}(r)=398\left(\frac{r-0.09}{a}\right)^{0.01}-t_{ref}$ [K], t_{inner}=100K,

t_{outer}=400K, t_{ref}=273K, m=3 and for λ and γ: m_1=2.3, p_{inner}=60MPa, p_{outer}=0MPa, ω=400 1/s.

Table 5.1 presents the material parameters of the constituent materials based on Eqs. (2.4.1) and (2.4.2). Figure 5.12 shows that the temperature field of thin disks depends on the radial coordinate by these symmetric boundary conditions.

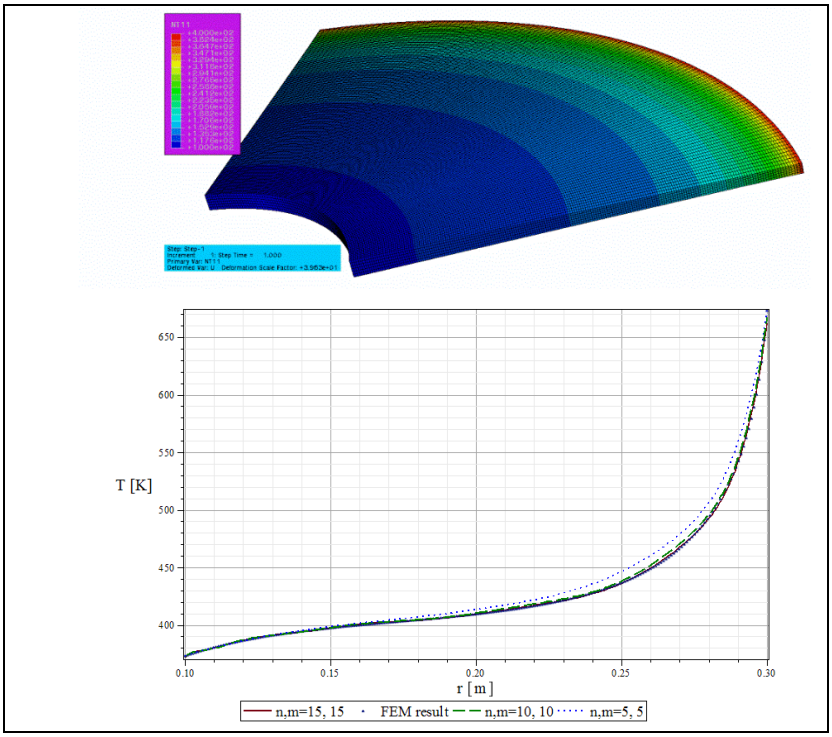

Figure 5.12. The finite element model with the absolute temperature field and the graphs.

The results of the displacements and normal stresses are in good agreement as it can be seen in Figs. 5.13-5.15. The approximation of the normal stresses can improve the accuracy of the multilayered method.

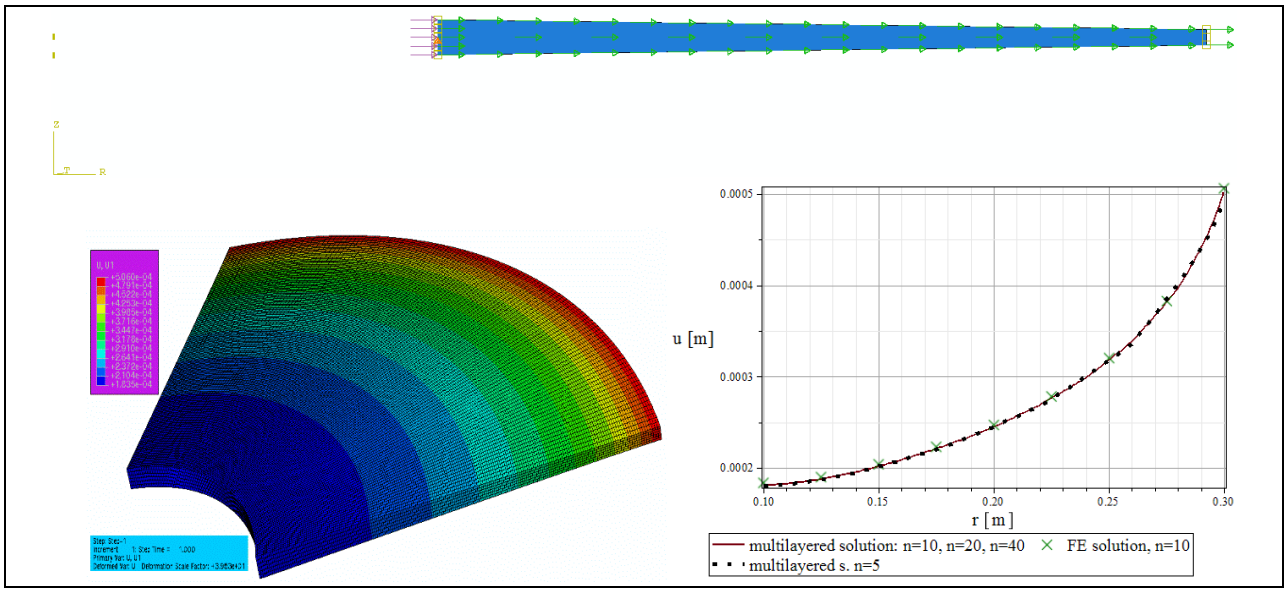

Figure 5.13. The finite element model of the disk with the radial displacement and the graphs of the different solutions.

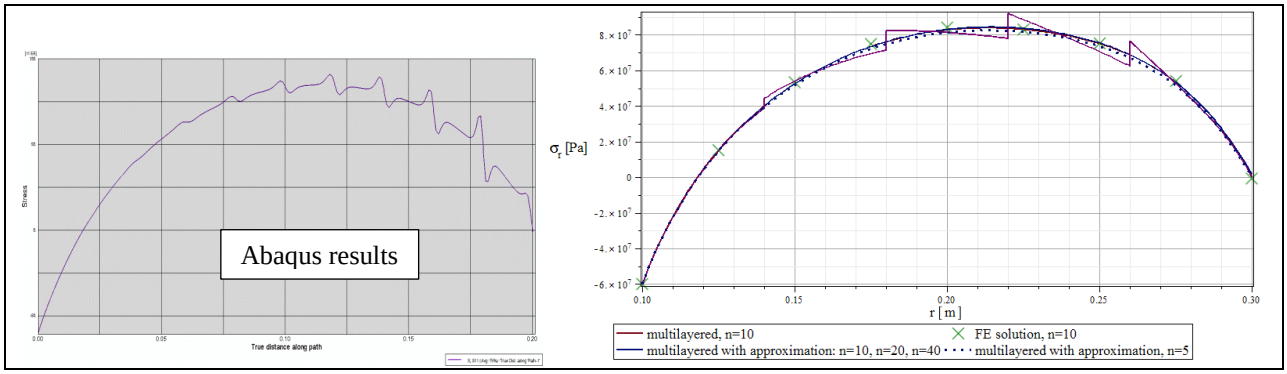

Figure 5.14. The radial normal stresses within the radially graded disk.

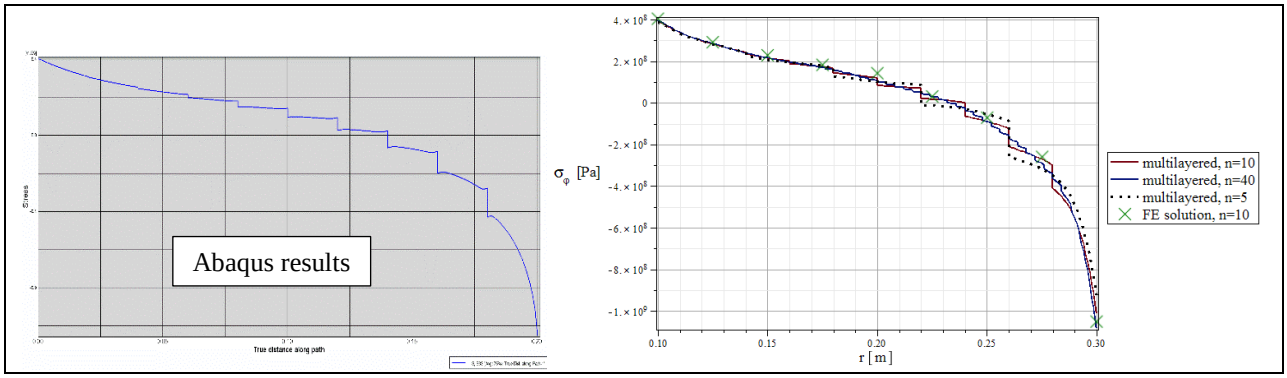

Figure 5.15. The graphs of the tangential normal stresses.

6. Thermoelastic problem of functionally graded beams and strips

In this chapter functionally graded beams and strips will be investigated. The problems of functionally graded prismatic beams are dealt with complementary energy method and a direct approach. The problems of functionally graded strips are solved with multilayered approach, furthermore the case of bimetallic strips in uniform temperature field is further analysed. At the end of this chapter numerical examples are presented and verified with finite element solutions.

6.1. Thermoelastic problem of functionally graded prismatic beams using complementary energy method

This section deals with the determination of thermal stresses in nonhomogeneous prismatic bars. The derivation of the formulae for stresses caused by mechanical and thermal loads is based on the principle of minimum of complementary energy. The cross section of the bar is an arbitrary bounded plain domain, moreover the material properties and the temperature field do not depend on the axial coordinate. The considered inhomogeneity means that the material properties are arbitrary functions of the cross-sectional coordinates. The presented analysis is valid for compound bars whose material properties are discontinuous functions of the cross-sectional coordinates and bars made from functionally graded materials, whose material properties are smooth functions of the cross-sectional coordinates. If there are no prescribed surface displacements than the theorem of minimum of complementary energy can be formulated [51], [52], which means that among all the sets of admissible stresses σ_x, σ_y, σ_z, τ_{xy}, τ_{xy}, τ_{xy} which satisfy all the equilibrium equations and the prescribed stress boundary conditions, the set of actual stress components makes the functional $\tilde{\Pi}_c\left(\sigma_x,\sigma_y,\sigma_z,\tau_{xy},\tau_{xz},\tau_{zy}\right)$ defined by Eq. (2.3.6) an absolute minimum as we can see in Section 2.3.

The considered nonhomogeneous prismatic bar and its mechanical loads are shown in Fig. 6.1, where $\mathbf{F}=F\mathbf{e}_z$ is the applied axial force and $\mathbf{M}=M_x\mathbf{e}_x+M_y\mathbf{e}_y$ is the applied bending moment. The material properties are functions of x and y, therefore we have $E=E(x,y)$ and $\alpha=\alpha(x,y)$. In our formulation the Poisson's ratio of the thermoelastic bar problem does not appear. The temperature difference field T also depends only on x and y and it is a given function. In the framework of strength of materials the equilibrium stress field is characterized by the equations (Fig. 6.1)

$$\sigma_x=\sigma_y=\tau_{yz}=\tau_{xy}=\tau_{xz}=0,\qquad \sigma_z=\sigma_z(x,y), \tag{6.1.1}$$

$$K_1\left[\sigma_z(x,y)\right]=\int_A\sigma_z(x,y)\mathrm{d}A-F=0, \tag{6.1.2}$$

$$\mathbf{K}_2\left[\sigma_z(x,y)\right]=\int_A\mathbf{R}\sigma_z(x,y)\mathrm{d}A-\mathbf{e}_z\times\mathbf{M}=\mathbf{0}. \tag{6.1.3}$$

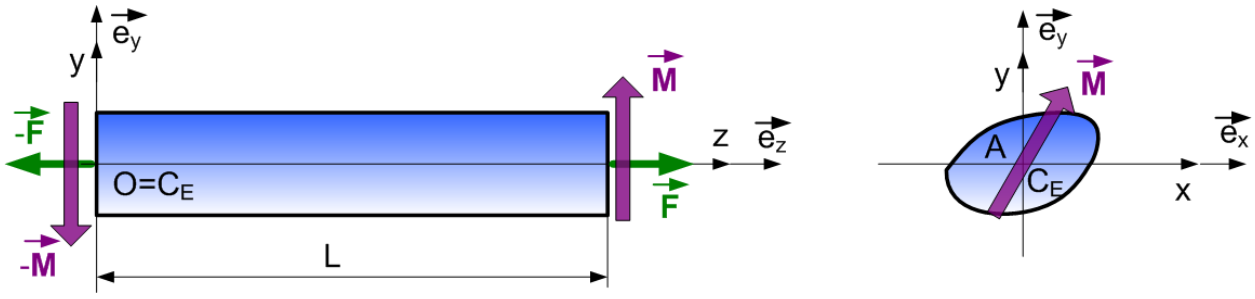

Figure 6.1. Nonhomogeneous prismatic bar.

Eqs. (6.1.1-6.1.3) refer to the coordinate system *Oxyz* with unit vectors $\mathbf{e}_x$, $\mathbf{e}_y$, $\mathbf{e}_z$ and

$$\mathbf{R} = x\mathbf{e}_x + y\mathbf{e}_y, \tag{6.1.4}$$

the cross between two vectors in Eq. (6.1.3) denotes their vectorial product and the cross section of the nonhomogeneous bar is *A*. Here we note that axis *z* is the *E*-weighted centerline of the nonhomogeneous bar, it connects of *E*-weighted centres of cross sections. The *E*-weighted centre C_E is defined by the next equation:

$$\int_A E(x,y)\mathbf{R}\mathrm{d}A = \mathbf{0}. \tag{6.1.5}$$

The state of stresses are independent of the axial coordinate *z*, from this it follows that the axial force and bending moment do not change along axis *z*. The complementary energy of nonhomogeneous bar according to Eq. (2.3.6) is as follows

$$\tilde{\Pi}_c = L\int_A \left\{ \frac{1}{2E(x,y)}\left[\sigma_z(x,y)\right]^2 + \alpha(x,y)T(x,y)\sigma_z(x,y) \right\}\mathrm{d}A, \tag{6.1.6}$$

where *L* is the length of the bar (Fig. 6.1). Let $\Pi_c\left[\sigma_z(x,y)\right]$ be defined as

$$\Pi_c = \int_A \left\{ \frac{1}{2E(x,y)}\left[\sigma_z(x,y)\right]^2 + \alpha(x,y)T(x,y)\sigma_z(x,y) \right\}\mathrm{d}A. \tag{6.1.7}$$

According to the minimum of complementary energy we look for the minimum of $\Pi_c\left[\sigma_z(x,y)\right]$ under the subsidiary conditions given by Eqs. (6.1.2), (6.1.3). The method of Lagrange multipliers will be used [70], [71]. We define a new functional which contains the constraints given by Eqs. (6.1.2) and (6.1.3)

$$F\left[\sigma_z(x,y),\, \lambda_1,\, \boldsymbol{\lambda}_2\right] = \Pi_c\left[\sigma_z(x,y)\right] - \lambda_1 K_1\left[\sigma_z(x,y)\right] - \boldsymbol{\lambda}_2 \cdot \mathbf{K}_2\left[\sigma_z(x,y)\right]. \tag{6.1.8}$$

In Eq. (6.1.8) the scalar product of two vectors is indicated by dot. The necessary condition of minimum is formulated by the next variational equation

$$\begin{aligned} \delta F = &\int_A \left\{ \frac{\sigma_z(x,y)}{E(x,y)} + \alpha(x,y)T(x,y) - \lambda_1 - \boldsymbol{\lambda}_2 \cdot \mathbf{R} \right\}\delta\sigma_z \mathrm{d}A - \delta\lambda_1 \left[\int_A \sigma_z(x,y)\mathrm{d}A - F \right] \\ &-\delta\boldsymbol{\lambda}_2 \cdot \left[\int_A \mathbf{R}\sigma_z(x,y)\mathrm{d}A - \mathbf{e}_z \times \mathbf{M} \right] = 0. \end{aligned} \tag{6.1.9}$$

Since $\delta\sigma_z$, $\delta\lambda_1$, $\delta\underline{\boldsymbol{\lambda}}_2$ are arbitrary we obtain the following equations from Eq. (6.1.9)

$$\sigma_z(x,y) = E(x,y)\left[\lambda_1 + \boldsymbol{\lambda}_2 \cdot \mathbf{R} - \alpha(x,y)T(x,y)\right], \tag{6.1.10}$$

$$F = \int_A \sigma_z(x,y)\mathrm{d}A, \quad \mathbf{e}_z \times \mathbf{M} = \int_A \mathbf{R}\sigma_z(x,y)\mathrm{d}A. \tag{6.1.11}$$

Combination of Eq. (6.1.5) with Eqs. (6.1.10) and (6.1.11) leads to

$$\lambda_1 = \frac{F + N_T}{A_E}, \tag{6.1.12}$$

$$N_T = \int_A E(x,y)\alpha(x,y)T(x,y)\mathrm{d}A. \tag{6.1.13}$$

In Eq. (6.1.12) the following notation is used

$$A_E = \int_A E(x,y)\mathrm{d}A. \tag{6.1.14}$$

Substitution of Eq. (6.1.10) into Eq. $(6.1.11)_2$ yields the next expression

$$\lambda_1 \int_A E(x,y)\mathbf{R}\mathrm{d}A + \boldsymbol{\lambda}_2 \cdot \int_A E(x,y)\mathbf{R} \circ \mathbf{R}\mathrm{d}A - \int_A E(x,y)\alpha(x,y)\mathbf{R}T(x,y)\mathrm{d}A = \mathbf{e}_z \times \mathbf{M}. \tag{6.1.15}$$

Here the circle between two vectors denotes their tensorial (dyadic) product. We introduce the Euler tensor $\mathbf{I}$ as

$$\mathbf{I} = \int_A E(x,y)\mathbf{R} \circ \mathbf{R}\mathrm{d}A = I_y \mathbf{e}_x \circ \mathbf{e}_x + I_{xy}\left(\mathbf{e}_x \circ \mathbf{e}_y + \mathbf{e}_y \circ \mathbf{e}_x\right) + I_x \mathbf{e}_y \circ \mathbf{e}_y, \tag{6.1.16}$$

where

$$I_y = \int_A E(x,y)x^2\mathrm{d}A, \quad I_{xy} = \int_A E(x,y)xy\mathrm{d}A, \quad I_x = \int_A E(x,y)y^2\mathrm{d}A. \tag{6.1.17}$$

Let $\mathbf{M}_T$ be defined as

$$\mathbf{e}_z \times \mathbf{M}_T = \int_A E(x,y)\alpha(x,y)\mathbf{R}T(x,y)\mathrm{d}A. \tag{6.1.18}$$

In Eq. (6.1.15) the coefficient of λ_1 vanishes, that is we have

$$\mathbf{I} \cdot \boldsymbol{\lambda}_2 = \mathbf{e}_z \times \mathbf{M}_T + \mathbf{e}_z \times \mathbf{M}. \tag{6.1.19}$$

Denote the unit vector in direction of $\boldsymbol{\lambda}_2$ is $\mathbf{m} = m_x \mathbf{e}_x + m_y \mathbf{e}_y$, which means that $\boldsymbol{\lambda}_2 = \lambda_2 \mathbf{m}$. Let $\mathbf{n} = \mathbf{m} \times \mathbf{e}_z = n_x \mathbf{e}_x + n_y \mathbf{e}_y$ be. From Eq. (6.1.19) we get

$$\lambda_2(\mathbf{I} \cdot \mathbf{m}) \times \mathbf{e}_z = \lambda_2 \mathbf{I} \cdot \mathbf{n} = \left(\mathbf{e}_z \times \mathbf{M}_T\right) \times \mathbf{e}_z + \left(\mathbf{e}_z \times \mathbf{M}\right) \times \mathbf{e}_z = \mathbf{M}_T + \mathbf{M}, \ \lambda_2 \mathbf{I} \cdot \mathbf{n} = \mathbf{M}_T + \mathbf{M}. \tag{6.1.20}$$

From Eq. (6.1.20) it follows that

$$\lambda_2 \mathbf{n} = \mathbf{I}^{-1} \cdot \left(\mathbf{M}_T + \mathbf{M}\right). \tag{6.1.21}$$

Eq. (6.1.21) gives a possibility to obtain the unit vector $\mathbf{n}$

$$\mathbf{n} = \frac{\mathbf{I}^{-1} \cdot \left(\mathbf{M}_T + \mathbf{M}\right)}{\left|\mathbf{I}^{-1} \cdot \left(\mathbf{M}_T + \mathbf{M}\right)\right|}. \tag{6.1.22}$$

On the other hand from Eq. (6.1.20) we have

$$\lambda_2 \mathbf{n}\cdot\mathbf{I}\cdot\mathbf{n} = \mathbf{M}_T\cdot\mathbf{n} + \mathbf{M}\cdot\mathbf{n}, \tag{6.1.23}$$

that is

$$\lambda_2 = \frac{M_{Tn}+M_n}{I_n}, \quad I_n = \mathbf{n}\cdot\mathbf{I}\cdot\mathbf{n} = I_x n_y^2 + 2I_{xy}n_y n_x + I_y n_x^2, \quad M_{Tn} = \mathbf{M}_T\cdot\mathbf{n}, \quad M_n = \mathbf{M}\cdot\mathbf{n}. \tag{6.1.24}$$

In Eq. (6.1.11)

$$\boldsymbol{\lambda}_2\cdot\mathbf{R} = \lambda_2\mathbf{m}\cdot\mathbf{R} = \lambda_2\left(\mathbf{e}_z\times\mathbf{n}\right)\cdot\mathbf{R} = \lambda_2\left(xm_x + ym_y\right) = \lambda_2\left(yn_x - xn_y\right). \tag{6.1.25}$$

Summarizing the obtained results the following formula can be derived for the axial normal stress σ_z

$$\sigma_z(x,y) = E\left\{\frac{F+N_T}{A_E} + \frac{M_n+M_{Tn}}{I_n}\left(yn_x - xn_y\right) - \alpha T\right\}. \tag{6.1.26}$$

Here we note that the Lagrange multipliers λ_1 and $\boldsymbol{\lambda}_2$ have mechanical meanings. The stress-strain relation for one-dimensional problem of thermoelasticity is formulated as [52], [60]

$$\sigma_z(x,y) = E(x,y)\left[\varepsilon_z(x,y) - \alpha T(x,y)\right]. \tag{6.1.27}$$

In Eq. (6.1.27) ε_z is the normal strain. Comparison of Eq. (6.1.10) with Eq. (6.1.27) gives

$$\varepsilon_z(x,y) = \lambda_1 + \boldsymbol{\lambda}_2\cdot\mathbf{R} = \lambda_1 + \lambda_2\mathbf{m}\cdot\mathbf{R}. \tag{6.1.28}$$

Eq. (6.1.28) shows that λ_1 is the normal strain at the E-weighted centre C_E of the cross section and $\boldsymbol{\lambda}_2$ is the curvature vector of the deformed E-weighted centre line:

$$\varepsilon_z(0,0) = \lambda_1 = \varepsilon_0, \qquad \boldsymbol{\lambda}_2 = \kappa\mathbf{m}, \tag{6.1.29}$$

where κ is the curvature of the deformed longitudinal fiber determined by x=0, y=0 and $0 \le z \le L$. The thermoelastic pure bending problem of nonhomogeneous prismatic bars, based on the Euler-Bernoulli beam theory was analysed by Stokes [72]. Stokes paper uses a direct approach starting from the assumed form of normal strain which is

$$\varepsilon_z(x,y) = \frac{\eta-\eta_n}{R}. \tag{6.1.30}$$

Here

$$\eta = \mathbf{m}\cdot\mathbf{R}, \qquad \kappa = \frac{1}{R}, \qquad \eta_N = -R\varepsilon_0. \tag{6.1.31}$$

The zero line of longitudinal strains is given by η_N. Our approach is different from the one presented by Stokes [72]. It demonstrates the efficiency of the variation method in solving the problems of mechanics of solids.

6.2. Thermoelastic problem of functionally graded beams using a direct approach

In our second model the nonhomogeneous bar is subjected to a given temperature field $T(x,y)$ and eccentric tension **F**, the sketch of the problem is shown in Fig. 6.2. The material parameters and the temperature field are functions of the coordinates x and y as in our previous problem.

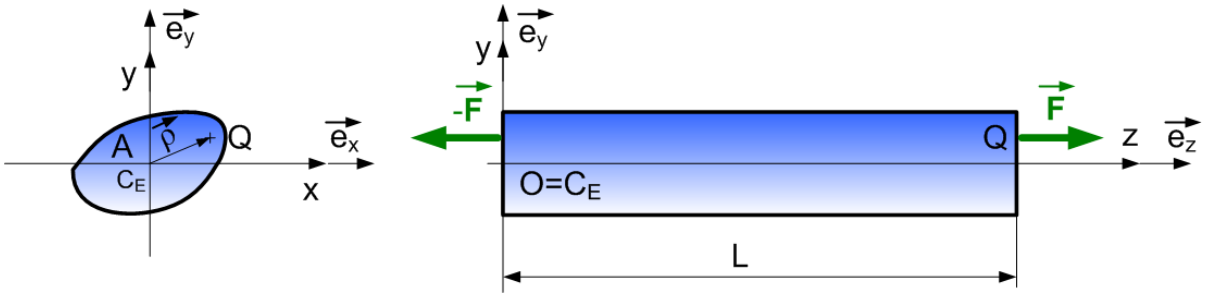

Figure 6.2. The sketch of the nonhomogeneous beam.

The mechanical loading can be expressed as:

$$\mathbf{F} = F\mathbf{e}_z\,,\ \mathbf{M} = F\boldsymbol{\rho}\times\mathbf{e}_z\,. \tag{6.2.1}$$

We will use a direct approach for the axial normal strain –according to Eqs. (6.1.30) and (6.1.31)- with the curvature and the longitudinal strain:

$$\varepsilon_z = \varepsilon_0 + \kappa\eta\,. \tag{6.2.2}$$

The stress-strain relation for this case can be expressed as

$$\sigma_z(x,y) = E(x,y)\left(\varepsilon_0 + \kappa\eta\right) - E(x,y)\alpha(x,y)T(x,y)\,. \tag{6.2.3}$$

The stress vector associated with a plane with normal unit vector $\mathbf{e}_z$ is

$$\mathbf{p}_z(x,y) = E\varepsilon_0\mathbf{e}_z + E\kappa\mathbf{R}\cdot\mathbf{m}\mathbf{e}_z - E\alpha T\mathbf{e}_z = E\varepsilon_0\mathbf{e}_z + E\kappa\mathbf{n}\times\mathbf{R} - E\alpha T\mathbf{e}_z. \tag{6.2.4}$$

From the equilibrium equation -and taking into account Eq. (6.1.5)- we get

$$F = \varepsilon_0\int_A E dA - \int_A E\alpha T\mathrm{d}A, \tag{6.2.5}$$

the unknown ε_0 can be determined as

$$\varepsilon_0 = \frac{F + F_T}{A_E}, \tag{6.2.6}$$

where we have introduced the notations

$$A_E = \int_A E\mathrm{d}A, \qquad F_T = \int_A E\alpha T\mathrm{d}A. \tag{6.2.7}$$

With the bending moment the following equation can be established

$$\mathbf{M}=\int_A \mathbf{R}\times\mathbf{p}_z \mathrm{d}A=\kappa\int_A E\mathbf{R}\times(\mathbf{n}\times\mathbf{R})\mathrm{d}A-\int_A E\alpha T\mathbf{R}\mathrm{d}A\times\mathbf{e}_z=$$
$$\kappa\int_A E\mathbf{R}\times(\mathbf{n}\times\mathbf{R})\mathrm{d}A-\mathbf{M}_T, \tag{6.2.8}$$
$$\mathbf{M}_T=\int_A E\alpha T\mathbf{R}\mathrm{d}A\times\mathbf{e}_z.$$

The combination of Eqs. (6.2.8) leads to

$$\mathbf{M}+\mathbf{M}_T=\kappa\hat{\mathbf{I}}\cdot\mathbf{n}, \tag{6.2.9}$$

Here we note that in Eq. (6.2.9) we have introduced

$$\hat{\mathbf{I}}=I_x\mathbf{e}_x\circ\mathbf{e}_x+I_{xy}\left(\mathbf{e}_x\circ\mathbf{e}_y+\mathbf{e}_y\circ\mathbf{e}_x\right)+I_y\mathbf{e}_y\circ\mathbf{e}_y. \tag{6.2.10}$$

The vector **n** can be determined according to Eq. (6.1.22) but with $\hat{\mathbf{I}}$ instead of **I**. Equation (6.2.10) can be rewritten into

$$\kappa\mathbf{n}=\hat{\mathbf{I}}^{-1}\cdot\mathbf{M}+\hat{\mathbf{I}}^{-1}\cdot\mathbf{M}_T, \tag{6.2.11}$$

From which we get

$$\begin{aligned}\kappa\left(\mathbf{m}\times\mathbf{e}_z\right)&=\left(\hat{\mathbf{I}}^{-1}\times\mathbf{e}_z\right)\cdot F\boldsymbol{\rho}+\hat{\mathbf{I}}^{-1}\cdot\mathbf{M}_T,\\ \kappa\mathbf{m}&=\left(\mathbf{e}_z\times\hat{\mathbf{I}}^{-1}\times\mathbf{e}_z\right)\cdot F\boldsymbol{\rho}+\mathbf{e}_z\times\hat{\mathbf{I}}^{-1}\cdot\mathbf{M}_T.\end{aligned} \tag{6.2.12}$$

The combination of Eqs. (6.2.12), (6.2.6) and (6.2.3) leads to the axial normal stress:

$$\sigma_z=E\left[\frac{F+F_T}{S}-F\mathbf{R}\cdot\left(\mathbf{e}_z\times\hat{\mathbf{I}}^{-1}\times\mathbf{e}_z\right)\cdot\boldsymbol{\rho}+\mathbf{R}\cdot\mathbf{e}_z\times\hat{\mathbf{I}}^{-1}\cdot\mathbf{M}_T-\alpha T\right]. \tag{6.2.13}$$

where the following notations are introduced:

$$\hat{\mathbf{I}}^{-1}=\frac{1}{\det\hat{\mathbf{I}}}\begin{bmatrix}I_y & I_{xy}\\ I_{xy} & I_x\end{bmatrix}=\frac{1}{\det\mathbf{I}}\left(I_y\mathbf{e}_x\circ\mathbf{e}_x+I_{xy}\left(\mathbf{e}_x\circ\mathbf{e}_y+\mathbf{e}_y\circ\mathbf{e}_x\right)+I_x\mathbf{e}_y\circ\mathbf{e}_y\right), \tag{6.2.14}$$

$$\mathbf{I}_1=\mathbf{e}_z\times\hat{\mathbf{I}}^{-1}=\frac{1}{\det\hat{\mathbf{I}}}\begin{bmatrix}-I_{xy} & -I_x\\ I_y & I_{xy}\end{bmatrix}, \tag{6.2.15}$$

$$\mathbf{I}_2=\frac{1}{\det\hat{\mathbf{I}}}\left(-I_y\mathbf{e}_y\circ\mathbf{e}_y-I_{xy}\left(\mathbf{e}_y\circ\mathbf{e}_x+\mathbf{e}_x\circ\mathbf{e}_y\right)-I_x\mathbf{e}_x\circ\mathbf{e}_x\right). \tag{6.2.16}$$

The axial normal stresses can be calculated as

$$\sigma_z=E\left[\left(\frac{F_T}{A_E}-\mathbf{R}\cdot\mathbf{I}_1\cdot\mathbf{M}_T-\alpha T\right)+F\left(\frac{1}{A_E}+\mathbf{R}\cdot\mathbf{I}_2\cdot\boldsymbol{\rho}\right)\right]. \tag{6.2.17}$$

6.3. Determination of the displacement field in inhomogeneous beams

In this section the determination of the displacement field in inhomogeneous prismatic bars is investigated when the material properties $E(x,y)$ and $\alpha(x,y)$ and temperature field $T(x,y)$ are

arbitrary functions of the cross-sectional coordinates *x* and *y* coordinates and do not depend on the axial coordinate.

According to the Euler-Bernoulli beam theory, the assumed form of the displacement field is

$$\mathbf{u}(x,y,z) = u(z)\mathbf{e}_x + v(z)\mathbf{e}_y + w(x,y,z)\mathbf{e}_z = \mathbf{U}(z) + w(x,y,z)\mathbf{e}_z . \tag{6.3.1}$$

The axial displacement can be expressed as

$$w(x,y,z) = -x\frac{\partial u(z)}{\partial z} - y\frac{\partial u(z)}{\partial z} + w_0(z) = -\mathbf{R}\cdot\frac{\partial \mathbf{U}(z)}{\partial z} + w_0(z) . \tag{6.3.2}$$

The non-zero normal strain is

$$\varepsilon_z = \frac{\partial w}{\partial z} = -x\frac{\partial^2 u(z)}{\partial z^2} - y\frac{\partial^2 u(z)}{\partial z^2} + \frac{\partial w_0(z)}{\partial z} = -\mathbf{R}\cdot\frac{\partial^2 \mathbf{U}(z)}{\partial z^2} + \frac{\partial w_0(z)}{\partial z} . \tag{6.3.3}$$

The constitutive equation for this case has the following form:

$$\varepsilon_z = \frac{\sigma_z}{E} + \alpha T . \tag{6.3.4}$$

The combination of Eqs. (6.3.4) and (6.3.3) gives the axial normal stress for the inhomogeneous beam.

$$\sigma_z = -E\mathbf{R}\cdot\frac{\partial^2 \mathbf{U}(z)}{\partial z^2} + E\frac{\partial w_0(z)}{\partial z} - E\alpha T . \tag{6.3.5}$$

The equilibrium equation gives the axial displacement of the centerline w_0

$$\int_A \sigma_z \mathrm{d}A = F = \frac{\partial w_0}{\partial z} A_E - N_T , \tag{6.3.6}$$

$$w_0 = \frac{F + N_T}{A_E} z . \tag{6.3.7}$$

For the moment **M** we have

$$\int_A \mathbf{R}\times\sigma_z\mathbf{e}_z \mathrm{d}A = \mathbf{M} , \tag{6.3.8}$$

$$\mathbf{e}_z\times\mathbf{M} = \int_A \mathbf{R}\sigma_z \mathrm{d}A = -\int_A E\mathbf{R}\circ\mathbf{R}\mathrm{d}A\cdot\frac{\partial^2\mathbf{U}}{\partial z^2} + \frac{\partial w_0}{\partial z}\int_A E\mathbf{R}\mathrm{d}A - \int_A E\alpha T\mathbf{R}\mathrm{d}A . \tag{6.3.9}$$

The combination of Eqs. (6.3.9), (6.1.18) and (6.1.5) leads to

$$\mathbf{e}_z\times(\mathbf{M}+\mathbf{M}_T) = -\mathbf{I}\frac{\partial^2\mathbf{U}}{\partial z^2} . \tag{6.3.10}$$

From Eqs. (6.3.10) and (6.3.1) we get, that

$$\mathbf{e}_z\times\left(\frac{\partial^2 u(z)}{\partial z^2}\mathbf{e}_x + \frac{\partial^2 v(z)}{\partial z^2}\mathbf{e}_y\right) = \mathbf{I}^{-1}\cdot(\mathbf{M}+\mathbf{M}_T) , \tag{6.3.11}$$

when **M** and $\mathbf{M}_T$ are constant,

$$u(z) = \frac{z^2}{2}\mathbf{I}^{-1}\cdot(\mathbf{M}+\mathbf{M}_T)\cdot\mathbf{e}_y, \tag{6.3.12}$$

$$v(z) = -\frac{z^2}{2}\mathbf{I}^{-1}\cdot(\mathbf{M}+\mathbf{M}_T)\cdot\mathbf{e}_x. \tag{6.3.13}$$

6.4. Curved layered beams and strips

In this section thermoelastic problems of curved beams are investigated for bimetallic curved strips and multilayered beams. The thermal stresses are caused by uniform temperature field. The functionally graded beam is approximated with the multilayered approach.

6.4.1. Bimetallic beams and strips

In this subsection a curved bimetallic beam is investigated, which can be seen in Fig. 6.3. The thin beam consists of two different elastic materials.

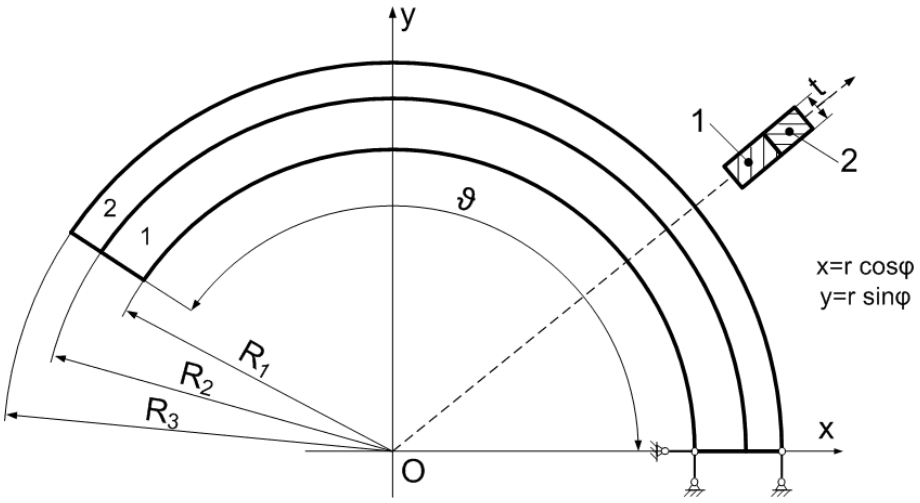

Figure 6.3. Bimetallic curved beam with rectangular cross section.

The governing equations and boundary conditions are formulated in the cylindrical coordinate system $Or\varphi z$, and the plane z=0 is the symmetry plane of the two-layered curved beam for its geometrical properties. The connection between beam component 1 and beam component 2 at the common cylindrical boundary surface $r=R_2$ is perfect, both the displacements and tractions have no jump at $r=R_2$. There are no present body forces and the whole boundary of the bimetallic curved beam is stress free. This means that

$$\sigma_r(R_1,\varphi) = \sigma_r(R_3,\varphi) = \tau_{r\varphi}(R_1,\varphi) = \tau_{r\varphi}(R_3,\varphi) = 0, \qquad 0 \le \varphi \le \vartheta, \tag{6.4.1}$$

$$\sigma_\varphi(r,\vartheta) = \sigma_\varphi(r,0) = \tau_{r\varphi}(r,\vartheta) = \tau_{r\varphi}(r,0) = 0, \qquad R_1 \le r \le R_3. \tag{6.4.2}$$

In the framework of generalized plane stress model the boundary condition

$$\sigma_\varphi(r,\vartheta)=\sigma_\varphi(r,0)=0, \qquad R_1\le r\le R_3, \tag{6.4.3}$$

will be satisfied only in weak form such as

$$N=\int_{R_1}^{R_3}\sigma_\varphi(r,\vartheta)\mathrm{d}r=\int_{R_1}^{R_3}\sigma_\varphi(r,0)\mathrm{d}r=0, \tag{6.4.4}$$

$$M=\int_{R_1}^{R_3}r\sigma_\varphi(r,\vartheta)\mathrm{d}r=\int_{R_1}^{R_3}r\sigma_\varphi(r,0)\mathrm{d}r=0. \tag{6.4.5}$$

The stress resultants and stress couple resultants vanish only at the end cross sections $\varphi=0$ and $\varphi=\vartheta$. Initially the temperature of the two-layer composite beam is the reference temperature. Its temperature is slowly raised to a constant uniform temperature, where the temperature change is T. The deformations and stresses are caused by only the uniform change of temperature. The solution of this problem is derived from the next displacement field

$$u_i(r,\varphi)=U_i(r)+f_1\cos\varphi+f_2\sin\varphi, \quad (i=1,2), \tag{6.4.6}$$

$$v_i(r,\varphi)=Cr\varphi+f_1\sin\varphi-f_2\cos\varphi+f_3 r, \quad (i=1,2), \tag{6.4.7}$$

where the displacement in the radial direction is denoted by u_i and the displacement in tangential direction is indicated by v_i, furthermore lower index i refers to curved beam component i (i=1,2). In Eqs. (6.4.6), (6.4.7) f_1, f_2 and f_3 are constants whose values obtained from the displacement boundary conditions (Fig. 6.3).

$$u_1(R_1,0)=0,\ v_1(R_1,0)=0,\ v_2(R_3,0)=0. \tag{6.4.8}$$

The constant C will be determined from the stress boundary conditions (6.4.1), (6.4.4), (6.4.5) and the continuity conditions of displacements and normal stress field σ_r at the common cylindrical boundary between beam component 1 and beam component 2. From Eqs. (6.4.6), (6.4.7) it follows that the strains can be expressed in terms of U_i and C as

$$\varepsilon_{\varphi i}=\frac{U_i}{r}+C, \qquad \varepsilon_{ri}=\frac{dU_i}{dr}, \qquad (i=1,2). \tag{6.4.9}$$

Combination of Eq. (6.4.9) with Eq. (6.4.10) gives the strain compatibility equation

$$r\frac{d\varepsilon_{\varphi i}}{dr}+\varepsilon_{\varphi i}-\varepsilon_{ri}-C=0, \qquad (i=1,2). \tag{6.4.10}$$

In the present problem the constitutive law of linear thermoelasticity [52], [60] has the next form

$$E_i\varepsilon_{ri}=\sigma_{ri}-\nu_i\sigma_{\varphi i}+E_i\alpha_i T, \qquad (i=1,2), \tag{6.4.11}$$

$$E_i\varepsilon_{ri}=\sigma_{\varphi i}-\nu_i\sigma_{ri}+E_i\alpha_i T, \qquad (i=1,2). \tag{6.4.12}$$

where σ_{ri}, $\sigma_{\varphi i}$ denote the radial and circumferential normal stresses of the i-th layer (i=1,2). Substituting Eqs. (6.4.11), (6.4.12) into Eq. (6.4.10) yields

$$r\frac{\mathrm{d}}{\mathrm{d}r}\left(-\nu_i\sigma_{ri}+\sigma_{\varphi i}+E_i\alpha_i T\right)-(1+\nu_i)\sigma_{ri}+(1+\nu_i)\sigma_{\varphi i}-E_i C=0,\quad (i=1,2). \tag{6.4.13}$$

In our case the equation of mechanical equilibrium is as follows

$$\frac{\mathrm{d}\sigma_{ri}}{\mathrm{d}r}+\frac{\sigma_{ri}-\sigma_{\varphi i}}{r}=0,\quad (i=1,2). \tag{6.4.14}$$

The general solution of Eq. (6.4.14) in terms of stress function V_i=V_i(r) can be given as

$$\sigma_{ri}=\frac{V_i(r)}{r},\ \ \sigma_{\varphi i}=\ \ \frac{\mathrm{d}V_i}{\mathrm{d}r},\quad (i=1,2). \tag{6.4.15}$$

Combination of Eq. (6.4.13) with formulae of normal stresses leads to the following differential equation

$$r^2\frac{\mathrm{d}V_i^2}{\mathrm{d}^2 r}+r\frac{\mathrm{d}V_i}{\mathrm{d}r}-V_i-E_i C r=0,\quad (i=1,2). \tag{6.4.16}$$

The solution of Eq. (6.4.16) is as follows

$$V_1(r)=c_1 r+\frac{c_2}{r}+\frac{E_1 C}{2}r\ln r,\quad R_1\le r<R_2, \tag{6.4.17}$$

$$V_2(r)=c_3 r+\frac{c_4}{r}+\frac{E_2 C}{2}r\ln r,\quad R_2<r\le R_3. \tag{6.4.18}$$

Here, we note that the stress field and strain field are independent of the polar angle φ. A simple computation shows that

$$N=\int_{R_1}^{R_2}\sigma_\varphi(r)\mathrm{d}r=\int_{R_1}^{R_2}\frac{d}{dr}(r\sigma_r)\mathrm{d}r=R_2\sigma_{r1}(R_2)-R_1\sigma_{r1}(R_1)+R_3\sigma_{r2}(R_3)-R_2\sigma_{r2}(R_2)=0 \tag{6.4.19}$$

if the stress boundary conditions

$$\sigma_{r1}(R_1)=\sigma_{r2}(R_3)=0, \tag{6.4.20}$$

and stress continuity condition

$$\sigma_{r1}(R_2)=\sigma_{r2}(R_2) \tag{6.4.21}$$

are satisfied. To obtain the stress field we must determine the five constants c_1, c_2, c_3, c_4 and C. The next equation will be used to get the value of the unknown constants

$$\sigma_{r1}(R_1)=0,\ \ \sigma_{r2}(R_3)=0,\ \ \sigma_{r1}(R_2)=\sigma_{r2}(R_2), \tag{6.4.22}$$

$$U_1(R_2)=U_2(R_2),\quad \int_{R_1}^{R_2}r\sigma_{\varphi 1}\mathrm{d}r+\int_{R_2}^{R_3}r\sigma_{\varphi 2}\mathrm{d}r=0. \tag{6.4.23}$$

We can reformulate Eq. $(6.4.23)_1$ by the use of Eq. $(6.4.9)_1$ as

$$\varepsilon_{\varphi 1}(R_2) = \varepsilon_{\varphi 2}(R_2). \tag{6.4.24}$$

Eq. (6.4.24) in terms of stresses is expressed as

$$\frac{1}{E_1}\Big[\sigma_{\varphi 1}(R_2) - \nu_1\sigma_{r1}(R_2)\Big] + \alpha_1 T = \frac{1}{E_2}\Big[\sigma_{\varphi 2}(R_2) - \nu_2\sigma_{r2}(R_2)\Big] + \alpha_2 T. \tag{6.4.25}$$

The following system of linear equations can be derived from Eqs. (6.4.22), (6.4.23) and (6.4.25)

$$\mathbf{M}\mathbf{x} = \mathbf{f}\ , \tag{6.4.26}$$

where

$$\mathbf{M} = \Big[m_{ij}\Big],\ \ (i, j = 1,2,3,4,5),\ \ \mathbf{f} = \big[0,0,0,f,0\big]^T,\ \mathbf{x} = \big[c_1, c_2, c_3, c_4, C\big]^T, \tag{6.4.27}$$

$$m_{11} = R_1,\ m_{12} = \frac{1}{R_1},\ m_{13} = m_{14} = m_{21} = m_{22} = 0,\ m_{15} = \frac{E_1}{2}R_1\ln R_1,$$

$$m_{23} = R_3,\ m_{24} = \frac{1}{R_3},\ m_{25} = \frac{E_2}{2}R_3\ln R_3,\ m_{31} = R_2,\ m_{32} = \frac{1}{R_2},\ m_{33} = -R_2,\ m_{34} = -\frac{1}{R_2},$$

$$m_{35} = \frac{E_1 - E_2}{2}R_2\ln R_2,\ m_{41} = \frac{1-\nu_1}{E_1},\ m_{42} = -\frac{1+\nu_1}{E_1R_2^2},\ m_{43} = -\frac{1-\nu_2}{E_2},\ m_{44} = \frac{1+\nu_2}{E_2R_2^2},$$

$$m_{45} = \frac{\nu_2 - \nu_1}{2}\ln R_2,\ m_{51} = \frac{1}{2}\Big(R_2^2 - R_1^2\Big),\ m_{52} = -\ln\frac{R_2}{R_1},\ m_{53} = \frac{1}{2}\Big(R_3^2 - R_2^2\Big),\ m_{54} = -\ln\frac{R_3}{R_2}, \tag{6.4.28}$$

$$m_{55} = \frac{E_1}{4}\left[R_2^2\ln R_2 - R_1^2\ln R_1 + \frac{1}{2}\Big(R_2^2 - R_1^2\Big)\right] + \frac{E_2}{4}\left[R_3^2\ln R_3 - R_2^2\ln R_2 + \frac{1}{2}\Big(R_3^2 - R_2^2\Big)\right],$$

$$f = \big(\alpha_2 - \alpha_1\big)T.$$

After the solution of system of linear equation (6.4.26) we can compute the stresses and displacements by the next formulae

$$\sigma_{r1}(r) = c_1 + \frac{c_2}{r^2} + \frac{E_1 C}{2}\ln r,\quad \sigma_{\varphi 1}(r) = c_1 - \frac{c_2}{r^2} + \frac{E_1 C}{2}(\ln r + 1), \tag{6.4.29}$$

$$\sigma_{r2}(r) = c_2 + \frac{c_3}{r^2} + \frac{E_2 C}{2}\ln r,\quad \sigma_{\varphi 2}(r) = c_3 - \frac{c_4}{r^2} + \frac{E_2 C}{2}(\ln r + 1), \tag{6.4.30}$$

$$U_1(r) = \frac{1-\nu_1}{E_1}c_1 r - \frac{1+\nu_1}{rE_1}c_2 + \frac{Cr}{2}\Big[\big(1-\nu_1\big)\ln r - 1\Big] + \alpha_1 T r, \tag{6.4.31}$$

$$U_2(r) = \frac{1-\nu_2}{E_2}c_3 r - \frac{1+\nu_2}{rE_2}c_4 + \frac{Cr}{2}\Big[\big(1-\nu_2\big)\ln r - 1\Big] + \alpha_2 T r, \tag{6.4.32}$$

$$f_1 = -U_1(R_1) = -\frac{1-\nu_1}{E_1}c_1R_1 + \frac{1+\nu_1}{R_1E_1}c_2 - \frac{CR_1}{2}\left[(1-\nu_1)\ln R_1 - 1\right] + \alpha_1 TR_1, \quad f_2 = f_3 = 0, \tag{6.4.33}$$

$$u_i(r) = U_i(r) - U_1(R_1)\cos\varphi, \quad (i = 1,2), \tag{6.4.34}$$

$$v_i(r) = Cr\varphi + U_1(R_1)\sin\varphi, \quad (i = 1,2). \tag{6.4.35}$$

6.4.2. Strength of materials solution for curved beams

According to paper by Ecsedi and Dluli [73] it is assumed that

$$u = U(\varphi), \quad v = r\phi(\varphi) + \frac{\mathrm{d}U}{\mathrm{d}\varphi} \tag{6.4.36}$$

is valid for the whole two-layer composite curved beam. From the strain-displacement relationships of linearized theory of elasticity we obtain

$$\varepsilon_r = \varepsilon_z = \gamma_{r\varphi} = \gamma_{\varphi z} = \gamma_{rz} = 0, \tag{6.4.37}$$

$$\varepsilon_\varphi = \frac{1}{r}\left(U + \frac{\mathrm{d}^2U}{\mathrm{d}\varphi^2}\right) + \frac{\mathrm{d}\phi}{\mathrm{d}\varphi}, \tag{6.4.38}$$

that is one strain component is different from zero. The next constitutive equation will be used

$$\sigma_{\varphi i} = E_i\varepsilon_\varphi - E_i\alpha_i T = \frac{E_i}{r}\left(U + \frac{\mathrm{d}^2U}{\mathrm{d}\varphi^2}\right) + E_i\frac{\mathrm{d}\phi}{\mathrm{d}\varphi} - -E_i\alpha_i T, \quad (i = 1,2). \tag{6.4.39}$$

The stress- and stress-couple resultants vanish since there are no applied mechanical load (Fig. 6.3), that is, we have

$$N = \int_{R_1}^{R_3}\sigma_\varphi \mathrm{d}r = k_1\left(U + \frac{d^2U}{d\varphi^2}\right) + k_2\frac{\mathrm{d}\phi}{\mathrm{d}\varphi} - \beta T = 0, \tag{6.4.40}$$

$$M = \int_{R_1}^{R_3} r\sigma_\varphi \mathrm{d}r = k_2\left(U + \frac{\mathrm{d}^2U}{\mathrm{d}\varphi^2}\right) + k_3\frac{\mathrm{d}\phi}{\mathrm{d}\varphi} - \gamma T = 0. \tag{6.4.41}$$

Here, the next notations are introduced

$$\begin{aligned} &k_1 = E_1\ln\frac{R_2}{R_1} + E_2\ln\frac{R_3}{R_2}, \quad k_2 = E_1\left(R_2 - R_1\right) + E_2\left(R_3 - R_2\right), \\ &k_3 = \frac{E_1}{2}\left(R_2^2 - R_1^2\right) + \frac{E_2}{2}\left(R_3^2 - R_2^2\right), \end{aligned} \tag{6.4.42}$$

$$\beta = \alpha_1 E_1 \left(R_2 - R_1 \right) + \alpha_2 E_2 \left(R_3 - R_2 \right), \ \gamma = \frac{\alpha_1 E_1}{2} \left(R_2^2 - R_1^2 \right) + \frac{\alpha_2 E_2}{2} \left(R_3^2 - R_1^2 \right). \quad (6.4.43)$$

From Eqs. (6.4.40), (6.4.41) we get

$$U + \frac{\mathrm{d}^2 U}{\mathrm{d}\varphi^2} = \frac{\beta k_3 - \gamma k_2}{k_1 k_3 - k_2^2} T, \ \ \frac{\mathrm{d}\phi}{\mathrm{d}\varphi} = \frac{\gamma k_1 - \beta k_2}{k_1 k_3 - k_2^2} T. \quad (6.4.44)$$

Combination of Eq. (6.4.39) with Eq. (6.4.44) leads to the expression of circumferential normal stresses

$$\sigma_{\varphi i} = E_i \left\{ \frac{1}{k_1 k_3 - k_2^2} \left(\frac{\beta k_3 - \gamma k_2}{r} + \gamma k_1 - \beta k_2 \right) - \alpha_i \right\} T, \quad (i = 1,2). \quad (6.4.45)$$

Knowing $\sigma_{\varphi i}$ (i=1,2) we can determine the normal stress σ_{ri} by the use of equation of equilibrium

$$\frac{\mathrm{d}}{\mathrm{d}r} \left(r \sigma_{ri} \right) = \sigma_{\varphi i} \quad (i = 1,2). \quad (6.4.46)$$

A simple computation gives

$$\sigma_{r1}(r) = E_1 \left\{ \frac{1}{\left(k_1 k_3 - k_2^2 \right) r} \left(\beta k_3 - \gamma k_2 \right) \ln \frac{r}{R_1} + \left(\gamma k_1 - \beta k_2 \right) \left(r - R_1 \right) - \alpha_1 \frac{r - R_1}{r} \right\} T, R_1 \le r \le R_2, \quad (6.4.47)$$

$$\sigma_{r2}(r) = \frac{R_2}{r} \sigma_{r1}(R_2) + E_2 \left\{ \frac{1}{\left(k_1 k_3 - k_2^2 \right) r} \left(\beta k_3 - \gamma k_2 \right) \ln \frac{r}{R_2} + \left(\gamma k_1 - \beta k_2 \right) \left(r - R_2 \right) - \alpha_2 \frac{r - R_2}{r} \right\} T, \quad (6.4.48)$$

$$R_2 \le r \le R_3,$$

Integration of Eq. (6.4.44) and using of boundary condition (6.4.8) lead to the expressions of radial and circumferential displacements

$$U(\varphi) = \frac{\beta k_3 - \gamma k_2}{k_1 k_3 - k_2^2} \left(1 - \cos \varphi \right) T, \quad (6.4.49)$$

$$v(\varphi, r) = \frac{\left(\gamma k_1 - \beta k_2 \right) r \varphi - \left(\beta k_3 - \gamma k_2 \right) \sin \varphi}{k_1 k_3 - k_2^2} T. \quad (6.4.50)$$

6.4.3. Radially graded strips

In this subsection the problem of functionally graded strips in uniform temperature field will be approximated with a multilayered method based on the one presented in Subsection 6.4.1. Let us consider a layered curved strip with perfectly bonded homogeneous layers, the number of layers is denoted by n. According to Subsection 6.4.1 the equations for this case are:

$$\sigma_{ri}(r) = c_{i1} + \frac{c_{i2}}{r^2} + \frac{E_i C}{2}\ln r, \tag{6.4.51}$$

$$\sigma_{\varphi i}(r) = c_{i1} - \frac{c_{i2}}{r^2} + \frac{E_i C}{2}(\ln r + 1), \tag{6.4.52}$$

$$U_i(r) = \frac{1-\nu_i}{E_i} c_{i1} r - \frac{1+\nu_i}{r E_i} c_{i2} + \frac{Cr}{2}\left[\left(1-\nu_i\right)\ln r - 1\right] + \alpha_i T r, \quad (i = 1,2,...,n). \tag{6.4.53}$$

The unknown constants c_{1i}, c_{2i} and C can be calculated from the boundary and fitting conditions similarly to Eqs. (6.4.22) and (6.4.23).

$$\begin{bmatrix}
1 & R_1^{-1} & 0 & 0 & 0 & 0 & 0 & \cdots & 0 & 0 & 0 & 0 & \frac{E_1}{2}\ln(R_1) \\
1 & R_2^{-1} & -1 & -R_2^{-1} & 0 & 0 & 0 & \cdots & 0 & 0 & 0 & 0 & \left(\frac{E_1 - E_2}{2}\right)\ln(R_2) \\
0 & 0 & 1 & R_3^{-1} & -1 & -R_3^{-1} & 0 & \cdots & 0 & 0 & 0 & 0 & \left(\frac{E_2 - E_3}{2}\right)\ln(R_3) \\
\vdots & & & & & & \ddots & & & & & & \vdots \\
0 & 0 & 0 & 0 & 0 & 0 & 0 & \cdots & 1 & R_n^{-1} & -1 & -R_n^{-1} & \left(\frac{E_n - E_{n-1}}{2}\right)\ln(R_n) \\
0 & 0 & 0 & 0 & 0 & 0 & 0 & \cdots & 0 & 0 & 1 & R_{n+1}^{-1} & \frac{E_n}{2}\ln(R_{n+1}) \\
\frac{1-\nu_1}{E_1}R_2 & -\frac{1+\nu_1}{E_1 R_2} & \frac{\nu_2 - 1}{E_2}R_2 & \frac{1+\nu_2}{E_2 R_2} & 0 & 0 & 0 & \cdots & 0 & 0 & 0 & 0 & \frac{R_2\ln(R_2)}{2}(\nu_2 - \nu_1) \\
\vdots & & & & & & \ddots & & & & & & \vdots \\
0 & 0 & 0 & 0 & 0 & 0 & 0 & \cdots & \frac{1-\nu_{n-1}}{E_{n-1}}R_n & -\frac{1+\nu_{n-1}}{E_{n-1}R_n} & \frac{\nu_n - 1}{E_n}R_n & \frac{1+\nu_n}{E_n R_n} & \frac{R_n\ln(R_n)}{2}(\nu_n - \nu_{n-1}) \\
\frac{R_2^2 - R_1^2}{2} & \ln\left(\frac{R_2}{R_1}\right) & \frac{R_3^2 - R_2^2}{2} & \ln\left(\frac{R_3}{R_2}\right) & & & & \cdots & & & & \ln\left(\frac{R_{n+1}}{R_n}\right) & \sum_{j=1}^{n} E_j\left[R_{j+1}^2\left(\ln(R_{j+1}) - \frac{1}{2}\right) - R_j^2\left(\ln(R_j) - \frac{1}{2}\right)\right]
\end{bmatrix}
\begin{bmatrix} c_{11} \\ c_{12} \\ c_{21} \\ c_{22} \\ c_{31} \\ c_{32} \\ \vdots \\ c_{n1} \\ c_{n2} \\ C \end{bmatrix} =
\begin{bmatrix} 0 \\ 0 \\ 0 \\ \vdots \\ 0 \\ 0 \\ (\alpha_1 - \alpha_2)TR_2 \\ \vdots \\ (\alpha_n - \alpha_{n-1})TR_n \\ 0 \end{bmatrix} \tag{6.4.54}$$

After the calculation of the stress field, the accuracy of the tangential normal stresses can be improved with curve fitting as we can see in Example 14.

6.5. Numerical examples

In this section four examples will be presented. In the first example a two-layered prismatic beam will be investigated in constant temperature field, in our second example a functionally graded beam will be examined loaded with concentrated force, moment and uniform temperature field. These problems will be solved with the method presented in Sections 6.1-6.3. In Subsection 6.5.3 a bimetallic- , in 6.5.4 a radially graded curved strip will be investigated.

6.5.1. Example 11

For this numerical example the cross section of the considered bar is shown in Fig. 6.4. This cross section is made of two different homogeneous materials with Young moduli $E_1=E$, $E_2=3E$ and the coefficients of linear thermal expansion are $\alpha_1=\alpha$, $\alpha_2=2\alpha$. There are no applied mechanical loads, that is $\mathbf{F}=\mathbf{0}$, $\mathbf{M}=\mathbf{0}$. The temperature difference T is constant on the whole cross section. For homogeneous cross section the uniform temperature does not produce any stress field, the homogeneous bar is stress free. The position of the E-weighted centre of cross section is given in Fig. 6.4. The elements of Euler tensor are

$$I_x = 512Ec^4,\ I_y = 64Ec^4,\ I_{xy} = -96Ec^4. \tag{6.5.1}$$

A simple computation gives

$$A_E = 48Ec^2,\ N_T = 72E\alpha Tc^2\,. \tag{6.5.2}$$

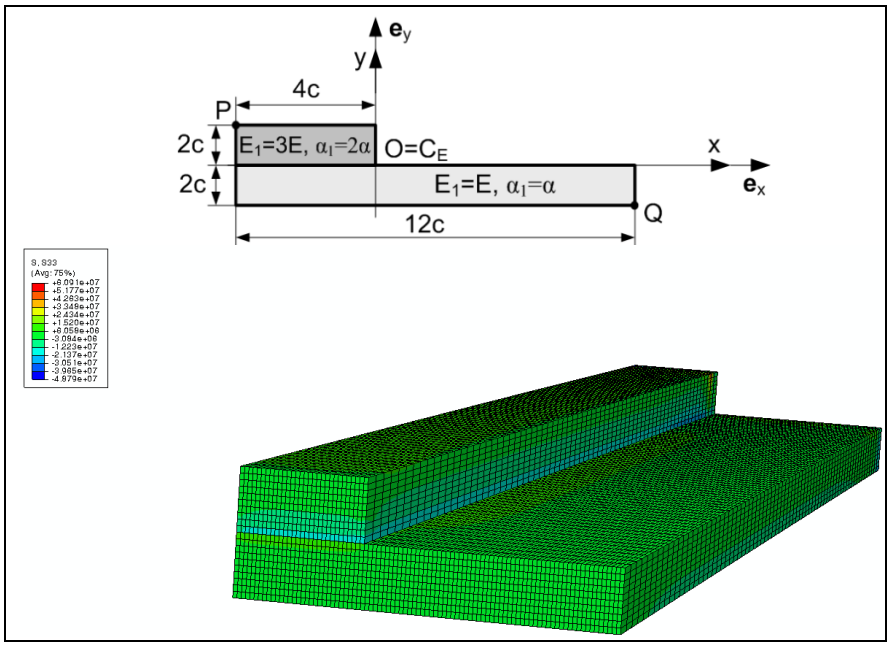

Figure 6.4. Nonhomogeneous cross section and its finite element model.

By the use of above computed values we can determine the stress field of composite bar caused by uniform temperature field. We determine the normal stresses at points $P(-4c, 2c)$ and $Q(8c, -2c)$. The computation gives

$$\sigma_z(P) = 20.002E\alpha T,\ \sigma_z(Q) = -5.0413E\alpha T. \tag{6.5.3}$$

From the finite element simulations in Abaqus CAE we get $\sigma_{zFE}(R) = 54.69\text{MPa}$, $\sigma_{zFE}(Q) = -45.33\text{MPa}$, from our calculations we get $\sigma_z(R) = 54.21\text{MPa}$, $\sigma_z(Q) = -45.87\text{MPa}$.

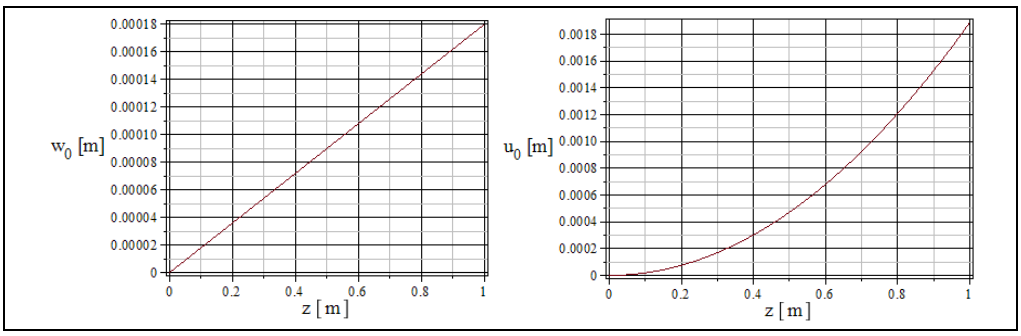

Figure 6.5. The displacement fields of the prismatic composite bar.

6.5.2. Example 12

In this example a functionally graded prismatic beam will be considered. The geometry of the beam, the loadings and the material parameters are:

$$a = 0.5 \text{ m}, b = 0.7 \text{ m}, \mathbf{F} = \mathbf{e}_z \text{kN}, \mathbf{M} = 150\mathbf{e}_x + 100\mathbf{e}_y \text{Nm}, T = 100\text{K},$$

$$E(r) = 2.1 \cdot 10^{11}(1 + 20x - 15y)\,\text{Pa}, \ \alpha(r) = 12 \cdot 10^{-6}(1 + 20x - 15y)\frac{1}{\text{K}}.$$

The finite element model can be seen in Fig. 6.6. The FE model was built from homogeneous segments (element lines as we can see in Fig. 6.6) with discrete values of the material properties calculated in the middle of each segment.

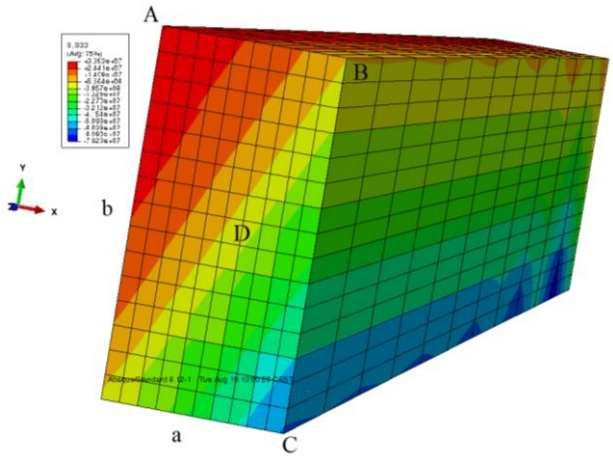

Figure 6.6. The finite element model of the functionally graded prismatic beam.

The results of the finite element model are in good agreement with the ones calculated with the previously presented method. The axial normal stresses of the marked points (in Fig. 6.5) are $\sigma_z \{A, B, C, D\} = \{32.65, 6.16, -60.3, 9.91\}\,\text{MPa}$.

6.5.3. Example 13

In this example a bimetallic curved beam will be considered (Fig. 6.3). This problem is solved with the two methods presented in Sections 6.4.1 and 6.4.2, then these results are compared to the finite element calculations. The next data are used in the numerical example:

$$R_1 = 0.5 \text{ m}, R_2 = 0.6 \text{ m}, R_3 = 0.7 \text{ m}, E_1 = 200 \text{ GPa}, E_2 = 70 \text{ GPa},$$

$$\nu_1 = 0.27, \nu_2 = 0.33, \alpha_1 = 11 \cdot 10^{-6}\,\frac{1}{\text{K}}, \alpha_2 = 23 \cdot 10^{-3}\,\frac{1}{\text{K}}, T = 200\text{K}, \vartheta = \frac{3}{2}\pi.$$

In Figs. 6.7 and 6.8 the graphs of normal stresses σ_r and σ_φ are illustrated in comparison with FE solution - which was carried out by Abaqus CAE software / coupled temperature-displacement solver.

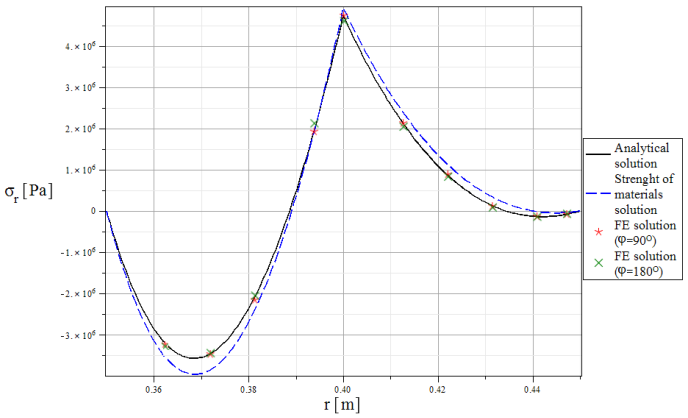

Figure 6.7. Plots of the radial normal stresses.

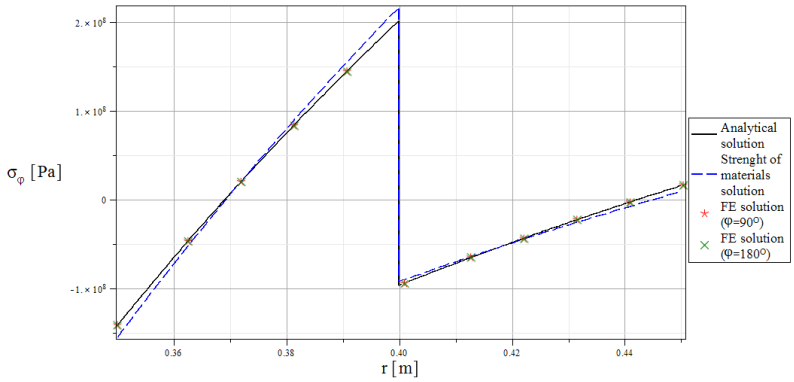

Figure 6.8. Plots of the circumferential normal stresses.

In Fig. 6.9 the finite element model of the problem and the von Mises equivalent stress field are presented, here we can see that the stress distribution does not depend on the polar angle φ except at the ends of the curved beam.

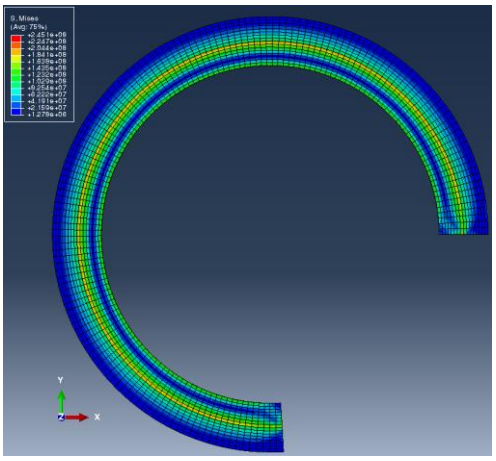

Figure 6.9. The finite element model with the equivalent stress field.

Figure 6.10 shows the 3D graphs of displacements *U(r, φ)* and *v(r, φ)* obtained by the previously presented elasticity solution when $R_1 \le r \le R_3$ and $0 \le \varphi \le \pi$.

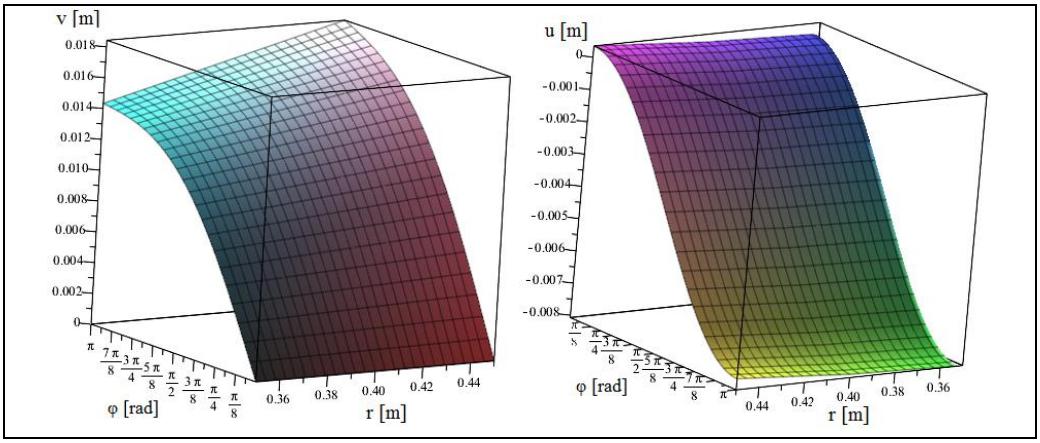

Figure 6.10. Plots of displacement field.

6.5.5. Example 14

In this example the problem of a functionally -radially- graded curved strip is replaced with the problem of a multilayered curved strip as we can see in Subsection 6.4.3, the number of layers is *n* and their thicknesses are equal. The next data are used in the numerical example:

$$a = 0.5\ \text{m}, b = 0.7\ \text{m}, \vartheta = \frac{3}{2}\pi,\ T = 100\text{K}, K(r) = \left(\frac{r - R_1}{R_2 - R_1}\right),\ \nu(r) = \left(0.32 - 0.24\right)K(r)^m + 0.24,$$

$$E(r) = \left(2.1 \cdot 10^{11} - 3.5 \cdot 10^{11}\right)K(r)^m + 3.5 \cdot 10^{11}\ \text{Pa}, \alpha(r) = \left(12 \cdot 10^{-6} - 3.8 \cdot 10^{-6}\right)K(r)^m + 3.8 \cdot 10^{-6}\ \frac{1}{\text{K}}.$$

The results were compared to finite element simulations and they are in good agreement (in the case of *n*=32 the maximum tangential stresses are $\sigma_{\varphi,\ FEmax}$=24.9MPa, $\sigma_{\varphi,\ multilayered\ max}$=24.01MPa). The graphs of the radial normal stress and displacement field are shown in Fig. 6.11.

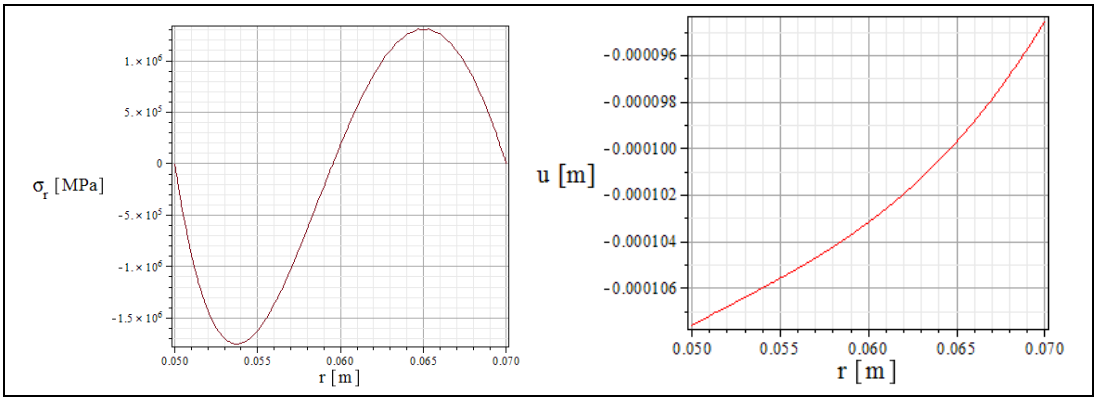

Figure 6.11. The radial normal stress and displacement field of the curved beam.

With curve fitting the accuracy of the tangential normal stresses can be improved. In our current case the fitting function of the tangential normal stress has the following recommended form (*m*<10):

$$\sigma_{app\,\varphi}(r) = F_0 + F_1 r + F_2 r^2 + F_3 r^3 + F_4 r^4, \tag{6.5.4}$$

the result can be seen in Fig. 6.12.

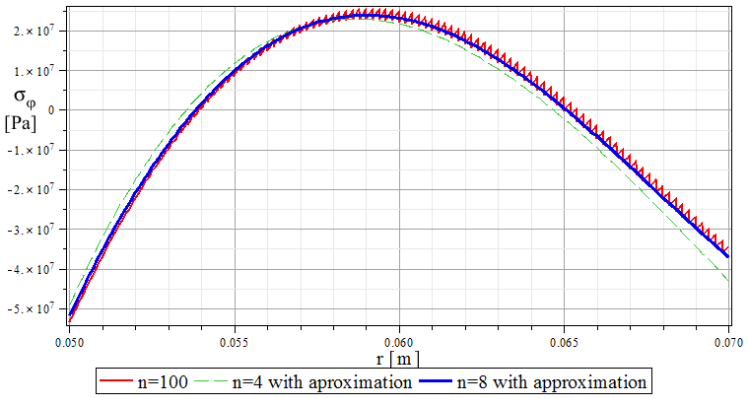

Figure 6.12. The plot of the normal tangential stresses in the curved functionally graded strip.

7. Summary and theses

The main goal of this dissertation was to present analytical and numerical methods to deal with the thermoelastic problem of composite and functionally graded simple structural components. The temperature-, displacement- and stress fields were determined in spherical bodies, disks and beams subjected to mechanical and thermal loads. Several methods were derived for steady-state thermoelastic problems of parts made from functionally graded materials, where the material properties are arbitrary functions of one (or two) coordinate(s) and the temperature field. The time-independence of the functions involved separates the analysis of the temperature field from that of the elastic field, therefore these problems become uncoupled.

After the introduction and the overview of the literature, the basic concepts and equations of thermoelasticity were presented in Chapter 2, such as the equilibrium equation and constitutive equations of linear thermoelasticity, functions of temperature-dependent material properties, etc.

In Chapter 3 two analytical methods were derived for layered composite spheres, where one based on the superposition of the cases of pure mechanical and pure thermal loading while the other used a direct form of the displacement field. Then two additional analytical methods were presented for radially graded spheres with special -mostly power-law based- functions for the material properties.

In Chapter 4 numerical methods were presented for determining the temperature-, displacement- and stress field within functionally -radially- graded spherical components, when the material properties are arbitrary functions of the radial coordinate and temperature. The possibility of approximating this one-dimensional static thermoelastic problem of functionally graded spheres with multilayered approach was investigated. A second method was derived which solves the problem of radially graded spheres with a coupled system of ordinary differential equations containing the radial displacement and stress function and transforms the two point boundary value problem to an initial value problem. This chapter contained special problems of functionally graded spherical bodies, such as incompressible materials or piezoelectric, radially polarized materials.

In Chapter 5 two numerical methods were developed for thin functionally graded rotating disks with arbitrary thickness profile when the material properties are arbitrary functions of the radial coordinate and the temperature field. There were combined thermal and mechanical loads on the cylindrical boundary surfaces. One method used the multilayered approach and the principle of superposition of the thermal and mechanical loads, while the other is an initial value method. The multilayered approach was applied to a generalized plane strain problem of radially bonded layered cylindrical bodies with axisymmetric loading which did not depend on the axial coordinate.

Chapter 6 dealt with the calculation of thermal stresses and displacements in nonhomogeneous prismatic bars caused by mechanical and thermal loads when the cross section of the bar is an arbitrary bounded plain domain, the material properties and the temperature field do not depend on the axial coordinate. Then the problem of curved layered composite and functionally graded curved beams was investigated when the structural components were subjected to special thermal and mechanical loads.

Furthermore numerical examples were presented in the end of each chapter to verify the developed methods, to demonstrate their accuracy, etc. The result were compared to each other, analytical solutions, to results obtained from the literature and FE simulations.

Theses

Thesis 1

I have derived two analytical methods to determine the displacements and stress field in layered composite spherical bodies subjected to axisymmetric mechanical and thermal loads exerted on the inner and outer boundary surfaces. The homogeneous layers were perfectly bonded. The first method uses a direct form of the displacement field, the second model derives the solutions of the combined loading from the superposition of the cases when there is only mechanical load and when there is only thermal load. An analytical solution is presented for the case when the distribution of the Young modulus is described by a certain power-law function, moreover the coefficient of thermal expansion depends on the radial coordinate and on the temperature in a prescribed way. I have solved the thermoelastic problem of radially graded spheres with stress function when the material properties follow a power-law distribution. I have investigated the possibilities of modelling the functionally graded spheres with the method of layered composite spheres. The developed methods have been verified by data obtained from the literature and comparisons have been made with each other and they have led to the same results.

Thesis 2

I have elaborated two numerical methods to deal with the thermoelastic problem of functionally graded spherical bodies subjected to axisymmetric thermal loading and constant pressure. The temperature field, displacements and normal stresses are determined when the material properties are arbitrary functions of the radial coordinate and temperature. The first model is based on the multilayered approach of Thesis 1. The second method uses a coupled system of ordinary differential equations containing the radial displacement and stress function and transforms the two point boundary value problem to an initial value problem. I have derived a numerical solution for radially graded piezoelectric spherical actuators and an analytical method for incompressible functionally graded spheres. By means of numerical examples the accuracy of the developed numerical methods have been investigated, compared to the analytical solutions of Thesis 1 and have been verified by finite element simulations. According to these, it turns out that the numerical models have good accuracy.

Thesis 3

I have derived two numerical methods for the thermoelastic analysis of thin functionally graded rotating disks subjected to combined axisymmetric thermal and mechanical loads. The temperature-dependent material properties of the rotating disk vary arbitrarily along the radial coordinate, moreover the thickness of the disk is an arbitrary function of the radial coordinate. The equations of the steady-state temperature fields have been presented for three cases with different thermal boundary conditions. In the first novel method the displacements and the normal stresses are determined by a multilayered approach which can be used as an analytical solution for layered composite disks with constant thickness. This method has been modified to tackle some thermoelastic problems of multilayered tubes which consist of radially bonded homogeneous layers. Furthermore, the tubes are loaded with constant temperature field and pressure. The second developed method uses a coupled system of ordinary differential equations containing the radial displacement and stress function which transforms the two point boundary value problem to an

initial value problem. An analytical method is proposed for the case when the distribution of the material properties are prescribed as power-law functions of the radial coordinate. The developed numerical methods have been compared to my analytical solution and finite element simulations. The results shows that the models have high accuracy.

Thesis 4

I have elaborated methods to determine the displacement- and stress field of functionally graded prismatic bars whose cross section is an arbitrary bounded plain domain. The material properties and the temperature field are arbitrary functions of the cross-sectional coordinates and do not vary in the axial direction. I have derived a model based on the principle of minimum of complementary energy for the case, when the prismatic bar is subjected to certain mechanical and thermal loads. Furthermore a method has been developed using a direct form of the axial normal strain. I have presented the equations for layered curved beam and I have focused on the problem of bimetallic curved beam in uniform temperature field. The method was extended to approximate the thermoelastic behaviour of functionally -radially- graded curved strips. The developed methods were verified by literature and finite element simulations.

Magyar nyelvű összefoglaló (Summary in Hungarian)

Napjainkban a modern mérnöki anyagok alkalmazása igen széles körben elterjedt. Gondoljunk például a kompozitok térhódítására, vagy a funkcionálisan gradiens anyagok és ezzel együtt az inverz tervezési eljárás előretörésére, melynek oka az ezen anyagokból készült szerkezeti elemek kiváló hő és mechanikai tulajdonságai. A tervezési folyamat során az anyagi viselkedés leírása kiemelt jelentőséggel bír, napjainkban egyre több könyv és folyóiratcikk foglalkozik a modern mérnöki technológiák anyagainak mechanikájával.

A disszertáció hő és mechanikai terhelésnek alávetett kompozit és funkcionálisan gradiens szerkezeti elemek hőrugalmasságtani problémáinak megoldásával foglalkozik. A vizsgálat tárgyát egyszerűbb geometriájú alkatrészek képezik, mint például tárcsák, gömb alakú testek és tartályok, rudak, bimetál szalagok és hengeresen rétegzett testek. A mérnöki gyakorlatban a funkcionálisan gradiens alkatrészeken belül általában egy irányban változik az anyagi összetétel, és ezzel az anyagjellemzők, emiatt a vizsgált problémák nagy részében -a rudak kivételével- ezt az esetet vizsgáltam. A folyamatok időtől való függésétől eltekintettem, így az eredetileg kapcsolt problémákat szét tudtam választani egy hővezetési és egy hőrugalmasságtani feladatra.

Funkcionálisan gradiens anyagok esetén az analitikus megoldások előállítása leszámítva néhány speciális eloszlás esetét, rendkívül körülményes. Éppen ezért a szakirodalomban fellelhető problémák különféle feltételezésekkel élnek. Ide sorolhatjuk például:

- speciális függvények -legtöbbször hatványfüggvény- által leírható anyagi eloszlás,
- a hőmérséklettől való függés elhanyagolása,
- geometriai egyszerűsítések,
- terhelésbeli megszorítások stb.

Ennek tükrében a célkitűzéseim:

(a) analitikus megoldások keresése rétegzett kompozit és funkcionálisan gradiens szerkezeti elemekben kialakuló hőmérséklet-, elmozdulás- és feszültségmező számítására,

(b) numerikus modellek kidolgozása funcionálisan gradiens alkatrészek problémáinak megoldására, amikor az anyagjellemzők a kitüntett koordináta –vagy koordináták- és a hőmérséklet tetszőleges függvényei,

(c) néhány speciális eset vizsgálata, mint például az összenyomhatatlan, vagy a piezoelektromos anyagok avagy a bimetal görbe rudak leírása,

(d) a kidolgozott módszerek pontosságának vizsgálata, összevetésük egymással, a szakirodalomban fellelhető és kereskedelmi szoftverekkel végrehajtott végeselemes szimulációk eredményeivel.

Tézis 1

Levezettem két analitikus módszert többrétegű, gömb alakú testek elmozdulásmezőinek és feszültségeinek meghatározására abban az esetben, amikor azokat forgásszimmetrikus, állandósult állapotú hő és mechanikai terhelések érik. A homogén gömbi rétegeket tökéletesen kapcsolatnak tekintettem. Az egyik módszer az elmozdulásmező egy feltételezett alakjából kiindulva, a másik módszer a tisztán hő és tisztán mechanikai terheléseket tartalmazó alesetek szuperpozíciójából és illesztéséből származtatja a feladat megoldását. Analitikus megoldás lett előállítva arra az esetre, mikor az anyagjellemzők a Poisson szám kivételével a helykoordinátának speciális alakú hatványfüggvényei és a lineáris hőtágulási együttható a hőmérséklet lineáris függvénye. Majd feszültségfüggvények alkalmazásával került kidolgozásra egy másik analitikus modell a hatvány függvény eloszlású anyagi összetétel esetére. Vizsgáltam a lehetőségeit a funkcionálisan gradiens anyagú gömbök hőrugalmassági feladatának közelítésére többrétegű gömbök modelljeivel. A levezetett módszereket összehasonlítottam egymással és szakirodalomban fellelhető eredményekkel, melyek kapcsán azonos eredményeket kaptam.

Tézis 2

Kidolgoztam két numerikus módszert funkcionálisan gradiens gömbök egydimenziós hőrugalmassági feladataira, amikor a testet forgásszimmetrikus hő és mechanikai terhelések érik. A hőmérsékletmezők, elmozdulások és feszültségek számítására szolgáló modellek abban az esetben érvényesek, ha az anyagjellemzők a sugárkoordináta és hőmérsékletmező –amely szintén csak a sugárkoordinátától függ- tetszőleges függvénye. Az egyik módszer a funkcionálisan gradiens anyagot az első tézisben ismertetett analitikus, többrétegű gömbre vonatkozó megoldással közelíti. A másik modell a feszültségfüggvényt és az elmozdulásmezőt, mint ismeretleneket tartalmazó kapcsolt egyenletrendszer segítségével kezdeti érték problémára vonatkozó, numerikus megoldásként oldja meg a feladatot. Egy-egy numerikus módszer lett kidolgozva a piezoelektromos, radiálisan polarizált, funkcionálisan gradiens, gömb alakú testek esetére és összenyomhatatlan gömbök problémáira is. Számpéldákon keresztül vizsgáltam a kidolgozott numerikus módszerek pontosságát, összevetve azokat az első tézisben kidolgozott analitikus megoldásokkal. A leírt modelleket végeselemes szimulációkkal is összevetettem és jó egyezés tapasztalható. Vizsgáltam a módszerek pontosságnövelésének lehetőségeit közelítő polinomok illesztésével. A numerikus példákból jól látszik, hogy a kidolgozott módszerek kielégítő pontosságúak.

Tézis 3

Levezettem két numerikus módszert vékony, forgó, funkcionálisan gradiens tárcsákra, amelyeket kombinált hő és mechanikai terhelések érnek. Az anyagállandók a hőmérsékletnek és a sugárkoordinátának, a tárcsa vastagsága a radiális koordináta tetszőleges függvényei. Az állandósult állapotú hőmérsékletmező három esetben lett kidolgozva három hőtani peremfeltétel-kombináció esetén. Az első numerikus módszer a radiálisan gradiens, változó profilú, forgó tárcsát több homogén rétegből felépített komponensként kezeli és a tisztán hő és tisztán mechanikai terheléseket tartalmazó alesetek szuperpozíciójából és illesztéséből származtatja a feladat megoldását. Ezen modell analitikus megoldásként alkalmazható állandó vastagságú, koncentrikusan rétegzett tárcsák hőrugalmasságtani feladataihoz, valamint ki lettek terjesztve többrétegű hengeres testek azon eseteire, amikor a rétegek radiálisan kapcsoltak, de axiálisan nem. Egy másik numerikus modellt vezettem le vékony, forgó, funkcionálisan gradiens tárcsák esetére, amely feszültségfüggvényt és az elmozdulásmezőt tartalmazó egyenletrendszer segítségével

kezdeti érték problémára transzformálja a feladatot, majd megoldja azt. Megadtam az analitikus megoldást hatvány függvény eloszlás esetére. Végezetül a numerikus modellek pontosságát vizsgáltam az analitikus megoldás segítségével, majd az eredményeket összevetett végeselemes szimulációkkal, és kiderült, hogy kielégítő pontosságúak.

Tézis 4

Kidolgoztam funkcionálisan gradiens prizmatikus rudak elmozdulás és feszültségmezőinek leírására szolgáló egyenleteit abban az esetben, amikor az anyagjellemzők és a hőmérsékletmező a keresztmetszeti koordináták tetszőleges függvényei, a keresztmetszet tetszőleges és a rudat koncentrált erő és nyomaték terheli. Az egyik módszer a kiegészítő energia minimuma elvet használja, a másik esetben az axiális nyúlás és elmozdulásmező egy adott alakjából indulva oldottam meg a feladatot. Levezettem egy modellt a többrétegű, görbe vonalú rudak hőrugalmasságtani feladatainak megoldására az általánosított síkfeszültségi állapot feltételezéseit használva. Részletesen megadtam a bimetál görbe vonalú szalagokra vonatkozó megoldást, majd kiterjesztettem a módszert radiális irányban gradiens görbe vonalú vékony rudakra is. Az eredményeket összevetettem kereskedelmi forgalomban kapható végeselem szoftverekkel végzett szimulációkkal és jó egyezést tapasztaltam.

Publications

The following publications were made in the topic of the dissertation:

Articles in journals:

- Gönczi D., Ecsedi I.: Thermoelastic analysis of functionally graded hollow circular disk. Archieve of Mechanical Engineering, Vol 62. (1), pp. 5-18., 2015.
- Gönczi D., Ecsedi I.: Thermoelastic stresses in nonhomogeneous prismatic bars. Annals of Faculty of Engineering Hunedoara – International Journal of Engineering, Vol 13. (2), pp. 49-52., 2015.
- Gönczi D.: Thermoelastic analysis in functionally graded incompressible spherical bodies. Annals of Faculty of Engineering Hunedoara – International Journal of Engineering, Vol 14. (2), pp. 103-106., 2016.
- Gönczi D., Ecsedi I.: Hőokozta feszültségek és elmozdulások számítása gömb alakú kivágással gyengített végtelen kiterjedésű rugalmas testben (Determination of thermal stresses and displacements in infinite elastic media with spherical cutting-out, in hungarian). Multidiszciplináris Tudományok: A Miskolci Egyetem Közleménye, Vol. 3.(2), pp. 279-288., 2013.
- Gönczi D., Ecsedi I.: Hőfeszültségek számítása üreges hengeres testekben hőmérséklettől függő anyagállandók esetén (Thermal stresses in hollow cylindrical bodies with temperature dependent material properties, in hungarian). GÉP, Vol. 64.(5), pp. 28-32., 2013.
- Gönczi D., Ecsedi I.: Hőokozta feszültségek és elmozdulások meghatározása rétegzett körhenger alakú testekben (Determination of thermal stresses and displacements in layered cylindrical bodies, in hungarian). Multidiszciplináris Tudományok: A Miskolci Egyetem Közleménye, Vol 2. (1), pp. 39-48., 2012.

Conference Papers:

- Gönczi D.: The determination of displacements stresses in functionally graded hollow spherical bodies. XXIX. MicroCAD International Scientific Conference, Miskolci Egyetem (ME), Paper D2, 2015.
- Gönczi D.: The determination of displacement field and normal stresses in multilayered spherical bodies. XXVIII. MicroCAD International Scientific Conference, Miskolci Egyetem (ME), Paper D35, 2014.
- Gönczi D.: Thermoelastic analysis of layered disks. XXXVIII. MicroCAD International Scientific Conference, Miskolci Egyetem (ME), Paper D36, 2014.
- Gönczi D., Ecsedi I.: Analysis of Bimetallic Circular Plate. Spring Wind Conference, Műszaki szekció, pp. 107-117., 2014.

- Gönczi D., Ecsedi I.: The Determination of Thermoelastic Stresses and DispIacement in Layered Spherical Bodies. XXVII. MicroCAD International Scientific Conference. Miskolci Egyetem (ME), Paper 6, 2013.
- Gönczi D., Ecsedi I.: Modelling of steady-state heat conduction and thermal stresses in a hollow cylinder. 8th International Conference of PhD Students, Paper F3, 2012.

Other works:

- Gönczi D.: Thermomechanical analysis of simple structural components subjected to mechanical and thermal loads. PhD students' Seminar, Report for István Sályi Doctoral School, pp. 1-27., 2014.
- Gönczi D.: Hő és mechanikai terhelésnek alávetett tárcsák, üreges gömb és körhenger alakú testek vizsgálata (Mechanical analysis of disks, spherical and cylindrical bodies subjected to mechanical and thermal loads, in hungarian). PhD students' Seminar, Report for István Sályi Doctoral School, pp. 1-24., 2013.
- Gönczi D.: Speciális feladatok végeselemes modellezése I. (Finite element modelling of special problems I., In hungarian) University of Miskolc, pp. 1-57., 2013.

References

[1] Rasheedat M. M., Esther T. A., Mukul S. and Sisa P.: Functionally Graded Material: An Overview, Proceedings of the World Congress on Engineering, 3, 2012.

[2] Craig B.: Limitations of Alloying to Improve the threshold for Hydrogen Stress Cracking of Steels Hydrogen Effects on Material Behavior, Moran, Wyoming, USA, 12-15 Sept., pp. 955-963., 1989.

[3] Wang S. S.: Fracture mechanics for delamination problems in composite materials, Journal of Composite Materials, 17 (3), pp. 210-223., 1983.

[4] Niino M., Hirai T. and Watanabe R.: The functionally gradient materials, J Jap Soc Compos Mat, 13, pp. 257-264., 1999.

[5] Report on: Fundamental study on relaxation of thermal stress for high temperature material by tailoring the graded structure, Department of Science and Technology Agency, 1992.

[6] Knoppers R., Gunnink J. W., Van den Hout J., and Van Vliet W.: The reality of functionally graded material products, TNO Science and Industry, The Netherlands, pp 38-43.

[7] Lin X. and Yue T. M.: Phase formation and microstructure evolution in laser rapid forming of graded SS316L/Rene88DT alloy, Mater Sci Engng, Vol. A402, pp.294-306., 2005.

[8] Elishakoff I., Pentaras D., Gentilini C.: Functionally Graded Material Structures, World Scientific Publishing Co, USA, 2015.

[9] Murín J., Kutiš V., Masný M., Ďuriš R.: Composite (FGM's) Beam Finite Elements, Computational Methods in Applied Sciences, 9, pp 209-23., 2008.

[10] Lutz M. P., Zimmerman R. W.: Thermal stresses and effective thermal expansion coefficient of a functionally graded sphere. Journal of Thermal Stresses, 19, pp. 39-54., 1996.

[11] Tutuncu N., Ozturk M.: Exact solutions for stresses in functionally graded pressure vessels. Composites, part B, 32, pp. 683-686., 2001.

[12] Obata Y., Noda N.: Steady thermal stress in a hollow circular cylinder and a hollow sphere of a functionally gradient materials. Thermal stress, 17, pp. 471-487., 1994.

[13] Kim, K.S., Noda, N.: Green's function approach to unsteady thermal stresses in an infinite hollow cylinder of functionally graded material. Acta. Mech., 156, pp. 61–145., 2002.

[14] Jabbari M., Sohrabpour S., Eslami M.R.: Mechanical and thermal stresses in a functionally graded hollow cylinder due to radially symmetric loads. Int. J. Press. Vessel. Piping, 79, pp. 493–497., 2002.

[15] Eslami M.R., Babaei M.H., Poultangari R.: Thermal and mechanical stresses in a fg thick sphere. Int. J. Press. Vessel. Piping, 82, pp. 522–527., 2005.

[16] Liew K. M., Kitipornchai S., Zhang X. Z., Lim C. W.: Analysis of the thermal stress behaviour of functionally graded hollow circular cylinders. Solids and Structures, 40, pp. 2355–80. (2003)

[17] Zamani N. M., Rahimi G.H.: Deformations and stresses in rotating FGM pressurized thick hollow cylinder under thermal load. Sci. Res. Essay, 4(3), pp. 131–140., 2009.

[18] Tutuncu N., Temel B.: A novel approach to stress analysis of pressurized FGM cylinders, disks and spheres. Compos. Struct., 91, pp. 385–390., 2009.

[19] Nayak P.; Mondal, S. C.: Analysis of a functionally graded thick cylindrical vessel with radially varying properties. Engineering science and technology, 3, pp.1551-1562., 2011.

[20] Shao Z. S.: Mechanical and thermal stresses of a functionally graded hollow circular cylinder with finite length. Pressure vessel and piping, 82, pp.155-163., 2005.

[21] Vitucci G., Mishuris G.: Analysis of residual stresses in thermoelastic multilayer cylinders. Journal of Internationaly Ceramic Society, 36, pp.2411-2417., 2016.

[22] Arefi M.: Two dimensional thermoelastic analysis of a functionally graded cylinder for different functionalyties by using the higher-order shear deformation theory. Journal of Applied Mechanics and Technical Physics, 56 (3), pp.494-501., 2015.
[23] You L. H., Zhang J. J., You, X. Y.: Elastic analysis of internally pressurized thick-walled spherical pressure vessels of functionally graded materials. Pressure vessel and piping, 82, pp.347-354., 2005.
[24] Ahmet N. E., Tolga A.: Plane strain analytical solutions for a functionally graded elastic plastic pressurized tube. Pressure vessels and piping, 83, pp. 635–644., 2006.
[25] Chen Y. Z., Lin X. Y.: Elastic analysis for thick cylinders and spherical pressure vessels made of functionally graded materials. Computational Materials Science, 44, pp.581–587., 2008.
[26] Shao Z. S., Ma G. W.: Thermo-mechanical stresses in functionally graded circular hollow cylinder with linearly increasing boundary temperature. Composite Structures, 83, pp.259–265., 2008.
[27] Nayak P., Mondal S. C., Nandi A.: Stress, Strain and displacement of a functionally graded thick spherical vessel. International Journal of Engineering Science and Technology, 3 (4), pp. 2660-2671., 2011.
[28] Bayat Y., Ghannad M., Torabi H.: Analytical and numerical analysis for the FGM thick sphere under combined pressure and temperature loading. Arch. Appl. Mech., 10, pp. 229-242., 2011.
[29] Pen X., Li X.: Thermoelastic analysis of functionally graded annulus with arbitrary gradient, Applied Mathematics and Mechanics (English Edition), pp. 1211-1220., 2009.
[30] Jabari M., Sohrobpoun S., Eslami M.R.: Mechanical and Thermal Stresses in a functionally graded hollow cylinder due to radially symmetric loads, Pressure Vessels and Piping 79, pp. 493-497., 2002.
[31] Timoshenko S., Goodier I. N.: Theory of Elasticity, McGraw-Hill, New York, 1951.
[32] Solecki R., Conant R, I.: Advanced Mechanics of Materials, Oxford University Press, Oxford, 2003.
[33] Barber I. N.: Intermediate Mechanics of Materials, 2nd edition, Springer, New York, 2011.
[34] Ragab A. R., Bayoumi S. E.: Engineering Solid Mechanics (Fundamentals and Applications), CRC Press, London, 1999.
[35] Hetnarski, R. B., Eslami, M. R.: Thermal Sresses – Advaned Theory and Applications, Springer, New York, 2010.
[36] Noda N., Hetnarski R. B. and Tanigawa Y.: Thermal Stresses. Lastran Corporation, Rochester, New York, 2000.
[37] Loghman A., Ghorbanpour A. A., Shajari R. A., Amir s.: Time-dependent thermoelastic creep analysis of rotating disk made of Al–SiC composite. Archive of Applied Mechanics, Springer, 81 (12), pp. 1853-1864., 2011.
[38] Afsar A. M., Go J.: Finite element analysis of thermoelastic field in a rotating FGM circular disk. Applied Mathematical Modelling, Elsevier, 34(11)., pp. 3309-3320., 2010.
[39] Hassani A., Hojjati M. H., Mahdavi E., Alashti R. A., Farrahi G.: Thermo-mechanical analysis of rotating disks with non-uniform thickness and material properties. International Journal of Pressure Vessels and Piping, Elsevier, 98., pp. 95-101., 2012.
[40] Dhamirchelli M., Azadi M.: Temperature and thickness effects on thermal and mechanical stresses of rotating FG-disks. Journal of Mechanical Science and Technology, Springer, pp. 11-23., 2011.
[41] Vivio F., Vullo V., Cifani P.: Theoretical stress analysis of rotating hyperbolic disk without singularities subjected to thermal load. Journal of Thermal Stresses. 37, pp. 117–136., 2014.

[42] Wang H. M.,Xu Z. X.: Effect of material inhomogeneity on electromechanical behaviors of functionally graded piezoelectric spherical structures. Comput. Mater. Sci., 48, pp. 440–445., 2010.
[43] Atashipour S. H., Sburlati R.: Electro-elastic analysis of a coated spherical piezoceramic sensor. Composite Structures, 130, 2015.
[44] Ghorbanpour A., Golabi S., Saadatfar M.: Stress and electric potential fields in piezoelectric smart spheres, Journal of Mechanical Science and technology, Springer, 20. (11), pp. 1920-1933., 2006.
[45] Chu P., Li X.-F., Wu J.-X., Lee K. Y.: Two-dimensional elasticity solution of elastic strips and beams made of functionally graded materials under tension and bending. Acta Mech, Springer-Verlag Wien, 226, pp. 2235-2253, 2015.
[46] Sankar B.V.: An elasticity solution for functionally graded beams. Compos. Sci. Technol., 61, pp. 689–696, 2001.
[47] Zhong, Z., Yu, T.: Analytical solution of a cantilever functionally graded beam. Compos. Sci. Technology, 67, pp. 481–488, 2007.
[48] Ying, J., Lu, C.F., Chen, W.Q.: Two-dimensional elasticity solutions for functionally graded beams resting on elastic foundations. Composite Structures, 84, pp. 209–219, 2008.
[49] Wang M., Liu Y.: Analytical solution for bi-material beam with graded intermediate layer. Compos. Struct., 92, pp. 2358–2368, 2010.
[50] Li Y. D., Zhang H. C., Zhang N., Dai Y.: Stress analysis of functionally gradient beam using effective principal axes. Int. J. Mech. Mater. Des. 2, pp. 157–164., 2005.
[51] Wallerstein D. V.: A Variational Approach to Structural Analysis. Wiley-Interscience, New York, 2001.
[52] Boley B. A., Weiner J. H.: Theory of Thermal Stresses, John Wiley & Sons Inc., New York, 1960.
[53] Shen H-S.: Functionally Graded Materials: Nonlinear Analysis of Plates and Shells. CRC Press, London, 2009.
[54] Reddy J.N., Chin C.D.: Thermomechanical analysis of functionally graded cylinders and plates. J. Thermal Stresses, 21, pp. 593-626., 1998.
[55] Mori T., Tanaka K.: Average stress in matrix and average elastic energy of materials with misfitting inclusions, Acta Metal, 21, pp. 568-582., 1973.
[56] Touloukian YS, Gerritsen JK, Moore NY. Thermophysical Properties Research Literature Retrieval Guide. Springer, 1967.
[57] Jiashi Yang: An introduction to the theory of piezoelectricity. Springer Science + Business Media Inc., Boston, 2005.
[58] Qing-Hua Qin: Advanced Mechanics of Piezoelectricity. Higher Education Press, Beiging, 2012.
[59] Carslaw H. S., Jaeger I. C.:Conduction of Heat in solids, Clarendon Press, Oxford, 1959.
[60] Nowinski I. L.: Theory of Thermoelasticity with Applications. Sythoff and Noordhoff, Alpen aan den Rijn, 1978.
[61] Wang H. M., Ding H. J., Chen Y. M.: Transient responses of a multilayered spherically isotropic piezoelectric hollow sphere. Arch. Appl. Mech., 74, pp. 581–599., 2005.
[62] Aignatoaie M.: FEA study on the elastic deformation process of a simple bimetal beam. Applied Mechanics and Materials, 371, pp. 448-452, (2013)
[63] Suhir E.: Interfacial stresses in bimetal thermostats. Journal of Applied Mechanics, 56 (3), pp. 595-600.,
[64] Ramos D., Mertens I., Callega M.,Tamayo I.: Study on the origin of Bending Induced by Bimetallic Effect on Microcantilever. Sensors, 7, pp. 1757-1765., 2007.

[65] Rao A. V., Prasad K.S.V., Avinash M., Nagababu K., Manohar V., Raju P.S.R., Chandra G.R., A Study on Deflection of a Bimetallic Beam under Thermal Loading using Finite Element Analysis. International Journal of Engineering and Advanced Technology, 2(1), pp. 81-82., 2012.
[66] Sadowski T., Birsan M., Pietras D.: Multilayered and FGM structural elements under mechanical and thermal loads. Part I: Comparison of finite elements and analytical models Archives of Civil and Mechanical Engineering, 15, pp. 1180-1192., 2015.
[67] Gönczi D., Ecsedi I.: Finite Element Modelling of Functionally Graded Spherical Pressure Vessels. Annals of Faculty of Engineering Hunedoara – International Journal of Engineering, 12 (2), pp. 179-184., 2014.
[68] Gönczi D., Ecsedi I.: Hőokozta feszültségek és elmozdulások meghatározása rétegzett körhenger alakú testekben (Determination of thermal stresses and displacements in layered cylindrical bodies, in hungarian). Multidiszciplináris Tudományok: A Miskolci Egyetem Közleménye, 2. (1), pp. 39-48., 2012.
[69] Gönczi D., Ecsedi I.: Thermoelastic analysis of functionally graded hollow circular disk. Archieve of Mechanical Engineering, Vol 62. (1), pp. 5-18., 2015.
[70] Shames I. H., Dym C. L.: Energy and Finite Element Methods in Structural Mechanics. Taylor and Francis, New York, 1985.
[71] Richards T. H.: Energy Methods in Stress Analysis: With Introduction to the Finite Element Technique. Ellis Harwood, Chichester, 1977.
[72] Stokes V. K.: Thermoelastic Pure Bending of Nonhomogeneous Prismatic Bars. Journal of Thermal Stresses, Vol. 14., pp. 499-518., 1991.
[73] Ecsedi I., Dluhi K.: A linear model for the static and dynamic analysis of non-homoeneous curved beams. Appl. Math. Modelling, 29 (12), pp. 1211-1231., 2005.
[74] Gönczi D.: Thermal stresses in thin anisotropic hollow circular disk. Annals of Faculty of Engineering Hunedoara – International Journal of Engineering, 14 (2), pp. 59-64., 2016.